# RHIC Beam Use Request
# For Runs 15 and 16

**The STAR Collaboration**

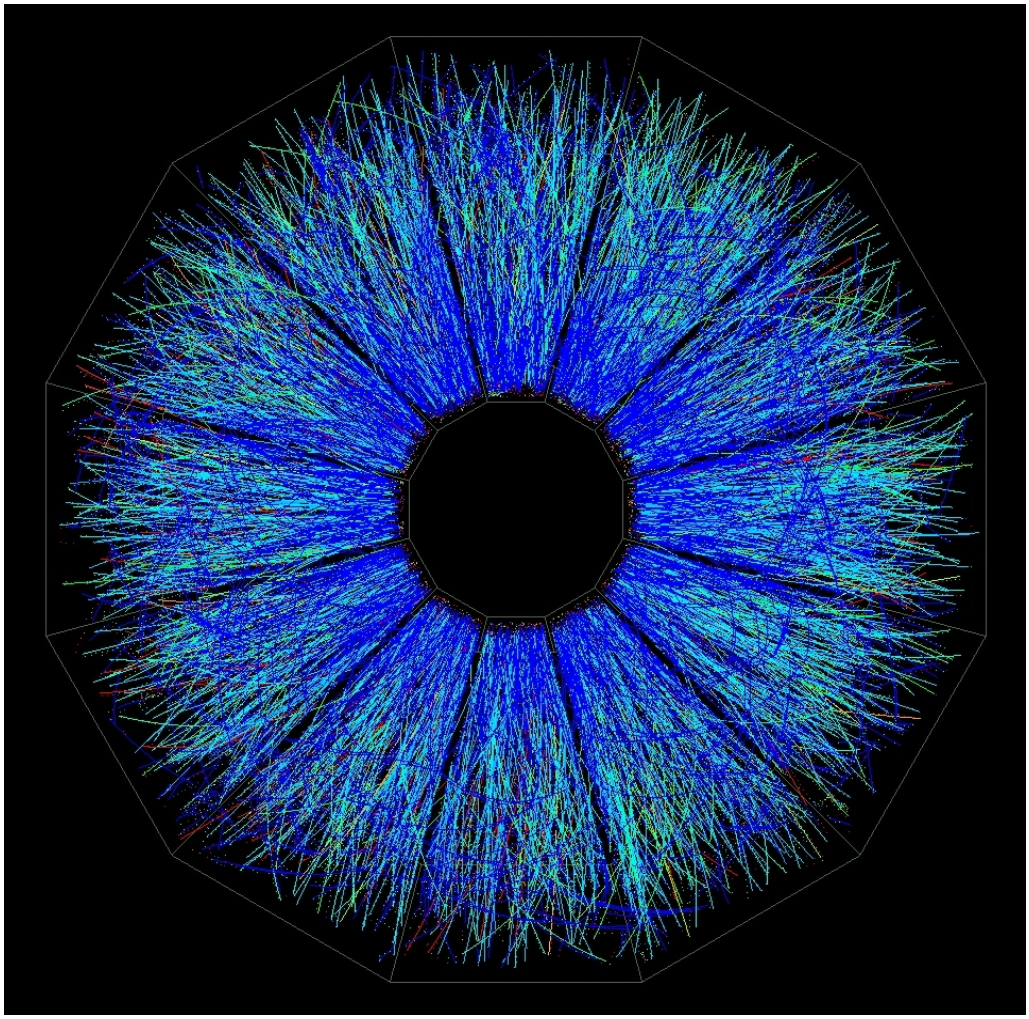

**June 2, 2014**

# 1. Executive Summary

With two new major upgrades, the Heavy-flavor Tracker (HFT) and the Muon Telescope Detector (MTD), the STAR Collaboration has positioned itself well for leading the field in several major scientific programs in the next few years. We have maintained a similar pace in our scientific productivity and training of the next generation of young scientists for the last 15 years. To continue our excellent track record on science, we, the members of the STAR Collaboration, have recently produced a road map for our future in the form of our decadal plan, eSTAR Letter of Intent, Beam Energy Scan Phase II Whitepaper and pp/pA Letter of Intent documents. This is a critical time for RHIC as a facility and STAR as a collaboration. The STAR Collaboration is fully committed to our priorities based on the scientific pillars of studying QGP properties, elucidating the nature of the spin of the proton, searching for a critical point in the QCD phase diagram and exploring the high-density gluon field in nuclei. A sustainable strong science program in STAR calls for realization of the proposed upgrades and substantial new initiatives, and requires continuous effort and involvement from each and every collaborator. The STAR Collaboration proposes the following two-year beam-use request for RHIC run periods in 2015 and 2016, in order to achieve its near-term spin and relativistic heavy ion physics goals. A detailed breakdown of the proposed run periods is shown in Table.1.1.

| Run | Energy | Duration | System | Goals | priority | sequence |
|---|---|---|---|---|---|---|
| 15 | $\sqrt{s_{NN}}$=200GeV | 5-week | Transverse p+Au | saturation physics, ridge and reference, $\mathcal{L}$=300 nb$^{-1}$ | 1 | 3 |
| | $\sqrt{s}$=200GeV | 12-week | 1) p+p | 1) HI reference $\mathcal{L}$=90 pb$^{-1}$, 500M MB | 2 | |
| | | | 2) transverse 6 weeks | 2) Study transversity, Sivers effects $\mathcal{L}$=40 pb$^{-1}$, 60% pol. | 2 | 2 |
| | | | 3) longitudinal 6 weeks | 3) Study $\Delta g(x)$ $\mathcal{L}$=50 pb$^{-1}$, 60% pol. | 2 | 1 |
| 16 | $\sqrt{s}$=200GeV | 10-week | Au+Au | $\Lambda_c$, D $v_2$, $R_{AA}$, $\Upsilon$ 10nb$^{-1}$, 2billion MB | 1 | 1 |
| | $\sqrt{s}$=510GeV | 7-week | Transverse p+p | $A_N$ of $W^{\pm}$, $\gamma$, Drell-Yan, $\mathcal{L}$=400 pb$^{-1}$, 55% pol | 2 | 2 |

*Table 1.1 STAR BUR for run15 and run16. Both requests assume 22 cryo-weeks for RHIC operation, and 17 weeks of physics run with two species in one RHIC year.*

**Run 15**:

The on-going run14 with Au+Au collisions at 200 GeV has been producing the first dataset with the complete MTD and all three subsystems of the HFT. Crucial to a successful run15 scientific program are our proposed incremental upgrades of other existing sub-systems. The necessary and on-going upgrades to the detectors are:

a) refurbishing the Forward Meson Spectrometer (FMS);
b) a scintillator-based pre-shower detector in front of the FMS,
c) Roman Pot Phase II*.

These upgrades are anticipated to be ready for the run. The proposed run15 programs with p+p and p+Au collisions at $\sqrt{s}$=200GeV provide crucial baseline measurements of charmed mesons and quarkonia. The same beam species will produce several important measurements to study the ridge phenomenon and the possible onset of gluon saturation effects using the unique polarized p+Au collisions in a collider mode.

A six-week run of p+p collisions at $\sqrt{s}$=200GeV with longitudinal polarization will provide a data-set to further constrain the gluon polarization through inclusive jet and di-jet measurements at mid-rapidity, especially for the medium momentum fractions *x*, and constitutes the main spin physics objective for Run 15 longitudinal running. The non-zero gluon contributions to the spin structure of the nucleon, extracted via the double-longitudinal polarization measurements of jet production, have generated significant interest in further improving the measurements and the kinematic reach. The same run configuration also allows one to measure the $A_{LL}$ of $\pi^0$ mesons in the forward meson spectrometer, extending to the unexplored lower *x* kinematics.

We propose a subsequent six-week run of p+p collisions at $\sqrt{s}$=200GeV with spins transverse to their momentum direction. These p+p collisions exhibit kinematic and dynamical effects that are directly sensitive to quark transversity and partonic motion within the proton. In addition to improving the existing measurements of Interference Fragmentation Function (IFF) and Collins analyses, a refurbished FMS with an additional pre-shower in the front will provide clean direct photon measurements at forward rapidity. This program is complemented by studies of polarized p+p elastic scattering and central exclusive production, in which an intact proton is detected at far-forward angles. The relocation of the Roman Pots allows concurrent data-taking with the nominal beam configuration, and enables new measurements on $A_N$ for exclusive J/Ψ production and inclusive diffractive production in p+p collisions.

A new program with an integrated 300 $nb^{-1}$ of luminosity of $\sqrt{s_{NN}}$ = 200 GeV p+Au collisions with a transversely polarized proton beam for a period of five weeks is proposed to follow the 12-weeks of p+p collisions. The program will address important physics, including gluon saturation, cold nuclear effects on open heavy flavor and heavy quarkonia production, the ridge effect in p+A, the Cronin effect and the strangeness enhancement in small-size systems. Utilizing RHIC's unique capability of colliding polarized proton with heavy nuclei, the ratios of single spin asymmetries in $\pi^0$ and direct photon production at forward rapidity between p+A and p+p collisions can be used to access the elusive nuclear Weizsaecker-Williams (WW) gluon distribution function. The asymmetry for exclusive J/Ψ production in ultra-peripheral p+A collisions measurable with the upgraded Roman-Pot detectors in STAR will explore the generalized parton distribution function for gluons.

**Run16**:

We propose a 10-week run period of Au+Au collisions at at $\sqrt{s_{NN}}$ = 200 GeV, integrating 10 $nb^{-1}$ of luminosity with rare triggers for Upsilon states, gamma-jet correlations, B→ J/ψ and J/ψ production, and 2 billion minbias events for $\Lambda_c$ and differential studies of charm flow and correlations.

A total integrated luminosity of over 20$nb^{-1}$ with the combination of run14 and run16 provides the necessary statistics for a measurement of each of the three Upsilon states. We also request to collect 2 billion minimum-bias Au+Au collision events at $\sqrt{s_{NN}}$ = 200 GeV in Run16. A new set of the inner HFT (PXL layers) with Aluminum cables will be installed for run16 with significantly reduced multiple-scattering. We have also proposed to improve the effectiveness of online vertex selection of collisions within the HFT fiducial coverage. The effective figure of merit in terms of statistics for the signal increases by about a factor of 6 for low $p_T$ D0 in comparison to the dataset taken in run14 due to reduced cabling material and improved online vertex selection. This significant improvement will allow us to perform differential studies on the charmed hadron yields, flow and correlations in several centralities. More importantly, the high statistics and the improved pointing resolution for low momentum tracks will make the $\Lambda_c$ measurement feasible ($c\tau$ of $\Lambda_c$ ~ 60 μm).

A seven-week run period in the second part of the run16 with transversely polarized p+p collisions at $\sqrt{s}$ = 510 GeV accumulating 400 $pb^{-1}$ integrated (600$pb^{-1}$ delivered) luminosity is proposed for measuring $A_N$ for $W^{\pm}$ at mid-rapidity, γ and exploratory DY measurements at forward rapidity. The possibility of measuring $A_N$ for DY, $W^{+/-}$, $Z^0$ Bosons and direct photons in one experiment would provide a unique world-class opportunity to test TMD evolution, access the Sivers function for sea quarks and test the prediction of non-universality for the Sivers function through three different processes. Measurement of $A_N$ for $W^{\pm}$ at mid-rapidity requires optimization of the instantaneous luminosity (β* squeeze) for best TPC performance and does not require additional detector upgrades. We have presented alternative upgrade options for a forward calorimeter, tracker and pre-shower and are in the process of evaluating the most cost-effective approach.

# 2. Highlights from STAR Science Programs

## 2.1 STAR Heavy-Ion Program

STAR had another successful and productive year with the publication of 5 PRL's [1,2,3,4,5] and 9 other articles in refereed journals from January 2013 thru April 2014 with another 4 letters submitted to PRL and a further 5 being refereed at other journals. These publications make significant steps towards meeting performance milestones of nuclear physics to measure jets and their correlations at top RHIC energies (DM10), measure the bulk properties of matter produced in the Beam Energy Scan and search for evidence of a Critical Point (DM11), measure the detailed production properties of identified heavy flavor particles (DM12), and determine how photons and low mass dileptons are emitted from collisions at RHIC (DM13). Thanks to the large statistics provided by recent RHIC runs combined with STAR's large acceptance and excellent particle identification, STAR has entered the era of precision measurements of the QGP properties at top RHIC energy using rare probes, namely heavy quarks and jets.

The reported jet-hadron correlations indicated that the energy lost due to interactions with the QGP as hard scattered partons leave the medium re-emerges as numerous soft particles that remain correlated with the original parton's trajectory[5]. This result is in qualitative agreement with the "2+1" hadron correlations analysis where a pair of high $p_T$ back-to-back hadron triggers were used as a di-jet proxy[6]. When compared to d+Au data a relative imbalance in the total $p_T$ between the hadrons attributed to the near-side and away-side jet-like peaks was observed. This relative imbalance increases with the asymmetry of the trigger pair, consistent with expectations from medium-induced energy-loss effects. A decrease in this imbalance for softer associated hadrons again suggests that the missing high $p_T$ particles are converted into softer hadrons. The energy loss likely has a pathlength-dependence, since di-hadron azimuthal correlations reveal an away-side modification that is more extreme in-plane than out-of-plane[7].

While fully reconstructed jets allow for a more differential investigation of the parton energy loss compared to single particle spectra, it is challenging due to a large population of combinatorial background that overwhelm the true hard jet population by several orders of magnitude. To overcome this challenging background STAR has recently focused on di-jet measurements and semi-inclusive recoil jet spectra measurements [1]. A significant di-jet transverse momentum asymmetry, $A_j$, is observed for the cutoff on the jet constituents of $p_T^{cut} > 2\ GeV/c$. However, these di-jet's energies become largely balanced for a very low cutoff $p_T^{cut} > 0.2\ GeV/c$ and the same resolution parameter $R$ ($R=0.4$) as shown in Figure 2.1. This observation is consistent with jet-hadron correlations[5] and suggests that most of the quenched energy is recovered within $R=0.4$ at RHIC, in contrast to the LHC measurements.

[1] J.Putschke QM2014

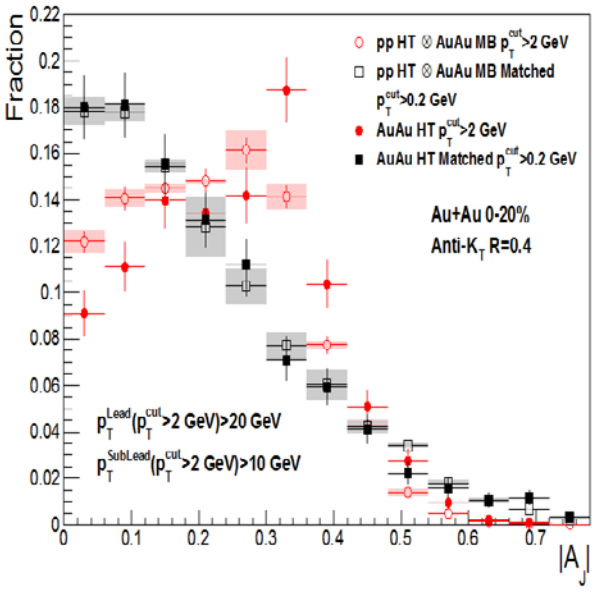


Figure 2.1: Preliminary di-jet transverse momentum asymmetry for 0-20% most central Au+Au collisions at 200 GeV (solid points) and p+p jets embedded into Au+Au collisions (open symbols) for two values of the cutoff on the jet constituents: $p_T^{cut} > 2\ GeV/c$ (red) and $p_T^{cut} > 0.2\ GeV/c$ (black).

To better constrain parameters of models of parton energy loss, it is essential to examine independently the dependence of the energy loss ($\Delta E$) on the initial energy of the parton ($E$), path length of the parton through the medium, and the parton type. Direct photons, $\gamma^{dir}$, serve as calibrated probes, providing experimental tools to explore energy loss of hard-scattered partons free from the uncertainties accompanying parton fragmentation[8]. STAR recently reported[2] preliminary detailed systematic studies of away-side azimuthal correlations of charged hadrons with respect to a direct-photon trigger in p+p and Au+Au collisions, using data collected in 2011. The away-side nuclear modification factor coincidence rate, $I_{AA}$, at low $z_T$ shows more suppression for photon triggered events than for $\pi^0$ triggered events.

Direct photons also provide an important cross-check for the finite $v_2$ of pions observed at high $p_T$ in Au+Au at 200 GeV. The observed anisotropy can originate either from jet-like correlations or a path length dependence of $\Delta E$ with respect to the reaction plane. Previous measurements[2] of $\gamma^{dir}$ $v_2$, with the event plane measured at mid-rapidity, showed a finite $v_2$ on the level of 0.03 – 0.05. Elliptic flow of $\gamma^{dir}$ measured with the event plane estimated with the Forward TPC (providing a larger rapidity separation between the reconstructed event plane and the $\gamma^{dir}$ measurement) is consistent with zero, while the charged hadrons $v_2 \approx 0.1$ for $p_T > 8$ GeV/c. This indicates that the azimuthal anisotropy at high $p_T$ arises from a path length dependence of $\Delta$E.

STAR has developed a new approach to the study of jet quenching, based on the semi-inclusive distribution of reconstructed jets recoiling from a high $p_T$ hadron trigger ("h+jet" coincidence). This approach enables the measurement of quenched jets in heavy ion collisions that is strictly infrared and collinear-safe (IRC-safe), without jet selection bias. It parallels a similar analysis by the ALICE Collaboration at the LHC, and allows direct comparison of IRC-safe jet quenching measurements at the two colliders. An important new development for the STAR analysis is the accurate measurement of the combinatorial background jet distribution using mixed events.

The upper left panel of Fig. 2.2 shows the distribution of all charged jet candidates (anti-$k_T$, R=0.3) in a 90 degree interval opposite in azimuth to a hadron trigger ($9<p_T^{trig}<19$ GeV), in central Au+Au

[2] A.Hamed QM2014

collisions at 200 GeV. The horizontal axis is the reconstructed charged jet energy, corrected event-by-event for the estimated average background energy density. Jet candidates with negative corrected energy are dominated by background; they are however not rejected in this analysis, but are used for precise measurement of background fluctuations. The grey histogram shows the distribution of jets reconstructed from mixed events, with the ratio of data/mixed events (lower left panel) showing that mixed events provide a precise representation of combinatorial jet background over several orders of magnitude in jet rate. The distribution of true coincident jet yield is the difference between the red points (data) and grey histogram (background), though with jet energy scale not yet corrected for smearing due to background fluctuations.

The middle panel compares the yield of the true coincident jet distribution with that from PYTHIA smeared by detector and underlying event effects, showing strong suppression of coincident jet yield in central Au+Au collisions. The PYTHIA distribution agrees well with the coincident jet yield in peripheral collisions (60-80%). The suppression in central collisions corresponds to a horizontal shift of the exponential distribution of about 5 GeV, representing the first direct measurement of jet energy loss at RHIC. The right panel shows the azimuthal distribution of recoil jets in central Au+Au collisions with (uncorrected) jet $p_T$ between 12 and 32 GeV. The width of the central peak is comparable in magnitude to that in peripheral collisions, and the tails do not show evidence for significant large-angle scattering in the medium. More precise characterization of these distributions is on-going.

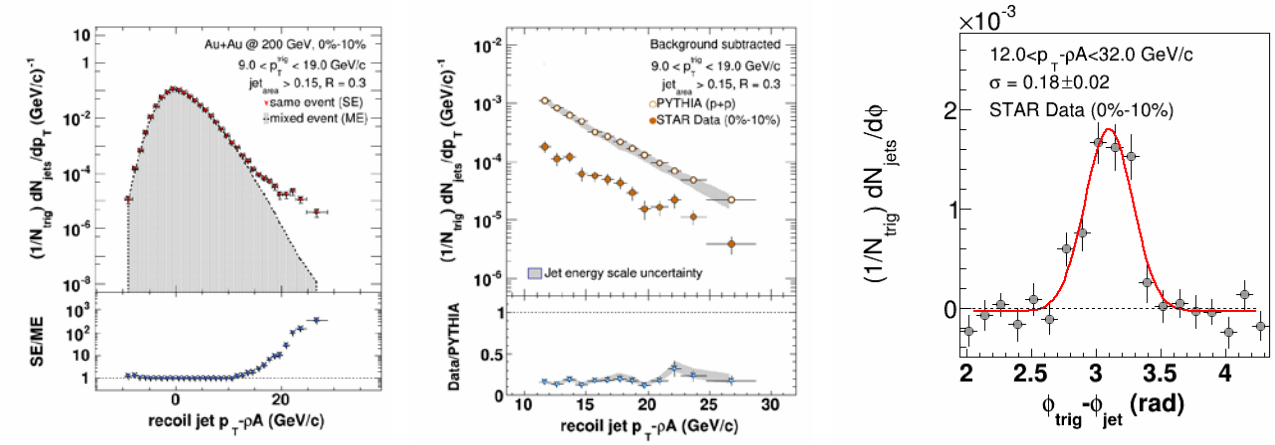


Figure 2.2: semi-inclusive h+jet measurement for 0-10% Au+Au collisions at sqrt(s)=200 GeV.

The properties of the bulk medium produced in Au+Au collisions from 7.7 to 200 GeV continue to be probed. The 200 GeV Kaon source functions are well described by a 3-D Gaussian, but generally narrower than those of pions. However, comparison with the Therminator model indicates that the lifetime and size of the emitting source is similar for $\pi$s and Ks. The Kaon's narrower shape suggests that long-lived resonances and/or the exponential emission duration, $\Delta\tau$, play a less important role in the K source emission. The breaking of the transverse mass scaling of longitudinal radii favors hydro-kinetic predictions over pure hydrodynamical calculations[ 9 ]. Triangular flow, $v_3$, at 200 GeV decreases as the mean pseudorapidity separation of the measured particles increases[10]. The good agreement of $v_3(p_T)$ with models including fluctuations indicates that triangular flow is mainly due to $\Delta\eta$ dependent fluctuations.

The system size dependence of the $p_T$ fluctuations and correlations were explored utilizing Cu+Cu collisions at $\sqrt{s_{NN}}$=62.4 and 200 GeV[11]. For similar mean number of participating nucleons, the dynamical $p_T$ fluctuations are comparable for the Cu+Cu and Au+Au systems, suggesting that the system size has little effect at those energies. Multi-phase transport models can best reproduce the invariance of the scaled $p_T$ correlations with both beam energy and centrality.

A study of the beam energy dependence of the directed flow of identified protons[1] reveals a minimum in the slope of $dv_1/dy$ between $\sqrt{s_{NN}}$ =11.5 and 19.6 GeV. This result is qualitatively consistent with predictions for hydrodynamical models containing first order phase transitions to a QGP. The first observation of a beam energy-dependent difference in the elliptic flow of antiparticles compared to particles [2,12] implies that the apparent universality of number-of-constituent quark scaling of $v_2$ observed at $\sqrt{s_{NN}}$ =200 GeV, which is one of the signatures in support of the QGP formation, is broken at lower collision energies. The difference increases with decreasing beam energy, it is larger for baryons compared to mesons and the NCQ scaling is broken at low energies across all centrality classes[3].

STAR measured also elliptic flow of light nuclei (deuteron, triton and helium) as a function of beam energy. Both nuclei and anti-nuclei show similar magnitudes of $v_2$ as well as clear centrality dependences. Balance functions are another observable studied as a function of beam energy, the widths of which are sensitive to the hadronization time. We observe a narrowing with increasing beam energy and centrality, even at $\sqrt{s_{NN}}$=7.7 GeV. These results are consistent with a delayed hadronization, which is expected in the case of the QGP formation.

One of main goals of the RHIC Beam Energy Scan program is a search for a critical point in the QCD phase diagram, where an ordered phase transition ends and becomes a crossover. Possible manifestations of the critical point are fluctuations in event-by-event multiplicity distributions of conserved quantities like net-charge, net-baryon number and net-strangeness. The net charge fluctuations however show no clear indication, within the current systematic and statistical precision, of any non-monotonic behavior with beam energy[13]. For beam energies less than 27 GeV, the products of higher moments ((the kurtosis times the variance, $\kappa\sigma^2$) of net-protons in central Au+Au collisions deviate significantly from Skellam expectations, and are reproduced by neither a hadronic resonance gas calculation nor the transport model URQMD[3]. However, the measurements are reasonably described by independent production of proton and anti-protons, indicating that there are no apparent correlations between the protons and anti-protons for that observable.

If local parity violating domains are formed within a QGP, they may manifest themselves as a charge separation in the produced hadrons along the magnetic field axis. Charge separation measurements consistent with this prediction using high statistics Au+Au data[14,15] confirmed our previous lower statistics results. An exploration of the beam-energy dependence of this separation revealed a gradually decreasing signal that vanished by 7.7 GeV[16]. This trend is consistent with local parity violation in a partonic phase for higher collision energies, but an increasing dominance of a hadronic phase at low $\sqrt{s_{NN}}$. In the high statistics data the source of an opposite charge parity-even suppression is likely explained as a parity conserving background, due to momentum conservation and collective flow. STAR uses U+U collisions for a cross-check in the search for the Chiral Magnetic Wave (CMW)[17] in Au+Au collisions. The integrated $v_2$ of $\pi^+(\pi^-)$ at low $p_T$ decreases (increases) linearly with the increasing net charge asymmetry $A^{\pm}$ . The $v_2$ difference between $\pi^+$and $\pi^-$ is proportional to $A^{\pm}$ and the slope parameters have magnitude of

[3] R. Haque QM2014

about 0.01. These observations are consistent with the predication based on CMW. The same linear relationship between $v_2$ of $\pi$ and $A^{\pm}$ has been confirmed in U+U collisions. Also a cross-check with third order harmonics, proposed in [18], indicates that it is unlikely that the background (local charge conservation at freeze-out) have a significant contribution to the splitting of $v_2$ of charged pions as a function of $A^{\pm}$.

The capability of selecting initial geometry in U+U collisions provides new opportunities to study possible Local Parity Violation and path-length dependent jet quenching in the future. To take advantage of Uranium nuclei's prolate shape, it is necessary to divide the U+U data into body-on-body vs. tip-on-tip enhanced samples. We already demonstrated that by combining cuts on the ZDC signals and charged particle multiplicity, one can select body-on-body or tip-on-tip enhanced samples of central U+ U collisions.

In nearly fully overlapping (small impact parameter) U+U collisions, the initial matter distribution can take on very different shapes. The two extremes are when the tip of one nucleus impinges on the tip of the other (tip-tip) or when the nuclei collide side-on-side or body-body. Tip-tip collisions have a larger number of binary collisions between constituent nuclei distributed over a smaller symmetric region while body-body collisions will have a more elliptic overlap region. The larger number of binary collisions in the tip-tip collisions are expected to lead to a larger number of produced particles[19] while the more elliptic shape of the body-body collisions are expected to lead to a larger second harmonic anisotropy $v_2$. Measurements of $v_2$ as a function of multiplicity in nearly fully overlapping U+U collisions therefore provide a unique test of our understanding of both particle production and $v_2$. It has been predicted that a unique knee structure will be present in high multiplicity collisions if one plots $v_2$ vs. charged multiplicity. However, the $v_2\{2\}$ results from U+U data show no indication of such a structure. A non-zero $v_2\{4\}$ combined with the lack of a knee structure in $v_2\{2\}$ could indicate that although the prolate geometry shape of Uranium nuclei do show up in the data, additional fluctuation might be washing out this "knee". The multiplicity dependence of $v_2\{2\}$ in central collisions was compared to Monte-Carlo Glauber model predictions and this model cannot explain the present results[4].

If body-body collisions produce smaller multiplicities than tip-tip collisions, we expect to see a negative slope in $v_2$ vs multiplicity. Figure2.3 shows the elliptic flow $v_2$ of all charged particles as a function of the normalized multiplicity for the ZDC selection of the 0.1% most central U+U and Au+Au collisions. The slope for Au+Au collision is close to zero indicating the variation in multiplicity in Au+Au is mainly driven by fluctuations. The negative slope for U+U collisions indicates that the variation of multiplicity in the 0.1% U+U collisions depends on the different geometries made possible by the oblate shape of the U nucleus. ZDC and multiplicity can therefore be used to select tip-tip and body-body enhanced samples: Those samples can then be used to study other topics like the path-length dependence of jet-quenching, or the extent to which three-particle charge-dependent correlations can be attributed to local parity violation or background effects. The data are also compared to expectations from our Glauber model calculations and from a gluon saturation (Color Glass Condensate) based calculation IP-Glasma. The Glauber model predicts a much larger slope for U+U collisions than is observed and a slightly positive slope for Au+Au collisions. The IP-Glasma model indicates a smaller slope in U+U collisions which is much closer to the data. Our data for nearly fully overlapping U+U and Au+Au prefer the IP-Glasma description of the initial conditions [20].

[4] H. Wang QM2014

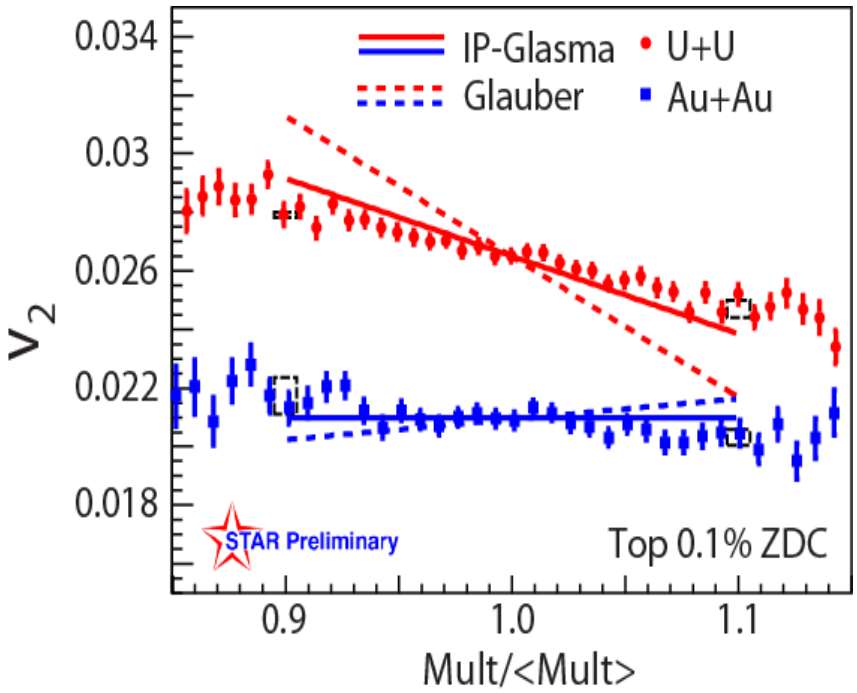

Figure 2.3: v2 as a function of multiplicity for top 0.1% central ZDC event selection.

The open charm $D^0$-meson suppression factor is measured for the first time revealing the first direct observation of charm quark energy loss in the medium [21]. A few models with different physical assumptions reproduce qualitatively the trends seen in the $D^0$ data and elliptic flow of non-photonic electrons [22]. Better precision and more differential measurements are necessary to discriminate between them. Azimuthal correlations of charmed mesons and hadrons ($D^0 - D^0$ and $D^0$-hadron) provide such additional observables. STAR made a first step in this direction and reported non-photonic electron - hadron correlation in Au+Au collisions at 200 GeV with high-statistics data taken in 2011[5]. We observe a similar pattern to that in the di-hadron correlations: there is away side broadening and a suppression in central events compared to peripheral collisions.

Elliptic flow of non-photonic was measured in Au+Au collisions at 200, 62.4 and 39 GeV[23] and shown in Figure 2.4 right panel. We observed a non-zero $v_2$ at low and intermediate transverse momentum at 200 GeV, and $v_2$ is consistent with zero at low $p_T$ at other energies. For Au+Au collisions at $p_T$<1 GeV/c, there is a statistically significant difference between elliptic flow at 200 GeV and at the two lower beam energies. This indicates that charm quarks interact less strongly with the hot and dense medium at 62.4 and 39 GeV compared to the top RHIC energy

Both the J/ψ and Υ production are highly suppressed compared to p+p collisions [24,25,26]. The Upsilon is the most accurate probe of the thermal suppression of quarkonium production via Debye screening in the heavy ion collisions; however it is experimentally challenging due to low cross section.: STAR reported a strong suppression of the $\Upsilon(1S)$ and combined *2S* and *3S* states in central Au+Au collisions (Figure 2.4)[25]. The $\Upsilon(1S + 2S + 3S)$ suppression increases with centrality and is consistent with a model that assumes complete suppression of $\Upsilon(2S)$ and $\Upsilon(3S)$ states. The suppression of $\Upsilon$ states in central Au+Au collisions confirms the presence of deconfined matter in heavy-ion collisions. Higher statistics d+Au or p+A datasets are needed in order to

[5] Zhenyu Ye, QM2014

strengthen the conclusions regarding cold nuclear modifications to ϒ production before a stronger connection between the deconfinement, color screening, and the observed ϒ suppression in Au+Au can be made.

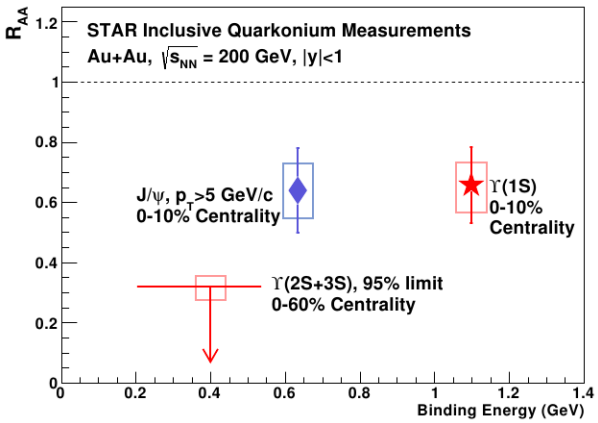


Figure 2.4: left, Nuclear modification factor of quarkonium states as a function of binding energy as measured by STAR. The horizontal line of the $\Upsilon(2S+3S)$ upper limit spans the range from the 3S to 2S binding energy; the arrow is placed at the weighted average of the binding energies.

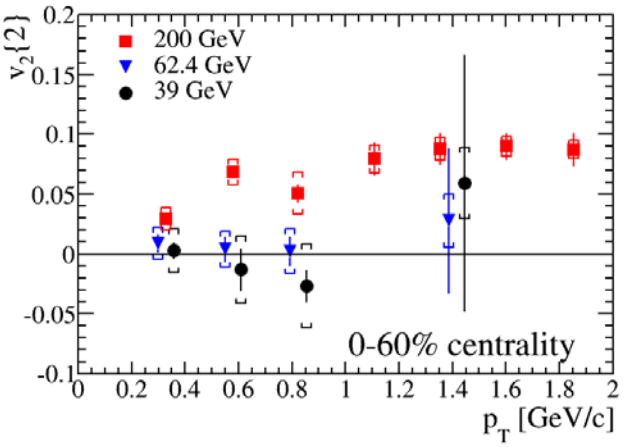


Figure 2.4: Right, Non-photonic electron $v_2$ in Au+Au collisions at $\sqrt{s_{NN}}$ = 39, 62.4, and 200 GeV.

The J/ψ suppression increases as $p_T$ decreases, probably due to the interplay of formation time, color screening, sequential suppression, and parton distribution functions in heavy nuclei. The first STAR J/ψ polarization measurements[27] in p+p collisions were made to further probe quarkonia production. The increase in longitudinal polarization with increasing $p_T$ is consistent with NLO calculations color singlet model but not with calculations including a color octet production mechanism. In Au+Au events evidence that J/ψ are not formed from the coalescence of thermalized flowing charm quarks, but rather earlier in the collision was revealed when the azimuthal anisotropy of J/ψ at large $p_T$ was shown to be consistent with zero[4].

In U+U collisions 20% higher energy densities can be achieved relative to Au+Au collisions (via orientation-averaged configurations). It allows us to study the dependence of quarkonium and open charm suppression as a function of initial energy density. $D^0$ $R_{AA}$ in Au+Au and preliminary U+U collisions show a similar behavior; namely a suppression at both small and large $p_T$ and an enhancement at intermediate $p_T$.[6] Quarkonia ($J/\psi$ and $\Upsilon(1S+2S+3S)$) production is also suppressed in U+U, and $R_{AA}$ as a function of $p_T$ and centrality follows trends observed in the Au+Au collisions[7].

An enhancement in the ρ-like region of the Au+Au di-electron mass spectrum cannot be explained by the presence of a vacuum ρ[28]. However, if one includes a broadened ρ spectral function, due to interactions with the hadronic medium, the calculations become consistent with the data. A significant excess in this low invariant mass range is observed over a broad range of a beam energies, as seen in Figure . Recently we reported a complimentary measurement of the direct

[6] Z. Ye QM2014
[7] W. Zha QM2014

virtual photon production derived from the di-electron continuum in the low invariant mass region[8]. An enhancement compared to PHENIX p+p baseline is observed for 1-5 GeV/c. Models, which includes contributions from the QGP, hadron gas, primordial and ρ production contributions[29] are consistent with measured invariant yield in that $p_T$ range.

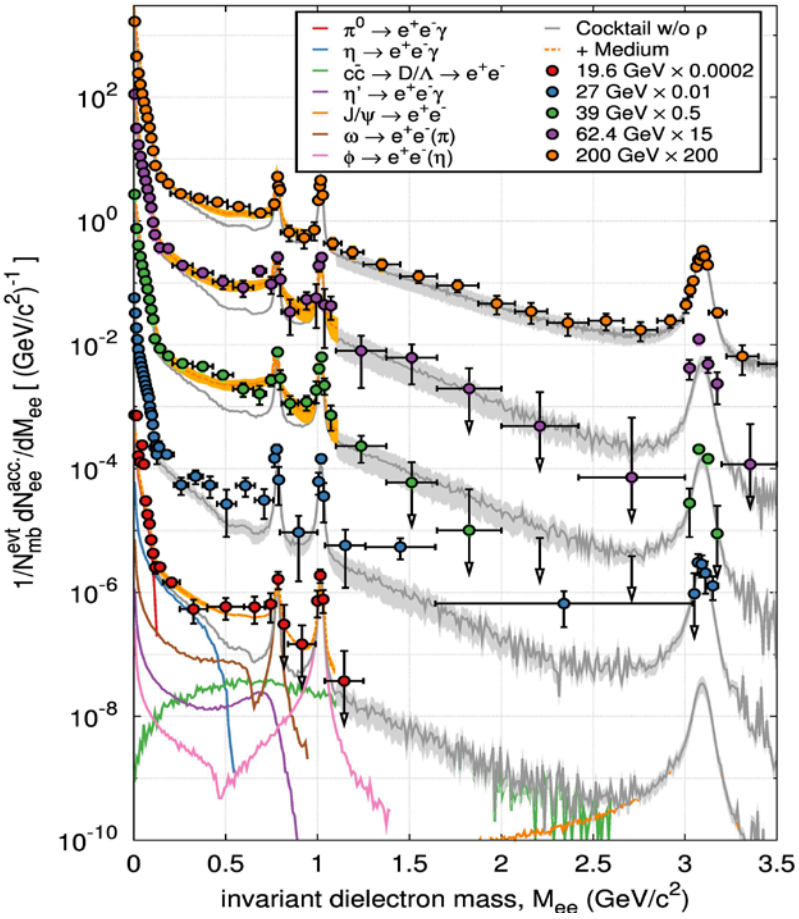


Figure 2.5: STAR Preliminary results of Background-subtracted dielectron invariant-mass distributions from Au+Au collisions at $\sqrt{s_{NN}}$ = 19.6, 39, 62.4, and 200 GeV. The (colored) dotted lines show the hadron cocktails (excluding contributions from ρ mesons). The (color) shaded areas indicate systematic uncertainties.

In the mass range 1.1<$M_{ee}$<2.9 GeV/$c^2$ the measured $v_2$ is consistent with that expected from the $c\bar{c}$ contributions. However, in the 0.14-0.3 GeV/$c^2$ range the extracted elliptic flow suggests that that from thermal radiation sources is smaller than from the low mass mesons[30].

A back-to-back double ridge was observed in p+Pb[31,32] and d+Au collisions[33] when di-hadron correlations in peripheral collisions were subtracted from those in the central events. STAR investigated the di-hadron correlations in d+Au and found that there is a significant difference between jet correlations in central and peripheral collisions, which has to be carefully taken into account when a "double ridge" is studied[9]. The difference could arise from a centrality selection, which biases the sampled jet populations, or a modification of jet correlations (for

[8] C. Yang QM2014
[9] Li Yi, QM2014

instance due to modification of the fragmentation functions).

## 2.2 Polarized Proton+Proton Physics

### 2.2.1 The Proton Helicity Structure

The STAR spin physics program seeks to advance our understanding of the spin and flavor structure of the proton in terms of its constituent quarks and gluons, exploiting the unique capability of RHIC to provide access to high-energy polarized p+p collisions. Using longitudinally polarized beams, one can probe the helicity preferences of the gluons and (flavor-separated) quarks and antiquarks, to gain insight in the contribution of each to the total spin of the proton. With spins transverse to the proton momentum direction, p+p collisions exhibit kinematic and dynamical effects that are directly sensitive to quark transversity and partonic motion within the proton. This program is complemented by studies of polarized p+p elastic scattering and central exclusive production, in which a far-forward proton is detected intact.
RHIC has completed very successful polarized p+p runs at $\sqrt{s}$ = 200 GeV, $\sqrt{s}$ = 500 GeV, and $\sqrt{s}$ = 510 GeV. The STAR recorded luminosity and the average beam polarization as measured by the H-jet polarimeter are summarized in Table 2-1 for runs since 2009.

| Year | $\sqrt{s}$ (GeV) | Recorded Luminosity for Transverse p+p | Recorded Luminosity for Longitudinal p+p | <P> |
|---|---|---|---|---|
| 2009 | 200<br>500 | | 25 $pb^{-1}$<br>10 $pb^{-1}$ | 55<br>39 |
| 2011 | 500 | 25 $pb^{-1}$ | 12 $pb^{-1}$ | 53/54 |
| 2012 | 200<br>510 | 22 $pb^{-1}$ | <br>82 $pb^{-1}$ | 61/58<br>50/53 |
| 2013 | 510 | | 300 $pb^{-1}$ | 50/53 |

Table 2-1: The STAR recorded luminosity and the average beam polarization as measured by the H-jet polarimeter.

These data sets formed the basis for papers and new preliminary results, which are highlighted in the following. Since the last PAC the STAR spin-working group published one paper in PRD [34] and submitted two to PRL [35,36].The latter two present milestones in our understanding of the proton helicity structure and address how the spin of the proton is distributed among it constituents.
The inaugural run at $\sqrt{s}$ = 500 GeV in 2009 yielded the first but still statistics challenged measurement of the longitudinal single-spin asymmetries $A_L$ in $W^+$ and $W^-$ production and their subsequent calculable leptonic decay [37]. The rapid analysis of the 2011 ($\sqrt{s}$ = 500 GeV ) and the high statistics 2012 ($\sqrt{s}$ = 510 GeV) longitudinal polarized p+p data sets yielded the first results for $W^{\pm}$ providing impact on the light sea (anti-)quark polarizations. Figure 2.6 shows the final result of the longitudinal single-spin asymmetry, $A_L$, for $W^{\pm}$ production as a function of lepton pseudorapidity $\eta_e$, in comparison to theory predictions. The STAR preliminary $A_L$ results based on the 2012 data set alone, have been included into the pQCD fits by the DSSV group [38]. A clear improvement on the determination of the polarization of the light sea quarks was observed. For $\Delta\bar{u}$ a shift away from the current best mean value was observed, reflecting that the new STAR data lie above the central curve based on DSSV fits to semi-inclusive and inclusive data. Already, with only the preliminary 2012 STAR data, the new global analysis showed a preference for $\Delta\bar{u} > \Delta\bar{d}$ in the range $x > 0.05$. New pQCD fits based on the published STAR data are already underway by the DSSV and NNPDF groups.

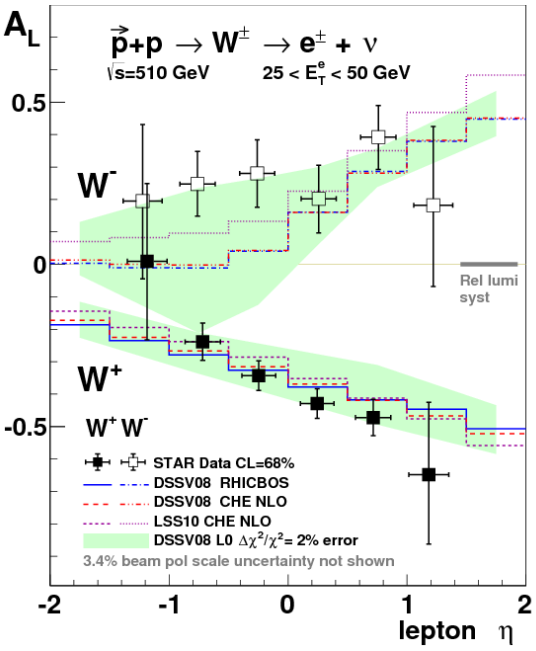


Figure 2.6: Longitudinal single-spin asymmetry, $A_L$, for $W^{\pm}$ production as a function of lepton pseudorapidity $\eta_e$, in comparison to theory predictions.

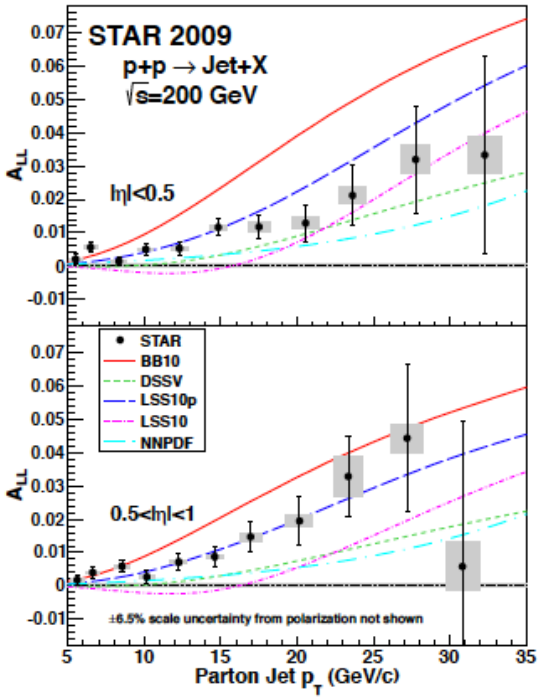


Figure 2.7: Midrapidity ($|\eta| < 0.5$, upper panel) and forward rapidity ($0.5 < |\eta| < 1$, lower panel) inclusive jet $A_{LL}$ vs. parton jet $p_T$, compared to predictions from several NLO global analyses. The error bars are statistical. The gray boxes show the size of the systematic uncertainties.

In 2009, with improved luminosity and polarization, as well as upgraded triggering and data acquisition systems at STAR, the uncertainties on the published inclusive jet $A_{LL}$ measurements at $\sqrt{s}$ = 200 GeV could be considerably improved. Figure 2.7 shows the final inclusive jet $A_{LL}$ vs. parton jet $p_T$ at midrapidity ($|\eta| < 0.5$, upper panel) and forward rapidity ($0.5 < |\eta| < 1$, lower panel) from 2009 data, compared to predictions from several NLO global analyses. The error bars are statistical. The gray boxes show the size of the systematic uncertainties. The impact of the new inclusive jet data on the polarized gluon distribution and its integral was studied using the reweighting method developed by the NNPDF group [ 39 ], which allows to include new experimental data into an existing PDF set without the need to repeat the entire fitting process. The obtained results are shown in Figure 2.8. The integral of $\Delta g(x,Q^2=10\ \mathrm{GeV}^2)$ over the range $0.05 < x < 0.5$ is $0.06 \pm 0.18$ for the original NNPDF fit and $0.21 \pm 0.10$ when the fit is reweighted using the STAR jet data. The DSSV group has performed a new global analysis [40] including the STAR jet $A_{LL}$ results. They find that the integral of $\Delta g(x,Q^2=10\ \mathrm{GeV}^2)$ over the range $x > 0.05$ is $\mathbf{0.20^{+0.06}_{-0.07}}$ at 90% C.L., consistent with the value STAR finds by reweighting the NNPDF fit. The jet data thus imply a polarization of gluons in the proton at intermediate momentum scales.

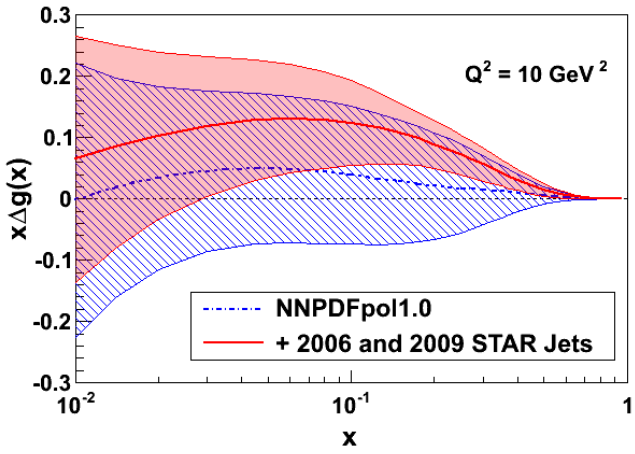


Figure 2.8: Gluon polarizations from NNPDF (blue dot-dashed curve, 135° hatched uncertainty band), and from modified versions of NNPDF that we obtain when including the 2006+2009 STAR inclusive jet $A_{LL}$ results through reweighting (red solid curve and uncertainty band).

### 2.2.2 The 2+1 Dimensional Structure of the Proton

A natural next step in the investigation of nucleon structure is an expansion of our current picture of the nucleon by imaging the proton in both momentum and impact parameter space. At the same time we need to further our understanding of color interactions and how they manifest in different processes. In the new theoretical framework of transverse momentum dependent parton distributions (TMDs) we can obtain an image in the transverse as well as longitudinal momentum space (2+1 dimensions). This has attracted renewed interest, both experimentally and theoretically, in transverse single spin asymmetries (SSA) in hadronic processes at high energies, which have a more than 30 years history. First measurements at RHIC have extended the observations from the fixed-target energy range to the collider regime up to the highest center-of-mass energies to date at RHIC. Figure 2.9 summarizes the measured asymmetries from different experiments as functions of Feynman-$x$ ($x_F \sim x_1$-$x_2$).

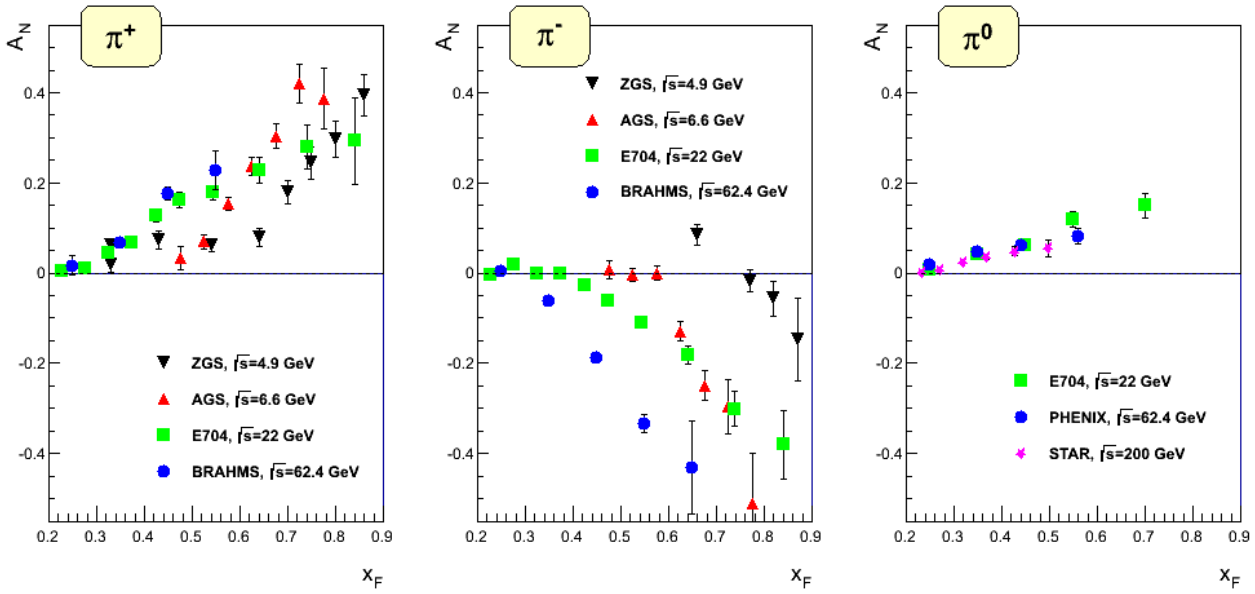


Figure 2.9: Transverse single spin asymmetry measurements for charged and neutral pions at different center-of-mass energies as function of Feynman-$x$.

The surprisingly large asymmetries seen are nearly independent of $\sqrt{s}$ over a very broad range. To understand the observed significant SSAs one has to go beyond the conventional collinear parton picture in the hard processes. Two theoretical formalisms have been proposed to generate sizable SSAs in the QCD framework: transverse momentum dependent parton distributions and fragmentation functions, which provide the full transverse momentum information, and the collinear quark-gluon-quark correlation, which provides information about the average transverse momentum. STAR has made several important contributions to this program, primarily through study of forward neutral pion production in p+p collisions (see, for example, ref. [34,41]). This effort has been extended to include the first measurements at $\sqrt{s}$ = 200 GeV of the transverse spin asymmetry $A_N$ for the $\eta$ meson [42].The Run-11 data taken with transverse polarization at $\sqrt{s}$ = 500 GeV have revealed several surprising results. Figure 2.10 shows the transverse single spin asymmetry $A_N$ for electromagnetic jets detected in the forward meson spectrometer (FMS) at 2.5 < $\eta$ < 4.0 as function of the jet $p_T$ and the photon multiplicity in the jet in bins of the jet energy. It can be clearly seen that with increasing number of photons in the electromagnetic jet (increasing jettiness of the event) the asymmetry becomes smaller and smaller. Jets with isolated $\pi^0$ have the largest asymmetry consistent with the asymmetry in inclusive $\pi^0$ events, as seen from the right-most panel in Figure 2.10. For all jet energies and photon multiplicities in the jet the asymmetries are basically flat as function of jet $p_T$, a feature also already seen for inclusive $\pi^0$ asymmetries.

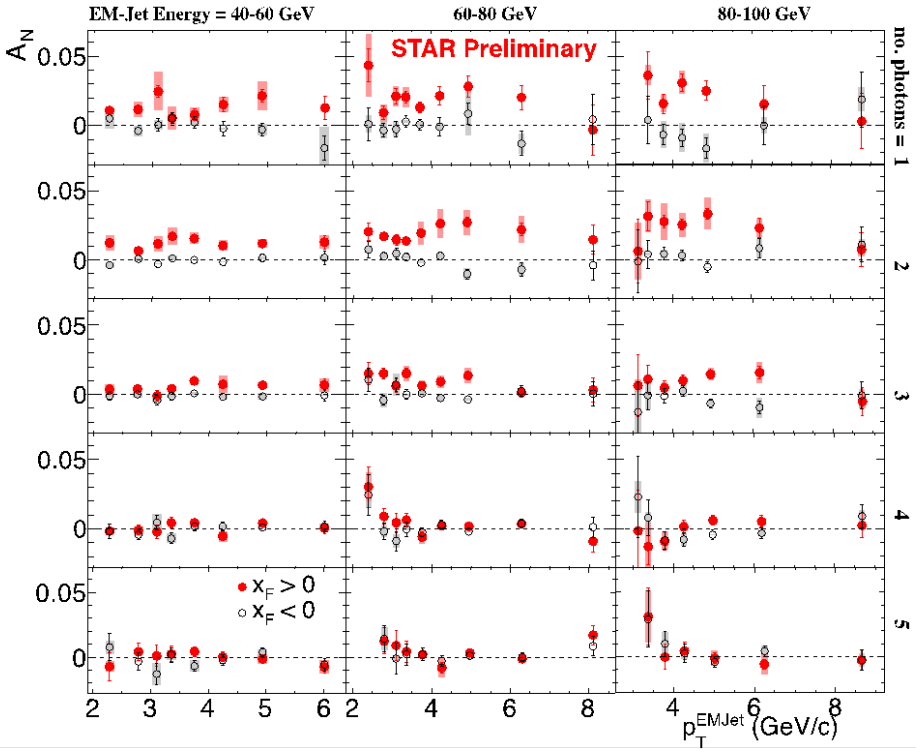


Figure 2.10: The transverse single spin asymmetry $A_N$ for electromagnetic jets detected in the forward meson spectrometer (2.5 < $\eta$ < 4.0) as function of the jet $p_T$ and the photon multiplicity in the jet in bins of the jet energy.

To further study these effects the transverse single spin asymmetry $A_N$ of these electromagnetic jets was measured if in addition a correlated away side jet in the rapidity range -1 < $\eta$ < 2 was required. Figure 2.11 shows clearly that for requiring an additional correlated away-side jet the asymmetry

for isolated forward $\pi^0$s becomes smaller[10]. All these observations raise serious questions how much of the large forward $\pi^0$ asymmetries is caused by 2→2 parton scattering processes.

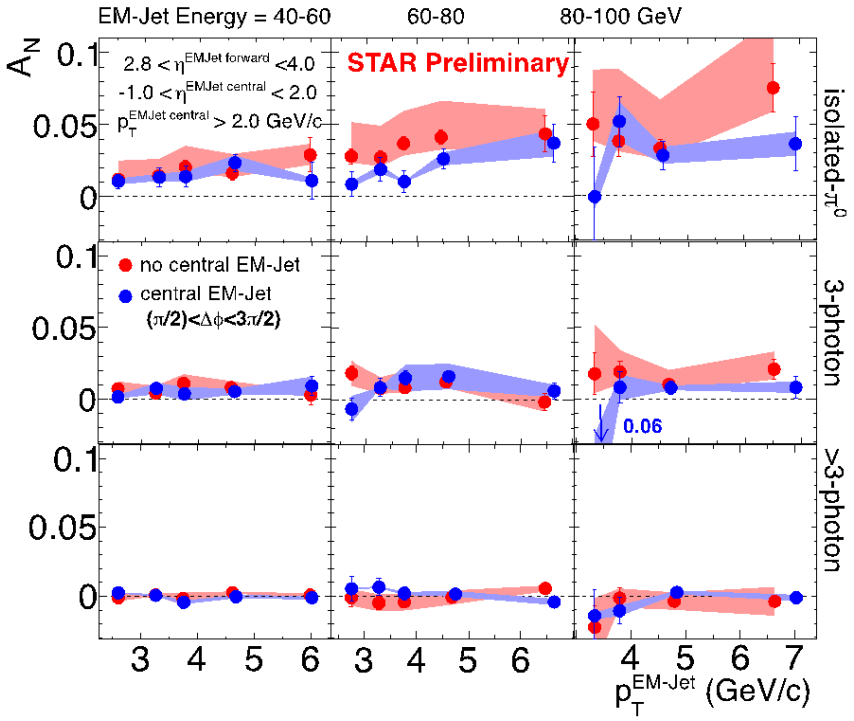


Figure 2.11: The transverse single spin asymmetry $A_N$ for electromagnetic jets detected in the forward meson spectrometer ($2.5 < \eta < 4.0$) as function of the jet $p_T$ and the photon multiplicity in the jet in bins of the jet energy (red points). The blue points represent the transverse single spin asymmetry $A_N$ if further a correlated away side jet in the rapidity range $-1 < \eta < 2$ was required. The blue and red bands represent the systematic uncertainties.

The Sivers function $f_{1T}^{\perp}$ is one of the transverse momentum dependent parton distribution functions of special interest. It describes the correlation of parton transverse momentum with the transverse spin of the nucleon. A non-vanishing $f_{1T}^{\perp}$ means that the parton distribution will be azimuthally asymmetric in the transverse momentum space relative to the nucleon spin direction. There is evidence of a quark Sivers effect in semi-inclusive DIS (SIDIS) measurements of the HERMES, COMPASS, and JLab Hall-A experiments [43]. An important aspect of the Sivers effect, which has emerged from theory lately, is its process dependence and the color gauge invariance. In SIDIS, the quark Sivers function is manifested in association with a final state effect from the exchange of (any number of) gluons between the struck quark and the remnants of the target nucleon. On the other hand, for the virtual photon production in the Drell-Yan process, the Sivers asymmetry appears as an initial state interaction effect. As a consequence, the quark Sivers functions are of opposite sign in these two processes and this non-universality is a fundamental prediction from the gauge invariance of QCD. The experimental test of this sign change is one of the key open questions in hadronic physics (NSAC performance measure HP13) and will provide a direct verification of QCD factorization.

While the required luminosities and background suppressions for a meaningful measurement of asymmetries in Drell-Yan production are challenging, other channels can be exploited in *p+p* collisions, which are similarly sensitive to the predicted sign change. These include prompt photons,

[10] M. Mondal, DIS 2014

$W^{\pm}$ and Z bosons, and inclusive jets. These are either already accessible with the existing STAR detector or need only modest upgrades and require continued polarized beam operations.
The transverse polarized data taking in Run-11 at $\sqrt{s}$ = 500 GeV allowed to reconstruct the transverse single spin asymmetries for $A_N$ for $W^{\pm}$ and $Z^0$ Bosons. Especially the measurement of the $A_N$ for $W^{\pm}$ Bosons is challenging as, contrary to the longitudinal case, it is required to completely reconstruct the W-Bosons as the kinematic dependences of $A_N$ cannot easily be resolved through the high $p_T$ decay lepton, for details see [44,45].Due to the large STAR acceptance it was possible to reconstruct the W-Boson kinematics from the recoil jet, a technique used at D0, CDF and the LHC experiments to reconstruct the W-Boson kinematics. Figure 2.12 shows the transverse single spin asymmetries for $A_N$ for $W^{\pm}$ as function of the W-Boson rapidity *y*. The asymmetries have also been reconstructed as function of the $p_T$ of the W-boson. For the $Z^0$-Boson the asymmetry could only be reconstructed in one bin in *y* due to the limited statistics (25 $pb^{-1}$) of the Run-11 transverse polarized data set. Details for this analysis can be found in [46].The Run-11 transverse analysis represents an important proof of principle, as the Run-9 $W^{\pm}$ $A_L$ measurement was in the longitudinal case. The proposed high statistics run for Run-16 will allow to access the sign change and to constrain the presently unknown sea quark Sivers functions.

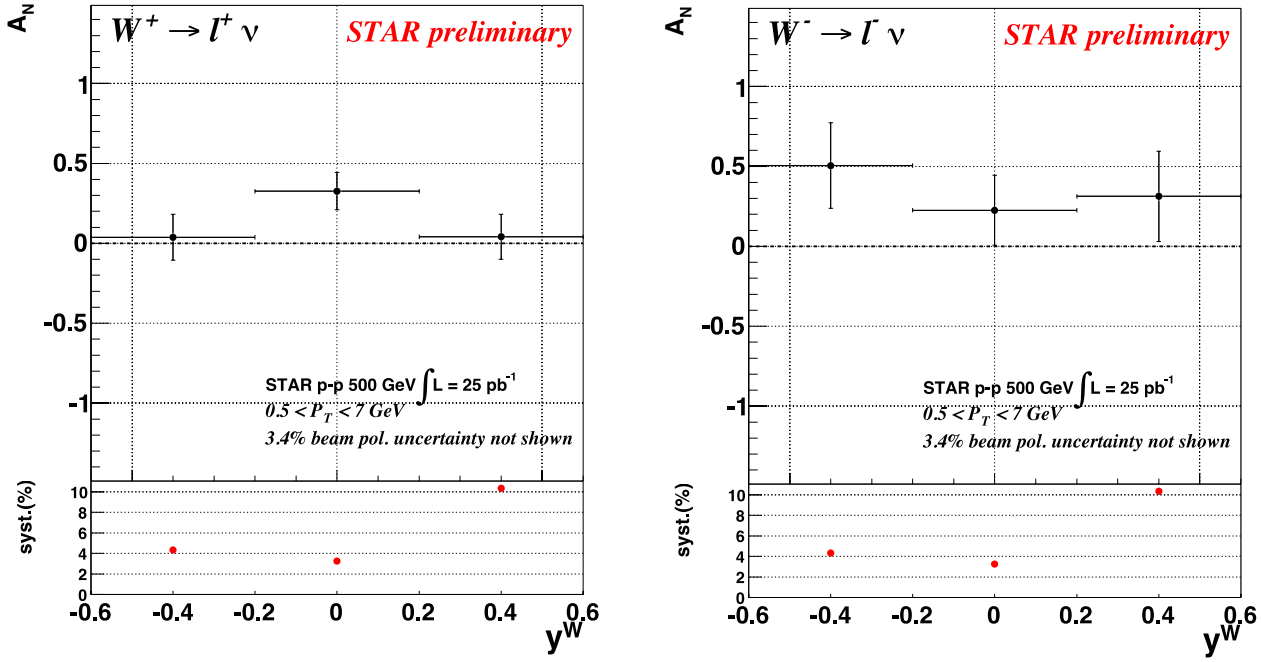


Figure 2.12: The transverse single spin asymmetries for $A_N$ for $W^{+/-}$ as function of the W-Boson rapidity *y*.

## 2.3 Cold Nuclear Matter

Prompted by the discovery of a long-range correlation in pseudo-rapidity ("ridge") in high-multiplicity *p*+*p* and *p*+*A* collisions at the LHC, STAR and PHENIX have been investigating the possibility of such a correlation in *d*+Au collisions at RHIC. PHENIX has reported an excess correlation when subtracting the per-trigger correlated yields in peripheral d+Au collisions from those measured in central *d*+Au collisions. Under the assumption that jet-correlated yields have no dependence on the event centrality, such an excess could be interpreted as a "ridge". The STAR detector has a large pseudo-rapidity coverage ideal for in-depth studies of the features of the correlations in *d*+Au collisions. In particular, STAR has studied the following aspects: 1) possible biases in the selection of centrality through multiplicity cuts resulting in larger jet-correlated yields in central vs. peripheral collisions; 2) the relative pseudo-rapidity ($\Delta\eta$) dependence of any excess

correlated yields over a large range of ($\Delta\eta$); 3) how the correlation depends on the trigger and associated particles being like-sign vs. unlike-sign pairs, and 4) the dependence of an excess in the correlated yields on the charge of the associated particle. We find that, after carefully subtracting any remaining biases due to the event centrality selection, there is indeed a significant dependence on the associated-particle charge. As seen in the figure, the near-side ($\Delta\Phi$~0) excess in the correlation at large $\Delta\eta$ is only prominent when the associated particle is positive, hinting toward a possible effect from the deuteron projectile in *d*+Au collisions.

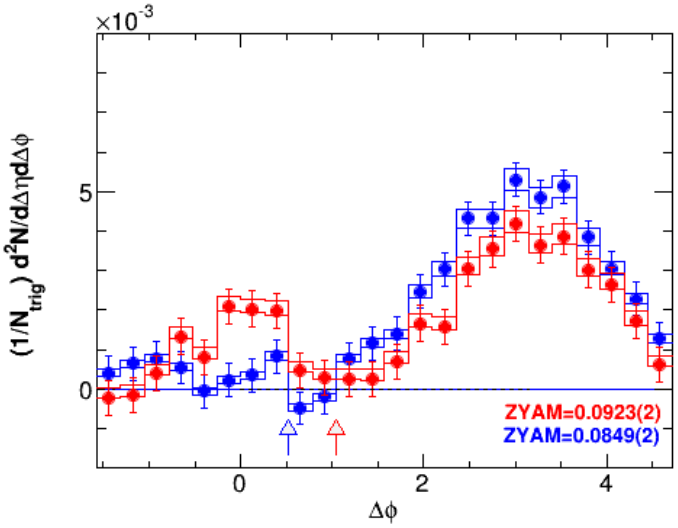


Figure 2.12: STAR Preliminary results on per-trigger correlated yields of particles for 0-20% central d+Au events, for -4.5<Δη<-2, for positive associated particles (red) and negative associated particles (black). The trigger particle is from the TPC and the associated particle is from the FTPC in the Au-beam direction. The centrality is determined by the Zero-Degree Calorimeter to minimize any bias from the jets in the events.

# 3. Run-14 Performance Report

## 3.1 Au+Au 15 GeV

Run 14 started with three-weeks of Au+Au collisions at $\sqrt{s_{NN}}$ = 14.5 GeV. This energy was selected to help fill in a large gap in chemical potential ($\mu_B$) in the Beam Energy Scan (BES) data sets. In 2010 and 2011, RHIC surveyed a series of low energies; Au+Au collisions were studied at 7.7, 11.5, 19.6, 27.0, 39.0, and 62.4 GeV. The goals of this energy scan were to study the evolution of various QGP signatures, to search for evidence of the postulated first order phase transition between the QGP and a hot hadronic gas, and to search for evidence of the critical end point of the phase transition boundary. Several signatures (NCQ scaling of elliptic flow, high $p_T$ suppression seen in $R_{CP}$ studies, Chiral magnetic effect correlations, and pion balance functions) were seen to smoothly evolve from no evidence for partonic behavior at 7.7 GeV to clear evidence at 200 GeV. Studies that are sensitive to compression were used to find the softest point which would be conclusive evidence for a first order phase transition. Although evidence of softening is seen in the average $m_t$-$m_0$ distributions and the average $E_T$, the most sensitive analysis appears to be the directed flow of net-protons. This analysis shows low (negative) values for the 11.5 and 19.6 GeV points, suggesting the minimum could lie somewhere between these two energies. The most challenging goal is the search for fluctuation signals indicating proximity to the critical point. The higher moments of the net-proton distributions exhibited an anomalously low point for the 19.6 GeV energy, however the magnitude of the error bars makes the result suggestive, but inconclusive. The possibility has been raised that the step size in $\mu_B$ of the beam energy scan was simply too large and we may have missed the critical point. The chemical potential for 11.5 GeV system is 316 MeV while that for the 19.6 GeV system is 206 MeV. The 14.5 GeV system, with a $\mu_B$ of 264 MeV helps to fill this gap. Results from this new BES energy will refine the evidence for localizing the softest point and will improve the coverage for finding the critical point.

The first collisions of Au+Au events at 14.5 GeV were detected on February 13th. After four days of collider development, data taking started on February 17th. By March 11th the online quality assurance available at the time suggested that STAR had met its data acquisition goals, and the collider shifted to operations at full energy (200 GeV). Preliminary analysis of the quality of these data and of the number of good events has been completed, and we conclude that the data set is consistent with the other BES energies. The table below shows the size of the sets for the BES energies.

| Collison Energy | 7.7 GeV | 11.5 GeV | **14.5 GeV** | 19.6 GeV | 27.0 GeV | 39.0 GeV |
|---|---|---|---|---|---|---|
| Good Events with | 4.3 M | 11.7 M | **24 M** | 35.8 M | 70.4 M | 130 M |

Table 3.1 1 A summary of the number of good Au+Au events with a vertex location near the center of the detector for various BES energies.

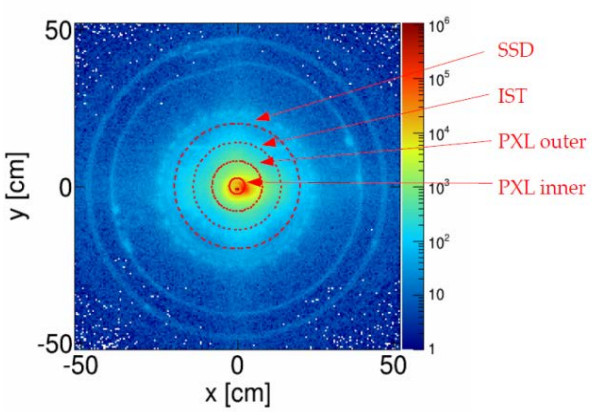


vertices shows the distribution of material inside the detector.

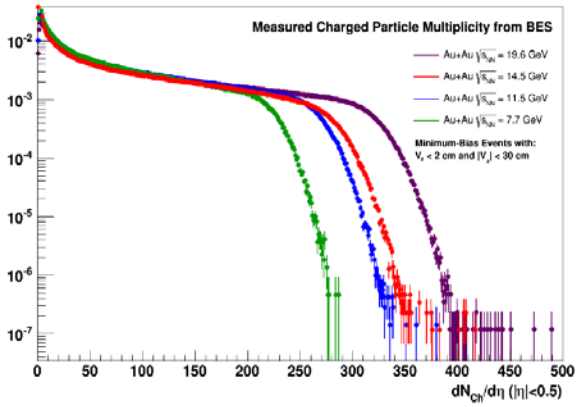


distribution for Au+Au events in the 14.5 GeV data (red) as compared to adjacent BES energies at 7.7 (green), 11.5 (blue), and 19.6 GeV (purple).

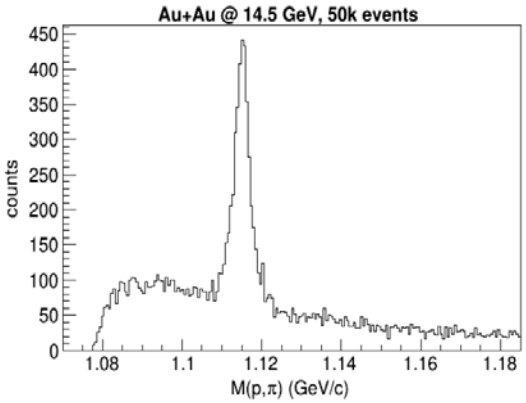


Figure 3.3 The proton-pion invariant mass spectrum showing reconstruction of the Lambda.

It should be noted that the detector configuration has changed since run 11, with the most significant change being the addition of the silicon detectors. A study of the location of vertices between multiple tracks shown in Fig. 3.1 shows the effect of this additional material. However, the total interaction length of the additional material is realtively small and this should have only minor effects of the qualitiy of the events. Figure 3.2 shows the multiplicity distribution for the 14.5 GeV data as compared to similar distributions for other BES data sets at 7.7, 11.5, and 19.6 GeV. One notes that the shape of the distribution is comparable to the other energies. However the maximum number of tracks seems to fall a little below the expected trend. This is due to the interactions in the inner silicon. This is due to the interactions in the inner silicon. This reduces the multiplicity by a few percent, which will not significantly effect the ablity to determine the event centrality, or have a significant effect on the physics analyses.

An important test of the quality of the reconstruction is the location and shape of the invariant mass peaks of unstable neutral hadrons. Figure 3.3 shows the invariant mass peak for the Lambda baryon. The mass peak position is coming in a little high. This is not unexpected as these preliminary data do not yet have the final calibrations. The width of the peak is consistent with the expected detector resolution and not the natural line width of the Lambda. These simple quality assurance results demonsrate that although the data are not fully calibrated, there are no performance issues with the detector during the 14.5 GeV about which we should be concerned.

Having verified that the data are of a high quality. We can then ask if there are sufficient statistics to preform the key physics analyses. The two most critical analysis are the study of the net-proton directed flow and the higher moments of the net-proton distributions. The key observable is the slope of the directed flow at mid-rapidity as a function of rapidity. Preliminary analysis shows negative slope for all three energies (11.5,14.5,19.6GeV). It is expected that as one approaches the critical point from the high energy side one will see a reduction in the kurtosis times squared variance ($\kappa\sigma^2$), while as one approaches from the lower energy side, one will see an increase in this observable. The magnitude of the disturbance from the trend is difficult to estimate as the final size of the system will have the effect of washing out any sharp features. The preliminary analysis of the

higher moments of the net-proton distributions shows suggestive features which could be consistent with the critical fluctuations. Analysis including all the datasets and with additional particle identification from TOF to extend the $p_T$ coverage are underway. These data are suggestive, but significantly improved statistics, which will only be available with major improvements to the collider, are needed.

## 3.2 Status of the Heavy Flavor Tracker (HFT)

The HFT detector system construction was completed by January 2014. The HFT consists of 4 layers of silicon detectors grouped into three subsystems with different technologies, guaranteeing increasing resolution when tracking from the TPC towards the vertex of the collision. The Silicon Strip Detector (SSD) is an existing detector in double-sided strip technology. It forms the outermost layer of the HFT. The Intermediate Silicon Tracker (IST), consisting of a layer of single-sided strip-pixel detectors, is located inside the SSD. Two layers of silicon pixel detector (PXL) are inside the IST. The pixel detectors have the resolution necessary for a precision measurement of the displaced vertex. With the HFT, MTD, the Time-of-Flight detector, the TPC, and the Barrel Electromagnetic Calorimeter STAR will study the physics of mid-rapidity charm and bottom production.

The IST detector was fully tested in July 2013, and installed on its support structures in August 2013. The SSD with the new ladders cards was mounted on the outer Support Cone (OSC). Initial testing took place in September and the IDS with IST and SSD was inserted into STAR in early October. The PXL first detector was completed with 8 sectors with Cu cables, and two with Al-cables on the inner ladders. All the outer ladders were made with Cu-Cables

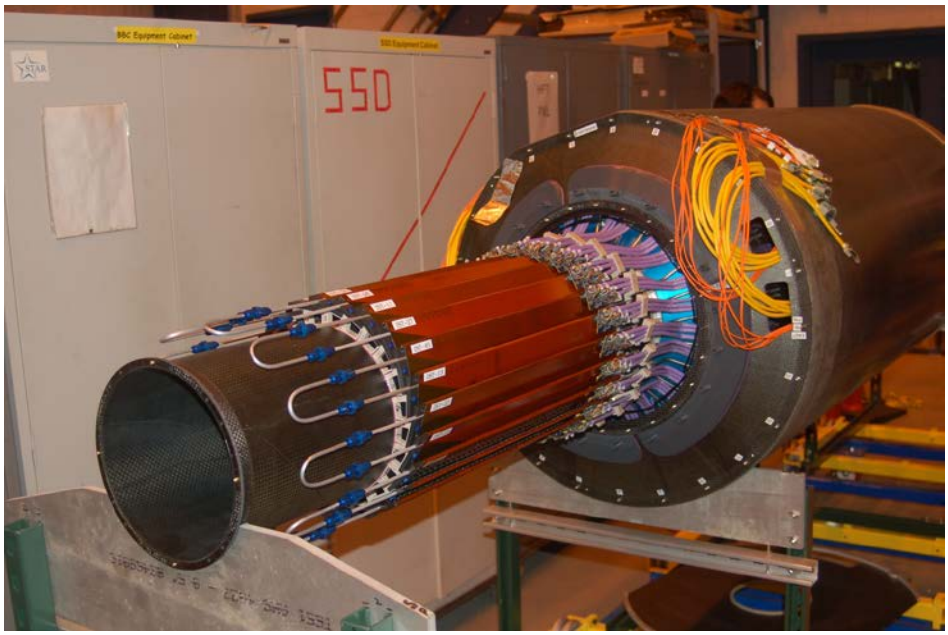

Figure 3.4 IST as mounted on the PXL support structures during assembly of IDS

Figure 3.5 SSD mounted on the support cylinders

The PXl sub-system was delivered to BNL in February, after having been fully tested at LBNL, tested again in the clean room and inserted into STAR ahead of the cosmic ray running at the end of February. At that time the detector was fully functional.

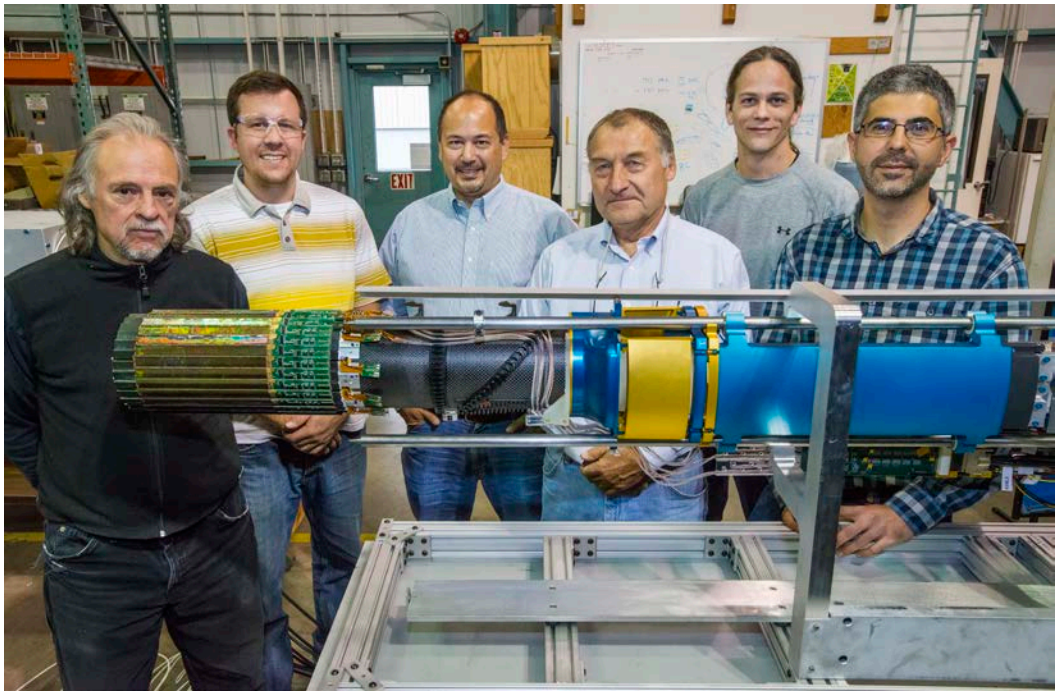


Figure 3.6 PXL one half at LBNL before being shipped to BNL.

Initial commissioning of IST and PXl was done during the cosmic ray run. In addition preliminary alignment of the two detector halves was performed, and the relative pointing resolution found to be within specifications. A number of issues were found with SSD, and commissioning of that detector has taken much longer time and is not (by end of April) included in regular running. It has been included at lower rate

(~600Hz) at end of May due to issues with baseline restoration at higher rates.

The beam conditions during the 15 GeV Au-Au run was so bad that it was decided to exclude PXL from any running conditions. In the early part of the 200 GeV running additional damage was found on the PXL inner layers, but as of late March operational procedures were put in place the has kept damage under control. At this time about 14% of the inner layers sensors are not operational.

By means of beam data the expected pointing resolution of the PXL has been achieved, and it's expected that significant data will be collected during the run-14 even with the non-optimal operational status. The root cause of the damage is not understood, but is under investigation. It is unlikely even when found that changes can be made to the production of the second detector and thus careful operational procedures have to be in place for operation in run-15 and run-16. During run-14, we have also continued to optimize our data-taking mode. Figure 3.11 shows the current status of total minbias events taken for HFT program. We have implemented slewing correction to the online vertex selection, which improved the vertex resolution by a factor of 2 for events selected within HFT fiducial acceptance. A high-level trigger (HLT) algorithm was also implemented to further tighten the vertex cut for events being saved to tape. We have also proposed to improve electronics for online vertex selection for run-16 by upgrading one of the components in the QT boards.

For run-15 the spare detector that is under final construction will be installed, and for run-16 the inner ladders of the first detectors will have been replaced. For both runs the detector will have Al-cable in the inner ladders resulting in increased significance for low-pt heavy quark measurements.

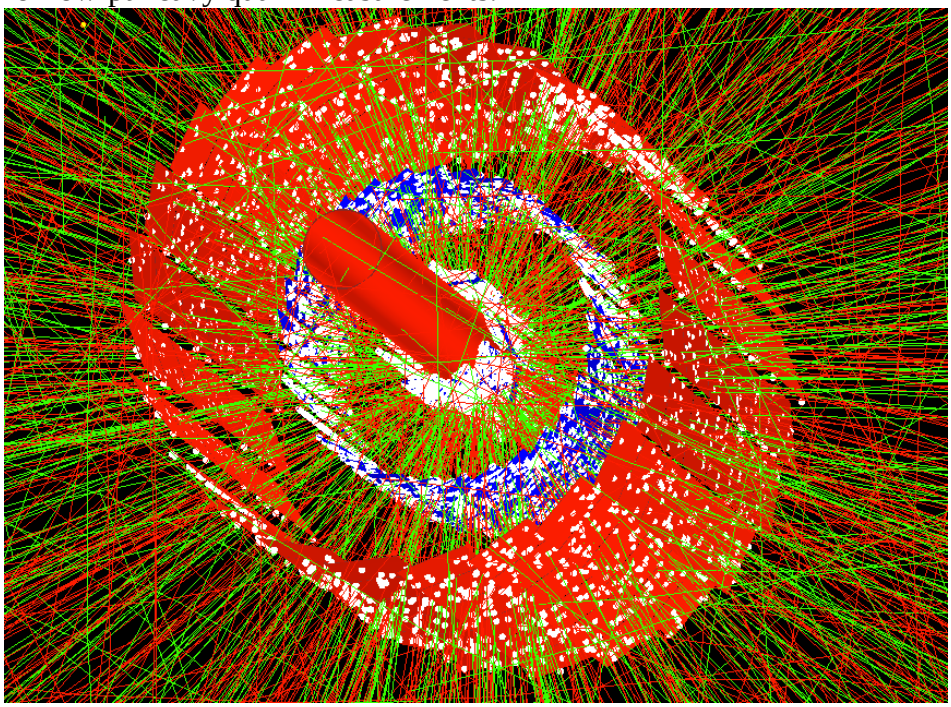

Figure 3.7, event display of Au+Au central event with tracks extrapolated from TPC to HFT.

The DCA resolution is very close to expected value based on using alignment from survey and zero-filed cosmic ray data taking.

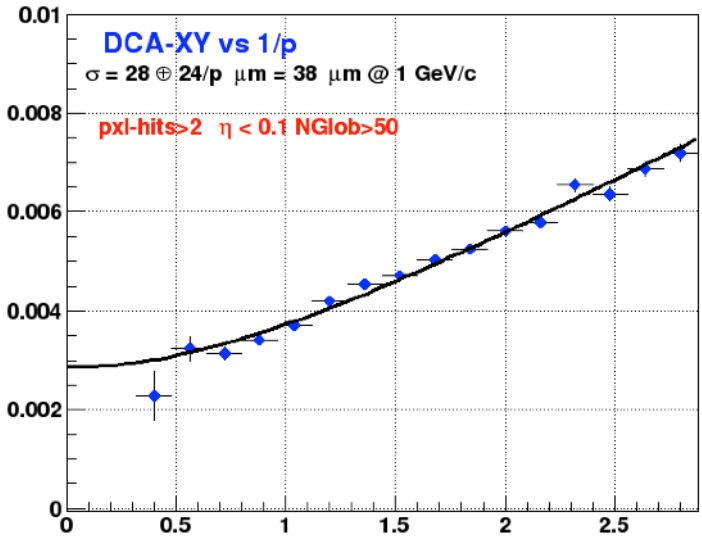


Figure 3.8 DCA resolution in r-phi for the HFT PXL system vs. 1/p

## 3.3 Muon Telescope Detector (MTD)

The goal of the MTD project is to measure J/ψ spectra from low to high $p_T$ and different ϒ states using di-muon channels, to perform a unique measurement of μ-e correlations from heavy-flavor decays, and to provide di-muon continuum measurements.

The full MTD system was installed and commissioned for Run 2014. Three MTD triggers including single-muon, dimuon, and μ-e triggers are running smoothly. The effective luminosity sampled by the dimuon trigger for Upsilon analysis will reach or exceed our Run 2014 goal in Au+Au collisions at 200 GeV. The details are summarized below.

**Installation of the full MTD system:**
The full system contains 122 trays. 117 trays were installed behind the 27 backlegs of the STAR magnet, corresponding to 96% of the full system before Run 2014 started. Among these 117 trays, 113 took data smoothly during 15 GeV Au+Au run. Four have gas leaks, 3 of which at backleg 19 were taken out of STAR and one of which at backleg 15 is not accessible and thus remains at STAR but not being used. During a bi-weekly maintenance day Apr. 2$^{nd}$, 2014, 8 new trays were installed. Five and three were installed to backlegs 8 and 19, respectively. This completed the full installation of the MTD system. The one inaccessible with gas leak will be replaced during summer shutdown.

**Evaluation of MTD trigger capabilities using Run 2013 data:**
With the full MTD system installed, it is important that our di-muon trigger capabilities can be maximally utilized. This requires a narrow trigger timing window cut on the MTD hits at the level-zero trigger level. Therefore a thorough study from the previous run (Run 2013) is necessary for us to obtain the important information.

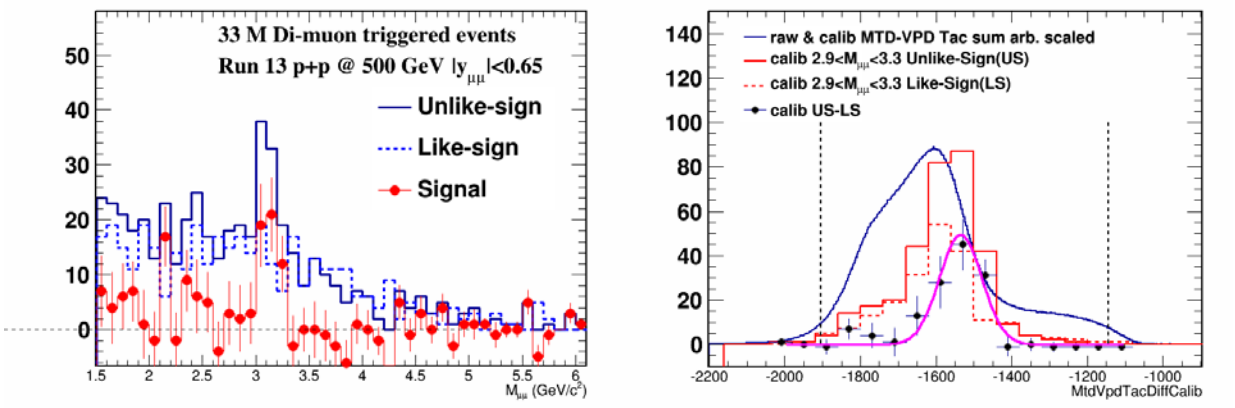


Figure 3.9 left: J/Psi invariant mass from dimuon channel. Right: muon timing distribution from J/Psi.

Among 75 MTD trays installed at STAR for Run 13, 74 took data smoothly. We implemented hit position correction online on the arrival time and took the single-muon, dimuon and μ-e triggers successfully. From 33 million produced dimuon offline data, we observed J/ψ signals. We present two plots from these data samples. Figure 3.9 left panel shows about 50 J/ψ counts are observed. The second plot shows after slewing correction, the timing difference between MTD and VPD from J/ψ is slightly shifted from the major background peak, which would give us additional background rejection online if we tightened the trigger timing window cut. The study also indicates that the resolution of the timing difference between MTD and VPD is 500 ps after the position and slewing correction. We note that the hits which arrive earlier at MTD have a larger value in the distribution of the timing difference between MTD and VPD.

**Implenmentation of the trigger algorithms online for 200 GeV Au+Au collisions in Run 2014**
In Run 2014, we had a three-week 15 GeV Au+Au run. A first physics store was delivered on Feb 16$^{th}$ for 15 GeV Au+Au collisions. On Feb. 18$^{th}$, we successfully implemented the hit position correction online and MTD triggers were in production mode since Feb. 21$^{st}$, 2014. On Feb. 28$^{th}$, 2014, we implemented slewing correction online for 15 GeV Au+Au collisions. These activities were to make sure that we smoothly commission mtd triggers in 200 GeV Au+Au collisions.

The 15 GeV run ended on Mar. 11$^{th}$, 2014. The first physics store for 200 GeV Au+Au collisions was delivered on Mar. 14$^{th}$, 2014. On Mar. 17$^{th}$, we successfully implemented the hit position correction and slewing correction online, determined the trigger window cut on the timing difference between MTD and VPD, and promoted the single-muon, dimuon, and μ-e triggers into production mode.

From the fastoffline data production, we observed that mtd hits can be matched with the tracks reconstructed in the Time Project Chamber (TPC). For each strip of the MRPC detector, we readout both ends. The timing difference between the two ends gives the measured position information along the beam line (z) direction. From the TPC tracks, we can obtain the extrapolated z position at the MTD. The distribution of the position difference (Δz) between the measured and the extrapolated is shown in the plot below. By selecting tracks with normalized ionization energy loss $0<n\sigma_{\pi}<3$ and $p_T$ larger than 2 GeV/c, we observe a clear narrow peak representing muon contribution, which sits on top of a broad distribution representing hadron contribution. Tightening the Δz cut helps to reject hadron background significantly.

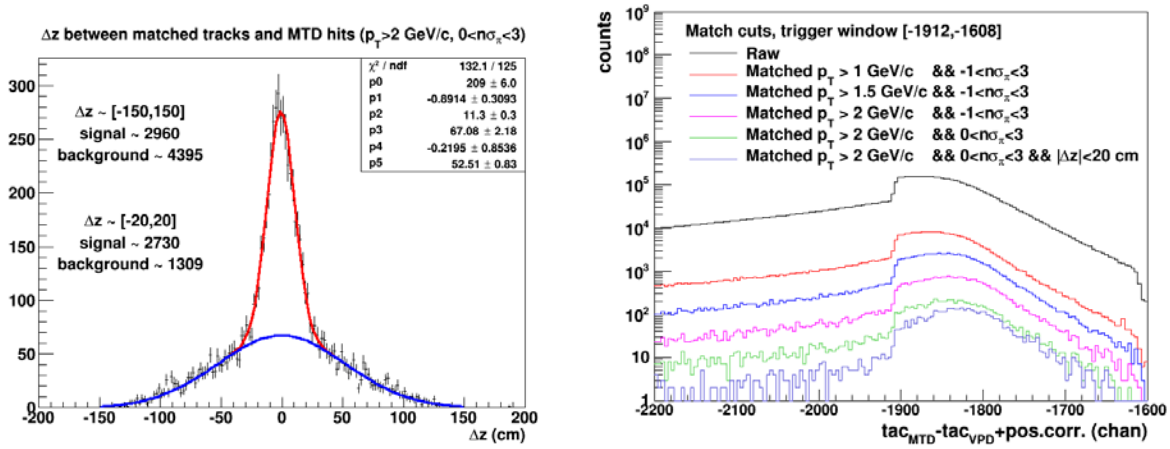


Figure 3.10 Left: MTD resolution from timing difference and TPC track projection. Right: timing difference from match tracks in MTD.

We obtain the timing difference between MTD and VPD for matched tracks, as shown in Figure 3.10 right.

Compared to the distribution of the raw hits, the peak position of the distribution for matched tracks at higher $p_T$ has a clear shift towards a larger value especially when we tighten the $\Delta z$ cut, which indicates that primary muons tend to arrive earlier compared to background hits.

From the above distributions, we estimate the efficiency of different trigger timing window cuts for matched tracks in different $p_T$ ranges. The results are listed in the table below:

| Tracks | Case A: [-1912,-1600] | Case B: [-1888,-1600] | Case C: [-1880,-1600] | Case D: [-1864,-1600] |
|---|---|---|---|---|
| pT>1 GeV/c, \|Δz\|<20 cm | 83.4% | 70.4% | 65.2% | 54.1% |
| pT>1.5 GeV/c, \|Δz\|<20 cm | 93.5% | 84.6% | 80.4% | 70.2% |
| pT>2 GeV/c, \|Δz\|<20 cm | 95.7% | 88.7% | 85.1% | 75.9% |

The cuts shown in Cases A nad B are selected to be the online trigger timing window cuts so that we can sample full luminosity for dimuon trigger and keep the Upsilon effciency high, 92% and 79% for Cases A and B, respectively. Taking into the trigger time window cut efficiency into account, we are on good track to sample 10 $nb^{-1}$ 200 GeV Au+Au collisions in Run 2014. The plot in Figure 3.11 shows the accumulated effective luminosity (shown by the black curve) sampled by dimoun trigger for Upsilon versus time. By the end of the run, we would expect to exceed our Run 2014 goal for Upsilon measurement, as indicated by the blue curve compared to the red one.

Part of the dimuon triggered events requires Heavy Flavor Tracker (HFT) detector readout. This is to study B→J/ψX→dimuonX using displaced vertex. The HFT contains two pixel layers, the Inner Silicon Tracker (IST) and the Silicon Strip Detector (SSD). Due to the possible band-width limitation issue of the IST, these dimuon triggered data samples require a cut of vertex-z value within 5 cm online.

In addition, enough data samples for single-muon and μ-e triggers are being taken for 200 GeV Au+Au collisions.

**Actual or anticipated problems**

The MTD is taking data smoothly in Run 2014. We are on good track to sample 10 $nb^{-1}$ luminosities in 200 GeV Au+Au collisions for the dimuon program. The only concern is related to disk space and data production time for these triggered data. The MTD group is working with STAR software group and STAR management to address this possible issue. In addition, the MTD group is proposing to add SF6 gas into the gas mixture of the MTD system, which will reduce the MTD noise rate and suppress the steamer possibility. This might reduce our dimuon trigger rate and thus reduce the needed disk space for these data sets.

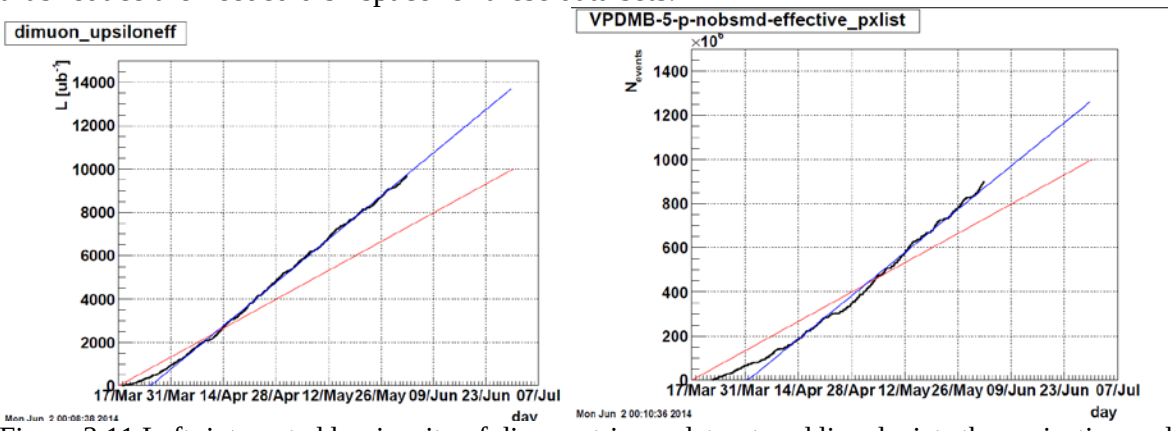


Figure 3.11 Left: integrated luminosity of dimuon trigger dataset, red line depicts the projection and target goal. Blue line is an extrapolation from the existing data taken. Right: Total minbias events with vertex (|Z|<5cm) selection for HFT program.

# 4. Run-15 Beam Use Request on p+p and p+A collisions

The proposed run15 programs with p+p and p+Au collisions at √s=200GeV provide crucial baseline measurements of charmed mesons and quarkonia. The 200GeV p+p beam request in run-15 is particularly driven by the precision for the $D^0$ $R_{AA}$ measurements. We will make use of both untriggered data (minimum bias triggers) for precision $D^0$ spectrum measurement at low $p_T$ and triggered data to extend the $p_T$ reach up to ~ 10GeV/c. The spectra will be used to provide baseline for nuclear modification factor and to study the cold nuclear effect in p+Au collisions.

We request 12 weeks of polarized p+p operation at $\sqrt{s}$ = 200 GeV in Run-15. The data would be split between longitudinally and transversely polarized data taking at STAR. As the polarization directions at IR-6 and IR-8 are completely independent from each other there is no interference between PHENIX and STAR choosing different polarization directions. Based on the latest guidance from CAD we assume a delivered integrated luminosity of 45 $pb^{-1}$ for the first 5 weeks and 15 $pb^{-1}$/week for the later weeks, for a total delivered integrated luminosity of ~150 $pb^{-1}$ with an average polarization of 60%. With an average data taking efficiency of 0.7 this would result in an integrated recorded luminosity of ~100 $pb^{-1}$. The running time would be split equally between transverse and longitudinal running. Such a data set would significantly advance the STAR spin physics effort; in particular, our analyses would focus on:

- Increased precision in measurements of the double-spin asymmetry $A_{LL}$ in inclusive jet and coincident di-jet production; the impact of such measurements is discussed in section 4.1
- Increased statistics in transversely polarized data together with the qualitatively new measurement capability afforded by equipment installed for Run-15 in the form of the Roman Pot Phase-II* and the FMS preshower. This will allow us to address the underlying physics causing the large transverse single spin asymmetries $A_N$ at forward rapidities by measuring less inclusive observables, including IFF, jets and direct photons as discussed in section 4.2

STAR assumes for 2015 a run with 22 cryo-weeks and proposes 5 weeks of transversely polarized p+A collisions, 6 weeks of longitudinally polarized p+p collisions, and 6 weeks of transversely polarized p+p collisions. The following smaller detector upgrades need to be completed for the proposed program:

1. the Roman pot system of pp2pp is moved to a new location in the DX-D0 region (for details see section 6.1)
2. a pre-shower detector is installed in front of the STAR FMS (for details see section 6.2)

## 4.1 Baseline reference data and Cold nuclear effect on open heavy flavor and heavy quarkonia production:

The 200GeV p+p beam request is to set the baseline reference for heavy ion measurements, particularly driven by the precision for the $D^0$ $R_{AA}$ measurements. We will make use of both untriggered data (minimum bias triggers) for precision $D^0$ spectrum measurement at low $p_T$ and triggered data to extend the $p_T$ reach up to ~ 10GeV/c. Therefore we request 500M p+p minimum bias events with $|V_z|<5$ cm to allow a first $R_{AA}$ assessment with reasonable precision. The fraction of events with real vertices within $|V_z|<5$ cm using an online 5 cm cut is about 40% due to the VPD $V_z$ resolution in p+p collisions with the software slewing correction. Therefore to record this data set needs about a 12-week beam time with 400Hz DAQ rate and 72 DAQ hours with HFT per week.

The precision of high $p_T$ heavy flavor hadron spectra can be improved by utilizing the EMCal higher tower (HT) triggered data set to trigger on one hadron leg and to sample the full luminosity. HT triggered data has been successfully used to measure the high $p_T$ $K_S$ and $\Lambda$ yield in p+p collisions to improve the baseline precision for $R_{AA}$ calculations [12]. Figure 4.1 left plot shows the trigger efficiency for charged pions with two different HT thresholds from 200GeV p+p in Run 6. This has been vetted using large minimum bias sample data. We will apply the same technique to measure the D-meson production with triggering on one charged daughter leg. At high $p_T$, the combinatorial background in the D-meson reconstruction in p+p collisions is small. To maximize the sampled luminosity, we will not be constrained by the HFT acceptance for this measurement. In a 12-week p+p 200GeV run in Run15, the total sampled luminosity within $|V_z|<30$cm with affordable bandwidth rate (BHT0*VPDMB with no prescale) and also considering the VPD minimum bias triggering efficiency and the vertex selection fraction is about 8 $pb^{-1}$. Figure 4.1 right plot shows relative errors of $D^0$ raw yields reconstructed in 100M 0-10% central Au+Au events, 500M p+p MB events and 8 $pb^{-1}$ sampled luminosity events in p+p with HT0 triggers. The triggered sample from p+p collisions will allow a comparable precision as central Au+Au collisions up to 10GeV/c. On the other hand, the comparison measurement at low $p_T$ is dominated by the statistic uncertainty from p+p collisions.

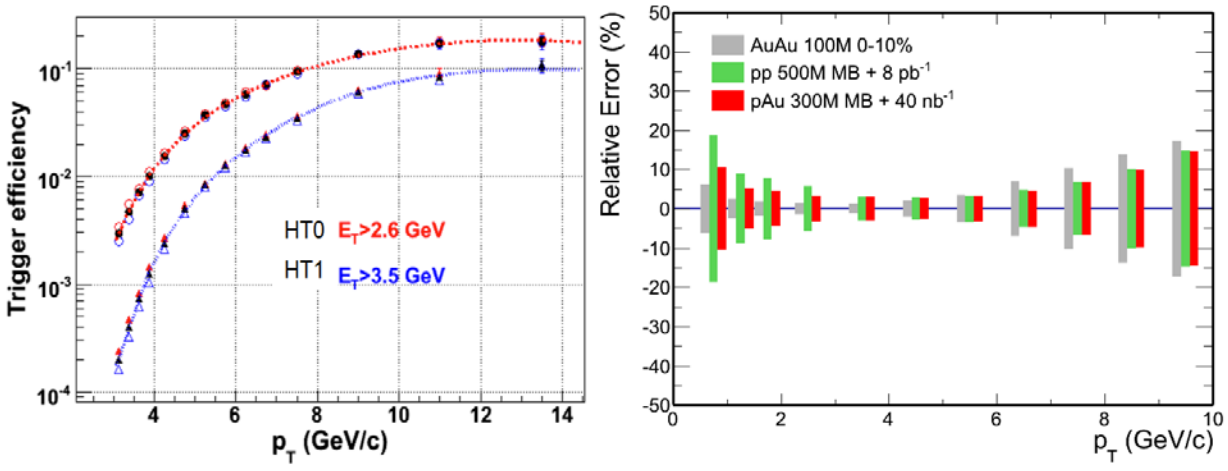


Figure 4.1: (Left) Barrel EMC trigger efficiency for charged pions with two different HT thresholds obtained from 2006 analysis. (Right) Projected relative statistical uncertainties for 100M 0-10% central Au+Au events, 500M p+p minimum bias events, and 8 $pb^{-1}$ sampled luminosity in p+p 200 GeV events with the HT0 ($E_T$ > 2.6GeV) trigger.

Measurements of the in-medium dissociation probability of the different quarkonium states are expected to provide an estimate of the initial temperature of the system. Dissociation of quarkonium in a thermal QCD system would ultimately provide evidence of color screening and free quarks in the medium. These measurements require a large integrated luminosity driven by the requirement in p+p reference data. Table 4.1 shows an estimate for the required luminosity for measurements of the 2S+3S and the 3S separately. We have investigated an alternative approach in obtaining the reference. Many experiments have measured the Upsilon yields and ratios of the three states. We have collected all the experimental results and survey the ratios of $\Upsilon$(2S)/$\Upsilon$(1S), $\Upsilon$(3S)/$\Upsilon$(1S) and $\Upsilon$(2S+3S)/$\Upsilon$(1S). Figure 4.2 left panel shows the results as a function of beam energy for all the p+p, p+pbar and p+A results. A small energy dependence of these ratios is observed within the broad collision energies. The solid line shown in the figure is a linear fit. The dashed line is a constant fit. The linear fit gives a better $\chi$2/NDF, where NDF is the number of degrees of freedom;

therefore we select the linear fit results to determine the nominal values for $p + p$ collisions at $\sqrt{s}$ = 200 GeV. The differences between these two fit results for 200 GeV $p + p$ collisions are considered to be the systematic uncertainties. The ratios are $\Upsilon(2S)/\Upsilon(1S) = 0.290 \pm 0.007$ (stat.) $\pm$ 0.014(syst.) and $\Upsilon(3S)/\Upsilon(1S) = 0.131 \pm 0.005$ (stat.) $\pm$ 0.003(syst.) for $p + p$ collisions at $\sqrt{s}$ = 200 GeV. Note that the error bars from these measurements are much smaller than that achievable at RHIC. The measurements with high statistics will nevertheless serve as important consistence checks for our extrapolations.

| **Collision system** | **Mini. lumi. for 10% uncertainty on $\Upsilon$(3S)** | **Mini. lumi. for 10% uncertainty on $\Upsilon$(2S+3S)** |
|---|---|---|
| p+p 200 GeV | 420 pb$^{-1}$ | 150 pb$^{-1}$ |
| p+p 510 GeV | 140 pb$^{-1}$ | 50 pb$^{-1}$ |

Table 4.2: Estimated luminosities for $\Upsilon$(2S, 3S) measurements.

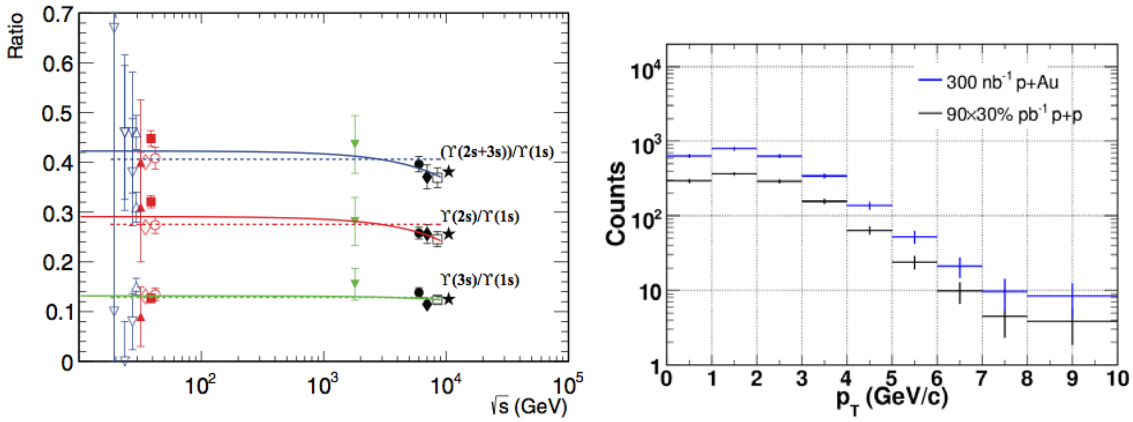


Figure 4.22: Left: Collision energy dependence of the yield ratio of Upsilon states in p+p, p+pbar and p+A collisions. The solid and dashed lines are fit curves. Right: projection of J/Psi yields from p+p and p+Au collisions in run15 with MTD trigger on dimuons.

***p+Au run request:***

To understand the cold nuclear matter (CNM) effect on the charmed meson production, we request to take 5 weeks of p+Au collisions at 200 GeV to collect 300M good minimum bias events and sample 40 nb$^{-1}$ luminosity within |Vz|<5 cm. The request datasets are determined to have comparable statistics for the nuclear modification factor measurement as that from the Au+Au 200 GeV dataset collected in Run14 and the p+p 200 GeV dataset requested above for Run15. The p+Au request in Run15 will be a starting point to provide a good precision measurement of the inclusive charmed hadron spectrum.

Figure 4.1 right plot also includes the statistical error projection from 300M minimum bias p+Au collisions at 200 GeV. It provides comparable precision with 500M $p$+$p$ reference data to allow the first assessment on the CNM effects on the charmed meson production.

The cold nuclear matter effects on heavy quarkonia production are critical in understanding the hot and dense medium effect of heavy quarkonia production in Au+Au collisions. It has long been a hot topic for discussion [38,47]. With the newly installed MTD, STAR will be able to sample the full luminosity with the di-muon trigger leading to high precision measurements of $J/\psi \rightarrow \mu^+\mu^-$ at

low $p_T$ shown in right panel of Figure 4.2. For $p_T$ = 0 – 4 GeV/c, the statistical uncertainty of the $J/\psi \rightarrow \mu^+\mu^-$ $R_{AA}$ measurements will be about 10% with 300 $nb^{-1}$ p+Au collisions and 90 $pb^{-1}$ p+p collisions sampled by di-muon trigger. For $p_T$ = 4 – 8 GeV/c, the statistical uncertainty of the $J/\psi \rightarrow e^+e^-$. $R_{AA}$ measurements will be about 5% with 50 $nb^{-1}$ p+Au collisions and 10 $pb^{-1}$ p+p collision sampled by HT1 ($E_T$ > 3.5 GeV) trigger in |Vz| < 30cm. For $p_T$ = 8 – 10 GeV/c, the statistical uncertainty of the $J/\psi \rightarrow e^+e^-$ $R_{AA}$ measurements will be about 15% with 300 $nb^{-1}$ p+Au collisions and 90 $pb^{-1}$ p+p collision sampled by HT2 ($E_T$ > 5.4 GeV) trigger.

***The ridge in p+A and d+A collisions at RHIC:***

In p+Pb collisions at the LHC, an unambiguous two-particle correlation is observed at large pseudorapidity $\Delta\eta$ and small azimuthal difference $\Delta\phi$. This is conventionally called the ridge. There are two leading theoretical explanations. One is the color glass condensate where small-x gluons are saturated below the saturation scale of *Qs* in transverse momentum. At transverse momentum ~*Qs*, two-gluon production is enhanced at small $\Delta\phi$ over a large range in $\Delta\eta$. The other is hydrodynamic expansion in response to initial interaction geometry fluctuations. The anisotropy in final-state azimuthal distribution can be as large as 10% to explain the LHC ridge observation.

The two physics mechanisms likely give difference predictions to the collision energy dependence of the ridge. It is therefore important to measure the ridge or the lack thereof at RHIC energies. STAR has analyzed the Run-3 d+Au data of approximately 10 million minimum bias events. Long-range near-side correlations (ridge) are observed in the TPC ($\Delta\eta$~1.5) and FTPC ($\Delta\eta$~3). The observed correlations have strong dependence on the particle charges. This suggests physics mechanisms other than anisotropic flow. In order to unravel the underlying physics mechanisms, detailed studies of the long-range correlations with much greater statistics are needed.

The long-range correlations in FTPC acceptance are dominated by positive associated particles, but no like- and unlike-sign difference is observed, while a difference between like- and unlike-sign correlations is observed at large $\Delta\eta$ in the TPC acceptance. In run15, there is no tracking system available in the forward direction. The FMS, which is sensitive to photons from neutral pions and other particle decays, is situated in the proton direction in p+Au collisions. This will enable us to study the ridge effect from correlation between neutral pions at $\eta$~=3 with hadrons at $\eta$~=0, and would require an integrated luminosity of 200 $nb^{-1}$.

***Cronin effect and strangeness enhancement in small-size systems:***

The reason for requesting *p*+Au collisions is to study the particle type dependence of the Cronin effect, and strangeness enhancement in small-size systems. From experiences in Run 8 *d*+Au collisions, the study of particle type dependence of the Cronin effect at intermediate $p_T$ requires more statistics compared to that to study the strangeness enhancement. Therefore we estimate the required statistics based on the measured $R_{dAu}$ from Run 8 *d*+Au 200 GeV collisions. The collected statistics in Run 8 is about 70M minimum bias events. After the event selection 30M events remain.

In the light flavor physics working group, one key study is to see whether there is a particle species dependence or baryon-meson dependence of the Cronin effect by comparing the $R_{dAu}$ of φ meson with other hadrons. The measured $R_{dAu}$ for $K_S^0$, φ mesons and Λ hyperons in 0-20% central collisions from Run 8 is shown in Figure 4-3. One can see a clear separation between $K_S^0$ and Λ hyperons at intermediate $p_T$. But for φ mesons the result is not as clear. The large uncertainties for the φ meson $R_{dAu}$ are mainly due to a poor p+p reference sample (only 6.5M p+p non-single diffractive events from the year 2002 have been used). The uncertainties for the p+p reference could be controlled within ~5% at intermediate $p_T$ (2-4 GeV/c) with about 0.5B events from Run 9 and Run 12. If we assume φ mesons $R_{dAu}$ is close to Λ hyperons at around 3 GeV/c, $R_{dAu}$ (φ) /$R_{dAu}$ ($K_S^0$) should be about 1.6. Considering that the ratio $R_{dAu}$ (φ) /$R_{dAu}$ ($K_S^0$) should decrease with the number of participant nucleons, the $R_{dAu}$ (φ) /$R_{dAu}$ ($K_S^0$) ratio should be about 1.3 in *p*+Au collisions at the

same centrality. To have a 3-sigma significance, we need to control the relative uncertainty on $R_{dAu}$ (φ) /$R_{dAu}$ ($K_S^0$) within 10% at $p_T$ around 3 GeV/c. In Run 8 *d*+Au 0-20% centrality, the relative uncertainty on φ meson raw yields at 3-3.5 GeV/c is about 8.3%. We need to control the error bar within 6% to make the uncertainty of $R_{dAu}$ (φ) /$R_{dAu}$ ($K_S^0$) within 10%. Therefore, a factor of 2 more statistics is needed compared to Run 8 *d*+Au collisions. Considering that φ meson yields in *p*+Au collisions are about a half of those in *d*+Au collisions, we need about 7022 = 280M minimum bias *p*+Au events to make a good measurement.

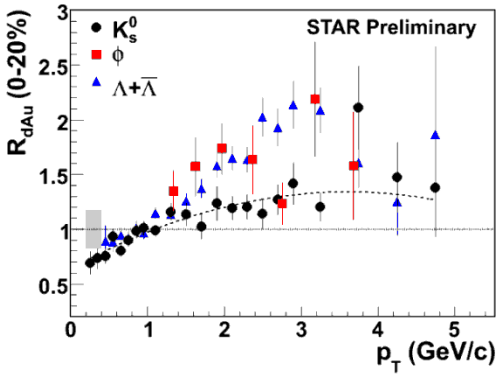


Figure 4.3 : $R_{dAu}$ for $K_S^0$, φ mesons and Λ hyperons in 0-20% *d*+Au central collisions from Run 8.

## 4.2 Physics with 200 GeV longitudinally polarized p+p collisions

The final results, obtained in Run-9, on the double-spin asymmetry $A_{LL}$ in inclusive jet production at √s = 200 GeV from 20 $pb^{-1}$ sampled with 58% average beam polarization are shown in Figure 2.7. Both from the latest $\Delta g(x,Q^2)$ extractions from DSSV and STAR through the NNPDF reweighting technique it is obvious that the uncertainties on the polarized gluon distribution need to be further decreased in the x-range currently already covered by measurements and that measurements are need to extend to the till today unexplored lower x-range.

The latest $\Delta g(x,Q^2)$ extractions from DSSV and from STAR through the NNPDF reweighting technique make it abundantly clear that the uncertainties on the polarized gluon distribution need to be further decreased in the x-range already covered by existing measurements as well as extended to the thus far unexplored low *x* range. Run-15 is an integral part of a three-step plan to further advance our knowledge about the polarized gluon distribution and its integral. The plan follows these steps: (1) reduce the statistical and systematic uncertainties of the workhorse of the STAR $\Delta g$ program, inclusive jet $A_{LL}$. (2) Make use of correlation measurements such as di-jets and di-hadrons, which give access to the partonic kinematics and thus the functional form of $\Delta g(x)$ (Note: $x_2 = p_T(e^{\eta_1} + e^{\eta_2})/\sqrt{s}$ and $x_1 = p_T(e^{-\eta_1} + e^{-\eta_2})/\sqrt{s}$, where $\eta_{1,2}$ represent the pseudorapidities of the two outgoing partons). The functional form of $\Delta g(x)$ also provides insight into the dynamical origin of gluons inside the proton. First results from di-jets from STAR have been released. (3) Access lower *x* by performing measurements at $\sqrt{s}$ = 500 GeV and at large forward rapidity. A first step in this direction has been made in [34]).

A new data set of 50 $pb^{-1}$ with 60% longitudinal polarization as anticipated from Run-15 will improve the uncertainties by a factor of nearly 2 at high $p_T$ > 15 GeV/*c* while a smaller improvement by about √2 is still achievable at smaller $p_T$, where the measurements will become systematics limited. Doing so will provide significant further constraints on the polarized gluon distribution, especially for large momentum fractions *x*. The anticipated improvement in statistics on $A_{LL}$ and the complementarity in kinematics with √s = 510 GeV data is shown in Figure 4.4. To

quantify the impact of these inclusive jet $A_{LL}$ data sets on $\Delta g(x,Q^2)$ a pQCD fit in the DSSV framework based on pseudo data of the different data sets has been performed. Figure 4.5 shows the improvement of the $\chi^2$ profile for the integrated gluon contribution in the $x$ region currently probed at RHIC. The current uncertainties for $\int_{0.05}^{0.2}\Delta g(x)dx = 0.1 \pm^{0.06}_{0.07}$ will be reduced by a factor of 2. The $\sqrt{s}$=510 GeV data sample will extend the x-range constrained by data down to $x \sim 0.02$.
Figure 4.6, Figure 4.7 and Figure 4.8 show the existing and projected statistical uncertainties for the di-jet $A_{LL}$ as function of di-jet mass for different di-jet combinations. It is clearly visible that the new Run-15 data set will lead to a significant improvement over the preliminary STAR measurements of the di-jet $A_{LL}$ at $\sqrt{s}$ = 200 GeV from Run-9 [48].
Figure 4.8 illustrates nicely how the probed $x_1$-$x_2$ correlation changes from high to low $x$ as function of the rapidity combination of the two jets.

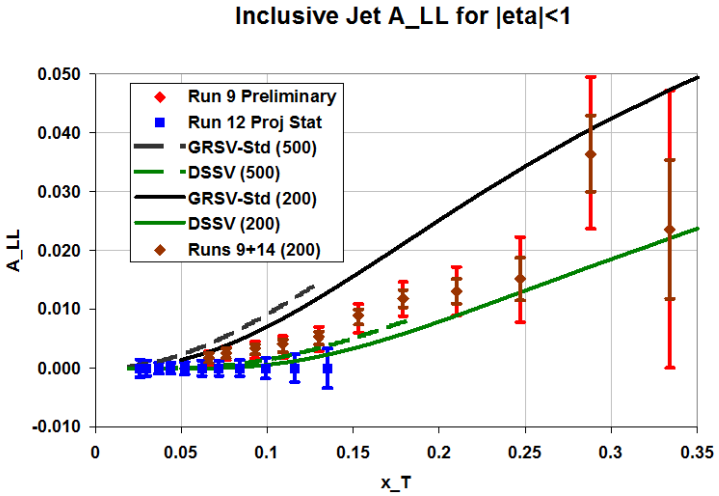


Figure 4.4 The expected precision for $A_{LL}$ vs. $p_T$ for inclusive jets at $\sqrt{s}$ = 200 GeV p+p collisions after the proposed Run-15 data are combined with the existing Run-9 measurements (brown diamonds). Also shown are the current Run-9 results (red diamonds) and the expected precision at $\sqrt{s}$ = 510 GeV from Run-12 (blue squares), together with model predictions for both energies from GRSV-Std and DSSV 2008.

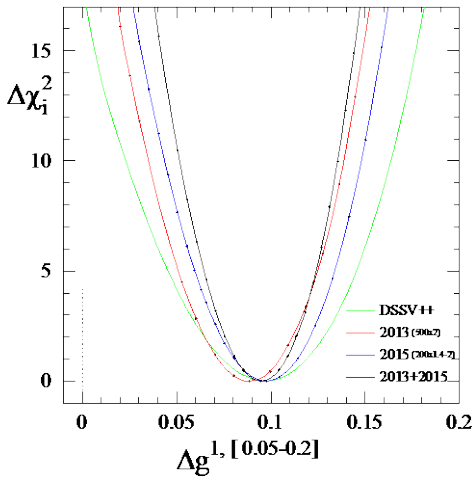


Figure 4.5: The improvement of the $\chi^2$ profile for the integrated gluon contribution in the $x$ region currently probed at RHIC for $\sqrt{s}$ = 200 GeV. The different curves represent including different data sets, red including the $\sqrt{s}$ = 510 GeV data from Run-12 and Run-13 (red), blue including the expected data from Run-15 (blue) and black represent a fit to all data at once..

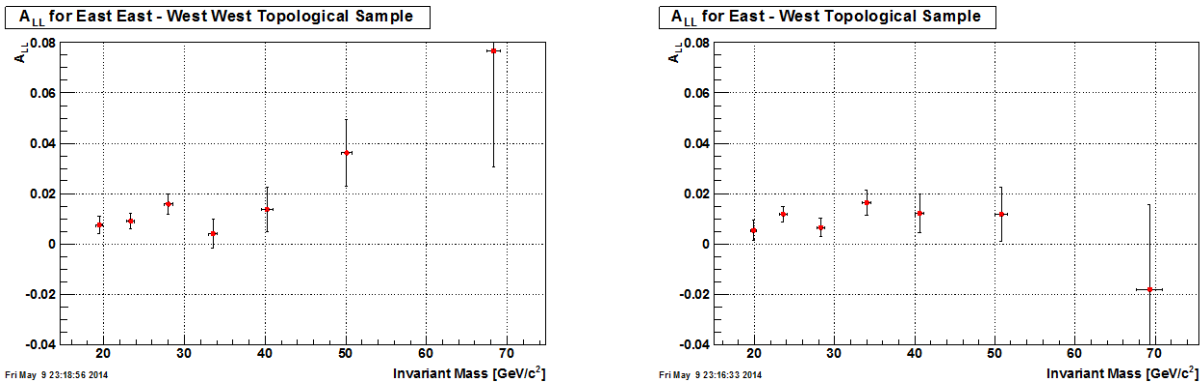


Figure 4.6: $A_{LL}$ di-jet as function of di-jets mass for different di-jet combinations from the Run-9 $\sqrt{s}$ = 200 GeV data taking [48].

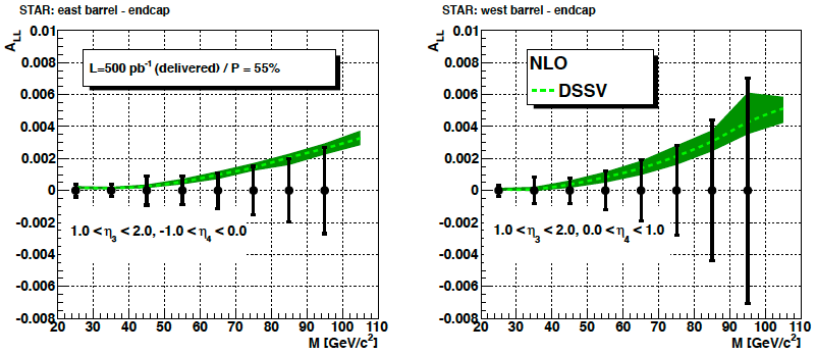


Figure 4.7: Projected statistical uncertainties for $A_{LL}$ of di-jets at mid-forward rapidity and into the STAR Endcap ($0.8<\eta<2.0$) at $\sqrt{s}$ = 510 GeV as function of the di-jet mass for two different di-jet combinations. The delivered luminosity of 500 pb$^{-1}$ corresponds to the sum of Run-11 to Run-13.

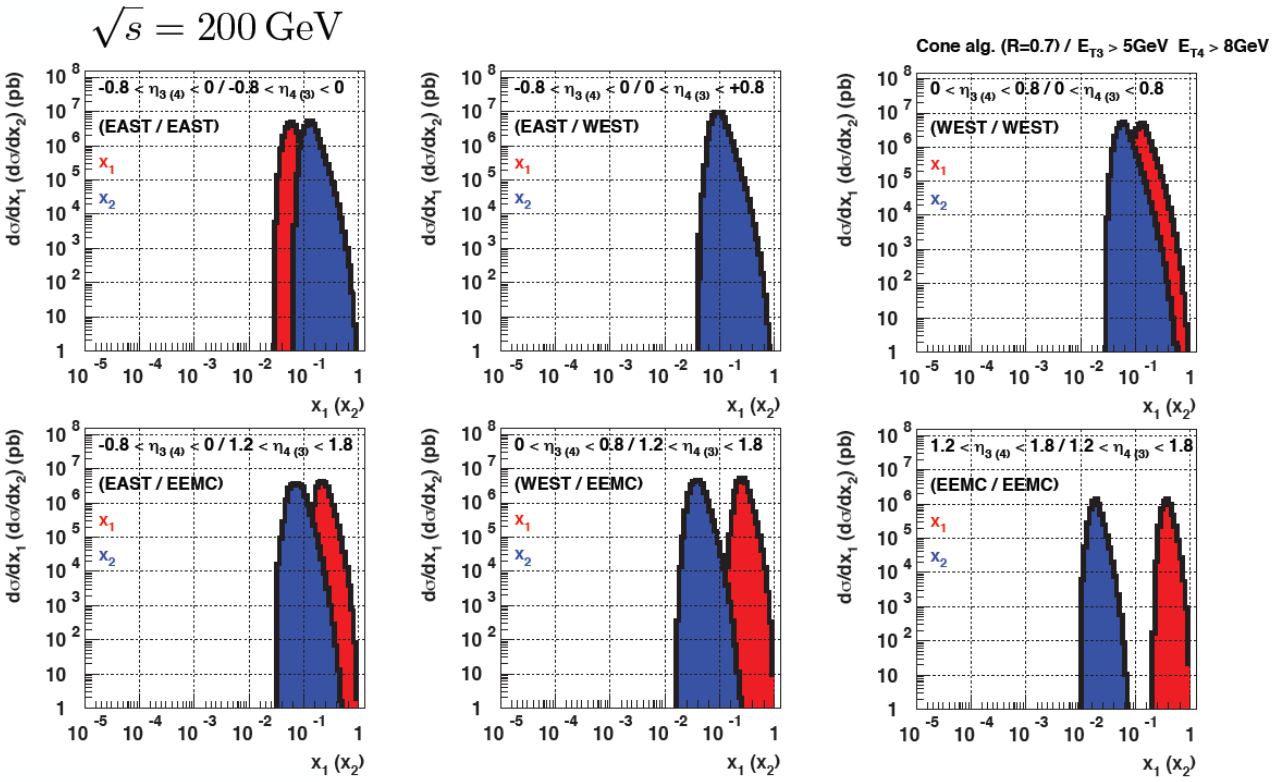


Figure 4.8: The probed $x_1$-$x_2$ correlation for di-jets as function of the rapidity combination of the two jets.

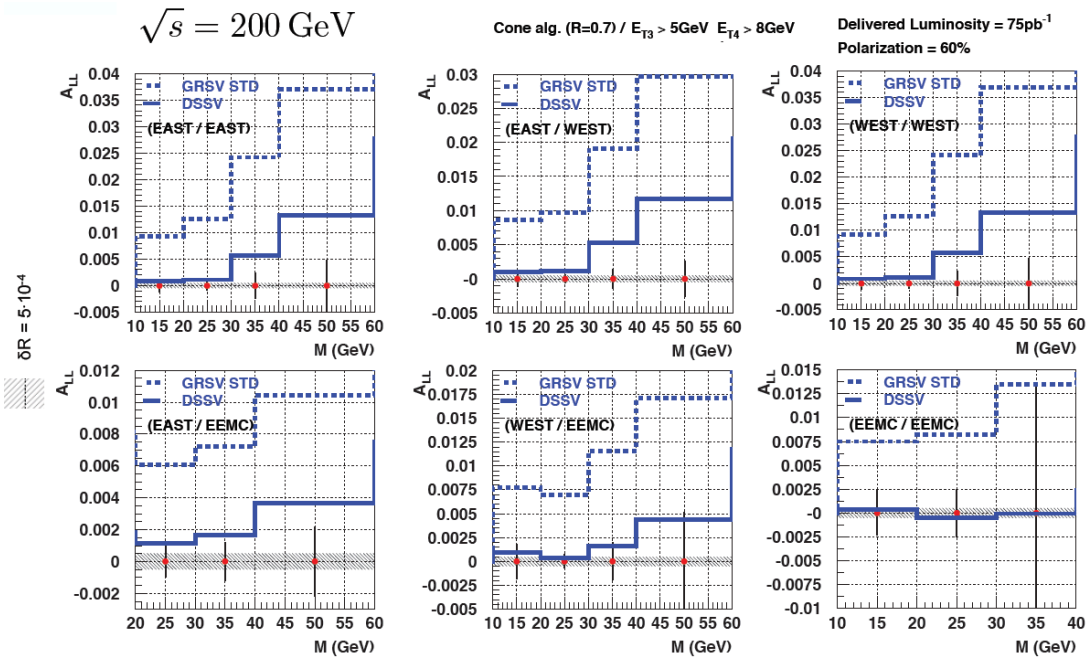


Figure 4.9: Projected statistical uncertainties for the di-jett $A_{LL}$ as function of di-jets mass for different di-jet rapidity combinations for the upcoming Run-15 $\sqrt{s}$ = 200 GeV data taking. The assumed delivered luminosity is 75 pb$^{-1}$ and a average polarization of 60%.

Combining the $\sqrt{s}$ = 200 GeV di-jet $A_{LL}$ results from Run-9 and Run-15 with the results already taken and currently analyzed $\sqrt{s}$ = 510 GeV di-jet $A_{LL}$ from Run-12 and Run-13 will provide stringent constrains on the functional shape of the gluon distribution as well as on the overall value. STAR can extend the physics reach of its gluon polarization measurement even further by tapping the low-$x$ region accessible with both inclusive $\pi^0$ and di-hadrons ($\pi^0$s) and direct photon $A_{LL}$ in the FMS. (Details about direct photon capabilities in the FMS are discussed in sections 4.2, 5.1, and 6.2).

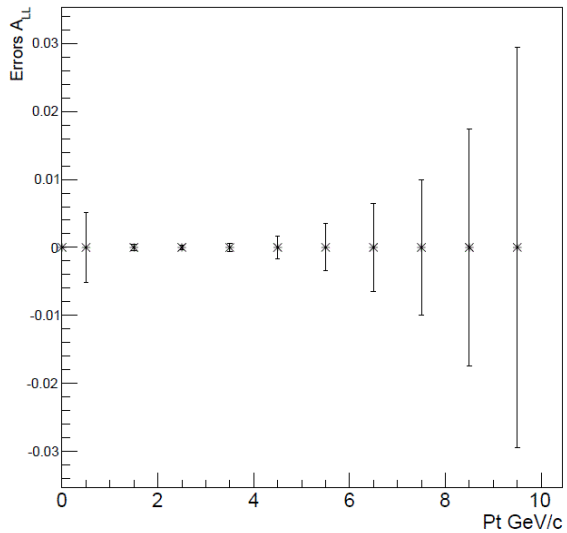


Figure 4.10 Projected statistical uncertainties for the $\pi^0$ double spin asymmetry for an integrated recorded luminosity of 50 pb$^{-1}$. The measurement is based on loose $\pi^0$ cuts (necessary for large $p_t$). This result uses a 35 mR cone for two photon selection.
The trigger from run 12 was FMS Jet Patch 2. It is this that defines the lower $p_T$ response and can be set to anything we choose. In Run 12 we used a Jet Patch 1 with prescaling to sample the distribution to lower $p_t$ (~ 1 GeV lower). The pseudo-rapidy range is the full range of the FMS 2.7<$\eta$<4.

Figure 4.10 shows the projected statistical uncertainties for inclusive $\pi^0$ in the FMS. The main systematic uncertainties will be the relative luminosity, the ongoing analysis of the Run-12 data reaches in the order of $10^{-3}$ or better. This measurement will provide an important first test for the future to measure double spin asymmetries at forward rapidity. Further systematic uncertainties

are a scale uncertainty in the order of 6% due to the beam polarization measurements and some point-to-point systematics due to background in the order of a 2-3%.

All these different measurements will have a direct impact on any polarized NLO pQCD global analysis such as DSSV by supplying data in a previously unexplored kinematic region.

## 4.3 Physics with 200 GeV transversely polarized p+p collisions

Determining the underlying physics process responsible for the large transverse single spin asymmetries at forward rapidities at high energy (see Figure 2.9) is the new spin puzzle for the 21st century. As discussed earlier the processes deemed to be responsible go beyond the conventional collinear parton picture in the hard processes. The two theoretical formalisms, which can generate sizable SSAs in the QCD framework are: transverse momentum dependent parton distributions and fragmentation functions, which provide the full transverse momentum information and the collinear quark-gluon-quark correlation, which provides the average transverse information. The most prominent mechanisms in these frameworks possibly responsible for the large $A_N$ are transversity in combination with the Collins fragmentation function or the Sivers distribution function together with transverse momentum dependent fragmentation functions. To disentangle the different subprocesses it is important to measure less inclusive processes. Table 4.1-1 identifies observables, which will help to separate the contributions from initial and final states, and will give insight to the transverse spin structure of hadrons. Depending the observable is a one-scale process, like most of the processes in p+p collisions we will probe the transverse spin structure of hadrons through the twist-3 formalism. Only 2-scale processes, like di-jets, $W^{\pm}$, $Z^0$ and DY, probe directly TMDs.

| **Sivers** | **Transversity *h(x)* x Collins FF** |
|---|---|
| $A_N$ as function of rapidity, $E_T$, $p_T$ and $x_F$ for inclusive jets, direct photons and charmed mesons<br><br>$A_N$ as function of rapidity, $p_T$ for $W^{\pm}$, $Z^0$ and DY | $A_N$ as function $p_T$ and the invariant mass of the hadron pair (IFF)<br>$A_{UT}^{\sin\Phi} = A_{UT}\sin(\Phi_R - \Phi_S) = \frac{\hat{\sigma}^{\uparrow} - \hat{\sigma}^{\downarrow}}{\hat{\sigma}^{\uparrow} + \hat{\sigma}^{\downarrow}}\sin(\Phi_R - \Phi_S)$<br><br>Hadron correlations within a jet<br><br>$A_{UT}$ as function of the azimuthal dependence of the correlated hadron pair on the spin of the parent quark |

Table 4.2: Observables to separate the contributions from initial and final states to the transverse single spin asymmetries. 2-scale processes are indicated in blue and 1-scale ones in black.

In the following the STAR capabilities to measure these different observables in Run-15 will be discussed. With its broad acceptance for charged particles in the TPC, STAR is well positioned to carry out the study of di-hadron correlations within a jet, *i.e.*, at relatively small opening angle, where one works with the transverse momentum $p_T$ and the invariant mass of the pair, rather than with individual particle $p_T$. These correlations can be described in terms of the product of the transversity *h(x)* and the so-called Interference Fragmentation Function, IFF, which is a chiral-odd quantity. Extracting the IFF in polarized *p+p* collisions at high energy is of particular interest as it will constrain *h(x)* at higher values of *x* than competing measurements in semi-inclusive DIS. Recent first results are shown in Figure 4.11.

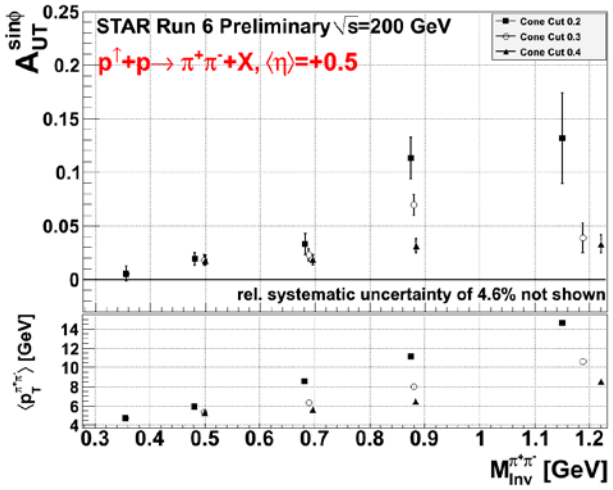


Figure 4.11: (top) Preliminary measurements of the transverse single-spin asymmetry $A_{UT}$, as defined in the text, as a function of the invariant mass of the unlike-sign di-pion. The choice of cone cut radius is strongly correlated with the average transverse momentum of the pair, as can be seen in the kinematic plot (bottom).

The second observable is leading charged pions inside a reconstructed jet. In this case one is looking for correlations between the azimuthal distribution of the pion inside the jet and the spin orientation of the parent proton. Similarly to the IFF case, these correlations are sensitive to the product of transversity *h(x)* and the Collins Fragmentation Function *ΔD(z)*, also a chiral odd quantity. Measurements in semi-inclusive deep inelastic and electron-positron scattering have shown *ΔD(z)* to be sizable and increasing with increasing pion momentum fraction *z*. Figure 4.12 shows a recent measurement of this Collins asymmetry $A_N$ made using mid-rapidity jets reconstructed at STAR. It was calculated by forming the ratio of the of sum of the $sin(\varphi_h-\varphi_S)$ weighted events and the sum of the polarization *P* weighted events. Systematic errors were conservatively estimated to be +/-0.023 for the $\pi^+$ and $\pi^-$ results independently.

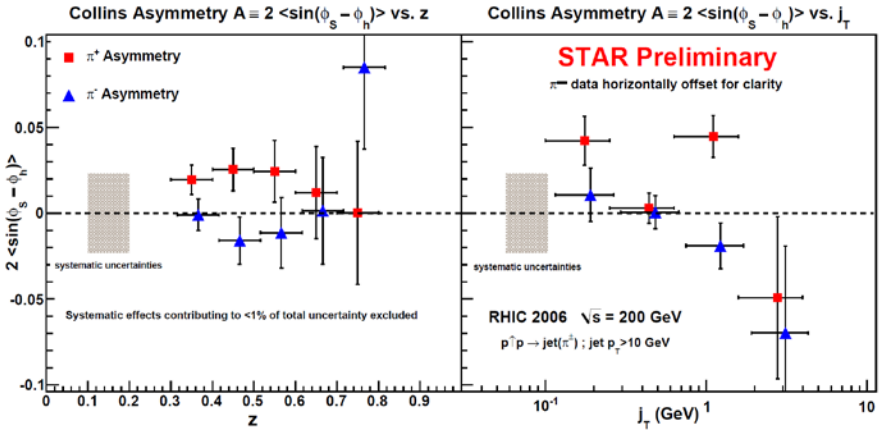


Figure 4.12: Preliminary results of the Collins moment for leading $\pi^+$(red) and $\pi^-$ (blue) particles within mid-rapidity jets reconstructed by the STAR detector. Statistical errors are shown on data points and the grey shaded band indicates the systematic error bar for $\pi^+$ and $\pi^-$ separately.

Both the IFF and Collins analysis were exploratory measurements made using Run-6 transverse data. Indications of non-zero asymmetries motivated the extended 200 GeV running during Run-12 and for Run-15. Exceptional accelerator performance and high sampling rates at STAR during the 2012 run resulted in a sampled FOM of ~ 7.74 $pb^{-1}$ in 5 weeks, compared to the ~2.2 $pb^{-1}$ of transverse data taken in 2006 used in the STAR analysis, which indicate non-zero asymmetries. Data collected in Run-12 will allow these asymmetries to be measured with higher precision and increased kinematic coverage, see for quantitative projections. These data will also be used to tighten the constraints on the mid-rapidity inclusive jet $A_N$, which will dominantly sensitive to the gluon Sivers contribution.

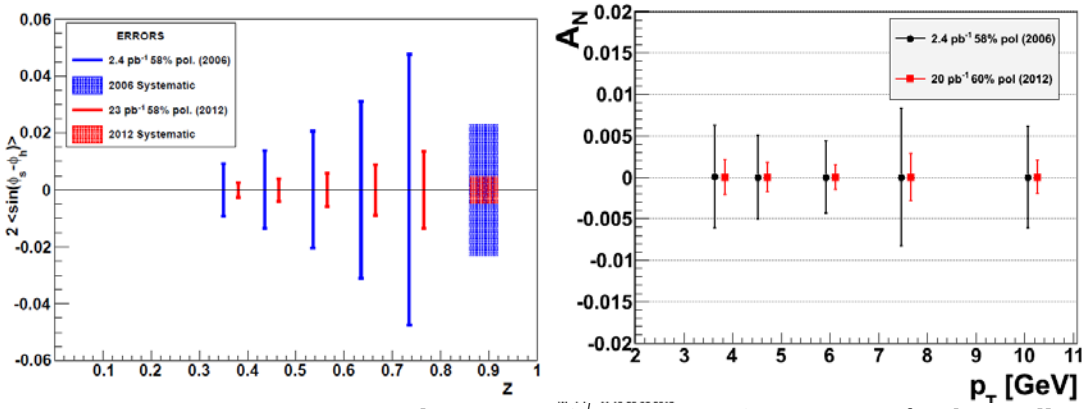


Figure 4.13: Run-6 errors compared to Run-12 ($\sqrt{s}$ = 200 GeV) projections for the "Collins-jet asymmetry'' (left) and for the mid-rapidity Interference Fragmentation Function (right).

Following the motivation for transverse polarized physics described in section 2.1.2, a transversely polarized $p+p$ run with an integrated sampled luminosity of 50 pb$^{-1}$ in Run-15 will allow us to answer several open questions. $p_T$-dependence for the different asymmetries shown in Figure 2.13 and Figure 2.14 turn over from flat and follow the pQCD expected $1/p_T$ behavior? Can the underlying sub-process(es) responsible for the large forward $A_N$ be identified and delineated?

Figure 4.14 shows the projected uncertainties for Run-12+Run-15 for IFF for different pion combinations. The uncertainties for the Collins asymmetry as shown will be reduced by a factor of 1.4 for Run-15 compared to Run-12. These two Run-15 results together with the Run-12 data will provide a powerful data set for global fits to extract transversity and to further constrain the Collins and interference fragmentation functions. The STAR data will be extremely crucial to constrain transversity at high $x$ where currently are absolutely no data available. Both data sets are very stringent tests to models trying to explain the transverse physics phenomena in p+p and especially the cause of the large forward pion $A_N$.

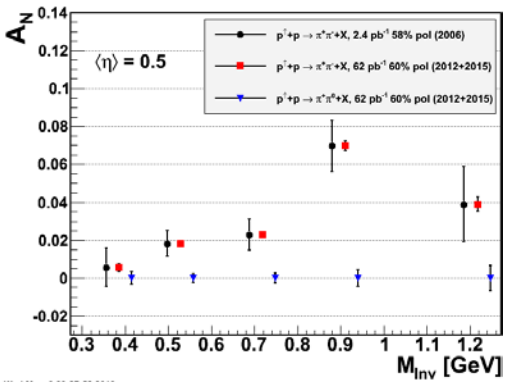


Figure 4.14: Run-12 + Run-15 projections for the mid-rapidity Interference Fragmentation Function compared to the results based on Run-6.

Having a first measurement of the direct photons $A_N$ with the FMS will be extremely crucial to understand the contribution of the Sivers-mechanism to the forward $A_N$. For the measurement of the direct photons it will be important to have the pre-shower described in section 6.2 installed in front of the FMS. Direct photons are a rare process. Therefore it is important to suppress background from leptons, hadrons and $\pi^0$ as much as possible. Figure 4.15 right shows the statistical and systematic uncertainties for the direct photon $A_N$. The asymmetry can be measured up to $x_F \sim 0.7$ where the $\pi^0$ asymmetries are largest. Figure 4.15 left shows the level of achieved background suppression for charged particles as well as photons from decays, i.e. $\pi^0$, using the forward meson spectrometer (FMS) and its preshower without any significant loss in the direct photon yield. Ideally, neutral pion asymmetries are measured simultaneously in the same $x_F$-range.

The background from charged tracks is removed by matching FMS clusters with hits in the preshower. The position resolution in the FMS is much better than the single tower size, so the preshower granularity is defining the limit on the matching cut. The matching distribution for charged particles exhibits a distinct peak at about half of the width of the preshower channels and it falls off steeply towards larger values, making the veto condition very effective to remove this kind of background from the direct photon signal. Photons from meson decays have to be separated from the direct photon sample by their event topology. For this, a two-fold selection is applied to the clusters in the FMS. Any event that contains two or more clusters above a certain threshold (1.0 GeV) is discarded. The remaining clusters are required to have an energy of 10.0 GeV or more. This initial cut is reducing the photon background more effectively with increasing $p_T$ (dashed line). Further refinement of this cut will be done with the real data to be able to study the $x_F$-dependence of the transverse single-spin asymmetries with good accuracy. For the background asymmetry, an upper limit of measured neutral pion asymmetries was used to estimate the systematic uncertainties ($0.0<A_N(x_F)<0.18$). An additional pT-cut of 2.0 GeV is used for the $x_F$-distribution.
Merged clusters in the FMS from pion decay become problematic at $p_Z \approx 60$ GeV or more; here the preshower/converter will help to increase the signal/background fraction and extend the reach in $x_F$.

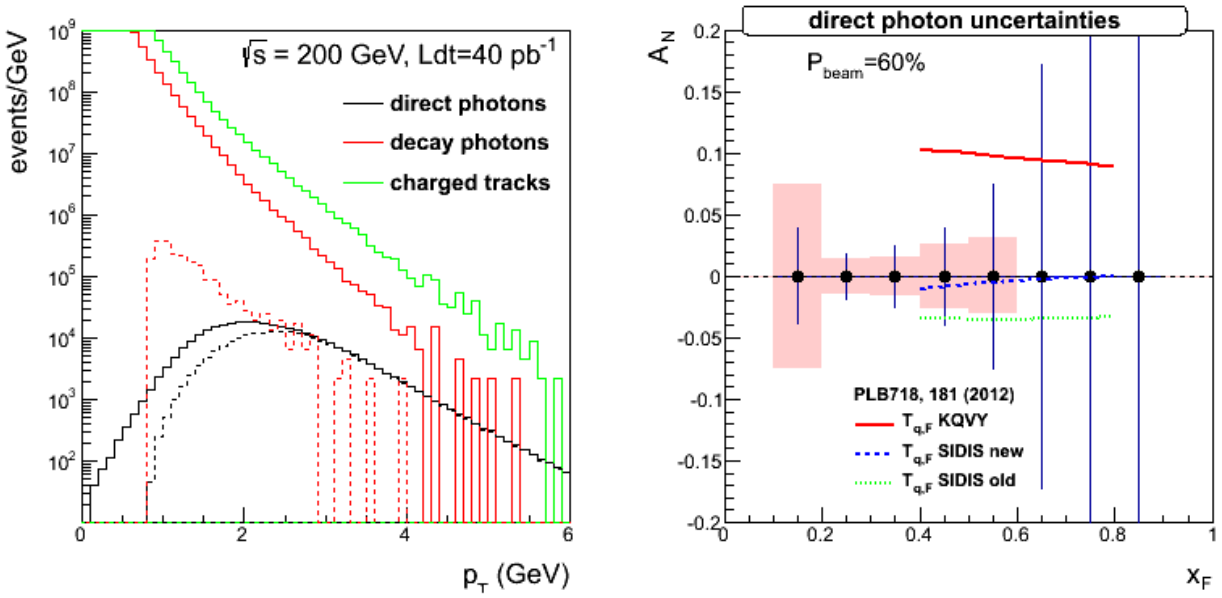


Figure 4.15: (Left) The number of events at $\sqrt{s}$=200 GeV for a recorded luminosity of 40 pb$^{-1}$ for direct photons, charged hadrons and photons from decays, i.e. $\pi^0$ before (solid) and after (dashed) detector responses have been applied. (Right) Statistical and systematic uncertainties for the direct photon $A_N$ after background subtraction compared to theoretical predictions based on different assumptions for the Sivers function [49].

The observation, see section 2.2.2, that the transverse single spin asymmetries drop with increased jettiness of the event, could indicate that the underlying subprocess causing the large transverse single spin asymmetries in the forward direction is of diffractive nature. The roman pot phase II* upgrade (see section 6.1) will allow to make a measurement of $A_N$ $\pi^0$ for single and double diffractive events by tagging one or both protons in the Roman Pots. A discovery of large transverse single spin asymmetries in diffractive processes would open a new avenue to study the nature of pomerons in $p+p$ collisions.

## 4.4 Physics with Tagged Forward Protons at STAR

There are two main reactions that can be studied with tagged forward protons: polarized proton-proton elastic scattering and Central Exclusive Production (CEP) in double Pomeron exchange (DPE). Since the proton beams at RHIC are polarized we will study the spin dependence of diffraction.
A process of unique interest at RHIC is the central production process through the DPE mechanism $pp \rightarrow pM_Xp$. The two protons stay intact after the interaction, but they lose momentum to the Pomeron and the Pomeron-Pomeron interaction produces a system $M_X$ at mid-rapidity of the colliding protons.

***Central Exclusive Production (CEP) in proton – proton collisions:***
Tagging and measuring the forward protons is important since it removes the ambiguity of a (complementary) rapidity gap tag, which has a background due to the low multiplicity of diffractive events. The momentum balance between the scattered protons and the centrally produced system, exclusivity condition, allows obtaining a relatively background free data sample, like the one obtained in Run-9 at $\sqrt{s}$ = 200 GeV, for which the statistics of the data sample was limited because of the luminosity and the *t*-range for that run.

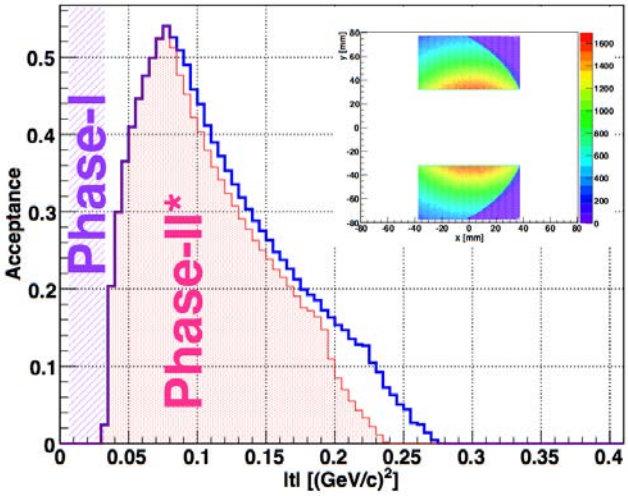


Figure 4.16 : Acceptance in t for Phase-II* setup. The acceptance for both RPs at 15.8 m and 17.6 m are shown in red and the acceptance for the front RP at 15.8m only are shown in blue. The acceptance for Phase-I is also shown for comparison. The inset plot shows the distribution of accepted protons in the front RP.

In Figure 4.17 a preliminary measurement of the invariant mass spectrum of the $\pi^+\pi^-$ pairs produced in the exclusive process $p+p$ -> $p+M_X+p$ is shown. The data were obtained with the STAR detector at RHIC at $\sqrt{s}$ = 200 GeV in 4 days running during Run-9. The Roman Pots were used to tag forward protons and the invariant mass of the pion pair was obtained using tracks reconstructed in the STAR Time Projection Chamber (TPC). To select CEP events the balance of momenta of the outgoing protons and central $\pi^+\pi^-$ pair was required.

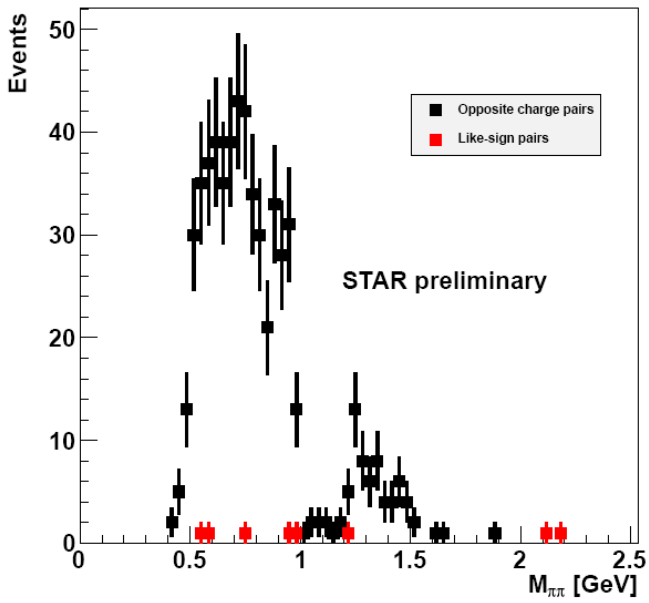


Figure 4.17: Invariant mass distributions for two opposite charged pions in the exclusive central diffraction in p+p -> p+ $M_X(\pi^+\pi^-)$+ p at $\sqrt{s}$ = 200 GeV. The distribution in red is non-exclusive background estimated from events with like-sign charge pion pairs. Errors are statistical only.

One of the interesting physics topics that can be explored at RHIC is a glueball search [50] in the Double Pomeron Exchange (DPE) process. Because of the constraints provided by the double Pomeron interaction, the glueballs, and other states coupling preferentially to gluons, are expected to be produced with much reduced backgrounds compared to standard hadronic production processes.

Two of the gluons in the DPE process, could merge into a mesonic bound state without a constituent quark, a glueball in the central production $p+p \rightarrow p+M_X+p$. The lattice QCD calculations predict the lowest-lying scalar glueball state will have a mass in the range 1500-2000 MeV/$c^2$, with tensor and pseudoscalar glueballs in the range 2000-2500 MeV/$c^2$ [ 51 ]. Experimentally measured candidates for the scalar glueball states are the $f_0(1500)$ and the $f_0(1710)$ in central production as well as other gluon-rich reactions such as $p\ \bar{p}$ annihilation, and radiative $J/\psi$ decay. The glueballs are expected to be intrinsically unstable and decay in diverse ways, yielding typically two or more mesons.

With the Phase-II* in Run-15 we expect to collect a data sample in a wider-$t$ range, allowing for much larger statistics. Simulations indicate that during 5 weeks of pp running in Run-15 (40 pb$^{-1}$) one can collect $1.5\times10^5$ exclusive $\pi^+\pi^-$ data sample (15k in $1< M_X < 2$ GeV/$c^2$) for analysis, estimated from the exclusive data sample collected during Run-9. The expected rate assumes 200 Hz DAQ rate for the physics.

### *Elastic scattering at medium |t|*

Elastic $pp$ (and $p\ \bar{p}$) scattering is a paradigm in the study of the diffraction process at the highest available energies. The special role of the elastic channel, contributing about 20% of the total cross section, can be interpreted in terms of the optical theorem, as the shadow of many inelastic channels, open at high energies: in this respect the elastic amplitude is considered to be mainly imaginary and helicity-conserving. This is reflected in the phenomenological features of a simple Pomeron Regge-exchange, with vanishing spin-flip, which implies a decrease of polarization asymmetries as energy increases.

Almost the entire energy range of this proposal has been inaccessible to proton-proton scattering in the past. A measurement of the total cross section, $\sigma_{tot}$ and spin dependence of the elastic scattering in the t-range [0.02, 0.12] will be studied.

## 4.5 Physics with transversely polarized p+A collisions

### 4.5.1 Unpolarized observables:

Our quest to understand QCD processes in Cold Nuclear Matter (CNM) centers on the following fundamental questions:

- What are the dynamics of partons at very small and very large momentum fraction (x) in nuclei, and at high gluon-density. What are the nonlinear evolution effects (i.e. saturation)?
- What are the pQCD mechanisms that cause energy loss of partons in CNM, and is this intimately related to transverse momentum broadening?
- What are the detailed hadronization mechanisms and time scales and how are they modified in the nuclear environment?

Various aspects of these questions are being attacked by numerous experiments and facilities around the world. Deep inelastic scattering on nuclei addresses many of these questions with results from HERMES at DESY [52], CLAS at JLab [53], and in the future at the JLab 12 GeV upgrade and eventually an Electron-Ion Collider [54]. This program is complemented with hadron-nucleus reactions in fixed target p+A experiments at Fermilab (E772, E886, and soon E906) [55] and at the CERN-SPS.

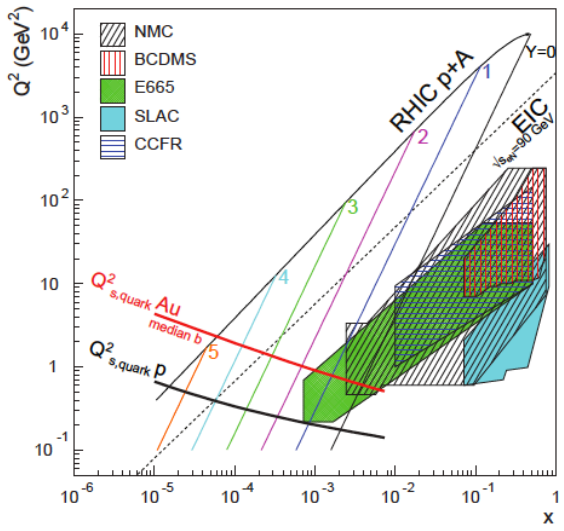


Figure 4.18: Kinematic coverage in the $x$-$Q^2$ plane for p+A collisions at RHIC, along with previous e+A measurements, the kinematic reach of an electron-ion collider (EIC), and estimates for the saturation scale $Q_s$ in Au nuclei and protons. Lines are illustrative of the range in $x$ and $Q^2$ covered with hadrons at various rapidities.

Current measurements at RHIC of the suppression of single hadrons [56,57] and back-to-back di-hadron correlations [58] in d+Au collisions have been interpreted as strong hints that the saturation scale, and the onset of saturation effects are accessible at forward rapidities at RHIC [59]. At this point, though, these interpretations are not unique, for two main reasons.

First, as shown in Figure 4.18 for the kinematic reach of RHIC energies the saturation scale is moderate, on the order of a few GeV$^2$, so measurements sensitive to the saturation scale are by necessity limited to semi-hard processes, and effects due to kinematic limits must be fully addressed. To some level this can be addressed at the LHC, where the larger energies allow for measurements deeper into the saturation regime, especially at forward rapidities. First measurements have been made at mid-rapidity by ALICE [60], which correspond approximately to $y$=3-4 at RHIC. This measurement shows no suppression of single hadrons for $p_T$ > 2 GeV/c, as predicted by saturation models [61,62], however, alternative models also predict this feature of the

data [63]. Key tests at the LHC will come at more forward rapidities, where saturation effects are expected to be stronger and distinct from other descriptions [62,63].

Second, and more importantly, in measurements to date in *p*+*A* collisions both the entrance and exit channels have components that interact strongly, leading to severe complications in the theoretical treatment. In *p*+*A* collisions, these complications can be ameliorated by removing the strong interaction from the final state, using photons and Drell-Yan electrons. Beyond this, the possibility of using polarized protons at RHIC to probe saturation phenomena is just beginning to be explored [64], utilizing the large transverse single-spin asymmetries seen in *p*+*p* collisions at forward rapidity (which do not require a polarized ion beam) to explore the onset of saturation.

Observables sensitive to parton saturation: Till today the golden channel at RHIC to observe strong hints of saturation are di-hadron correlations. The STAR di-hadron correlation results from Run-8 are shown in Figure 4.19, it shows the (efficiency uncorrected) probability to find an associated $\pi^0$ given a trigger $\pi^0$, both in the forward region covered by STAR's Forward Meson Spectrometer (FMS). Shown is the coincidence signal versus azimuthal angle difference between the two pions in p+p collisions (left) compared to peripheral (center) and central d+Au collisions (right) [65]. The trigger and associated $p_T$ ranges are indicated in the figure. All the distributions present two signal components, surmounting a constant background representing the underlying event contribution (larger in *d*+Au). The near-side peak represents the contribution from pairs of pions belonging to the same jet. It is not expected to be affected by saturation effects, therefore it is a useful tool to check the effective amount of broadening in the away-side peak. This away-side peak represents the back-to-back contribution to the coincidence probability, which should disappear in going from *p*+*p* to d+Au if saturation sets in. The data show that the width of the near-side peak remains nearly unchanged from p+p to d+Au, and particularly from peripheral to central *d*+Au collisions. Central d+Au collisions show a substantially reduced away side peak that is significantly broadened. Shown in the right plot of Figure 4.19 is a comparison with theoretical expectations using the CGC framework. The calculation uses a fixed saturation scale $Q_s$ and considers valence quarks in the deuteron scattering off low-*x* gluons in the nucleus with impact parameter $b = 0$ [66,67].

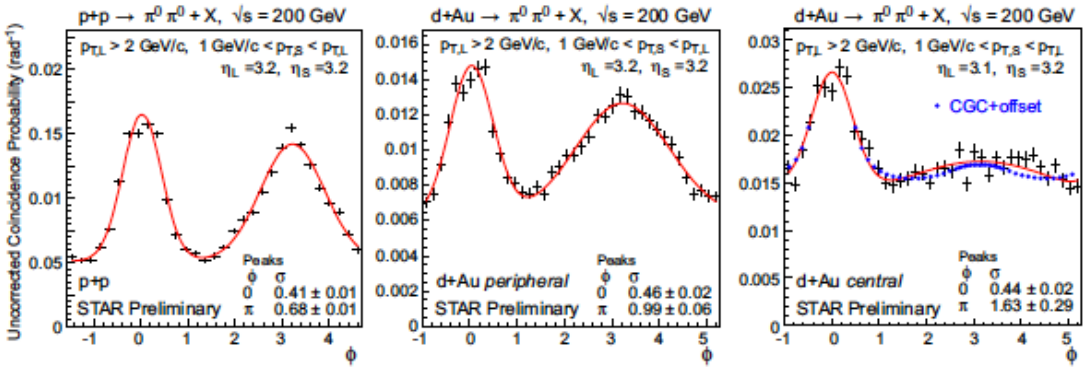


Figure 4.19 Uncorrected coincidence signal versus azimuthal angle difference between two forward neutral pions in p+p collisions (left) compared to peripheral (center) and central *d*+Au collisions (right) [31]. Data are shown with statistical errors and fit with a constant plus two Gaussian functions (in red). CGC expectations [66,67] have been superimposed (in blue) on the data for central *d*+Au collisions.

These data have been obtained from a sampled luminosity of 44 $nb^{-1}$. For an upcoming p+Au Run at RHIC the projection is 175 $nb^{-1}$/week after startup of the machine assuming a data taking efficiency of 70% and a run length of 5 weeks STAR could record 300 $nb^{-1}$. This would give the unique opportunity to vary the trigger and associated particle $p_T$ from low to high values and such crossing the saturation boundary as shown in Figure 4.18 and reinstate the correlations for central p+A collisions for forward-forward π0's (see Figure 4.19 right plot). At forward rapidities $\eta > 3$, $\pi^0$

cross section falls with $1/p_T^6$ so that to obtain the same statistical accuracy for $p_T^{trig}>3$ GeV a factor 11 in recorded luminosity would be needed. The requested 300 nb$^{-1}$ would give a factor of 6 increase in sampled luminosity, which together with the improved performance of the FMS and the STAR triggering, should make it possible to study the di-hadron correlations also at higher $p_T$ and such crossing the the saturation boundary. To conclude the investigation the suppression of di-hadrons at forward rapidities at RHIC are a clear sign of saturation, a high-statistics *A*-scan will be needed in the future.

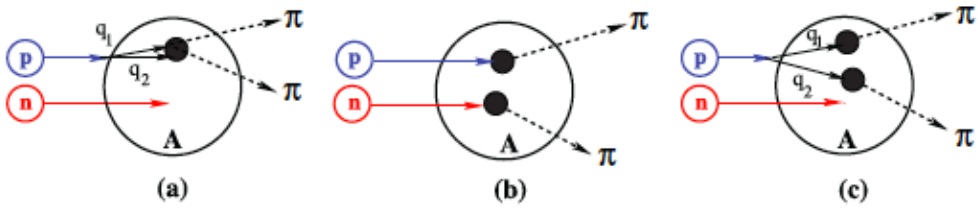


Figure 4.20: Contributions to two-pion production in d+A collisions through the double-interaction mechanism [68].

Studying di-hadron correlations in *p+A* collisions instead of *d+A* collisions has also the advantage that certain alternative interpretations can be ruled out. In reference [68], the authors point out that the contributions from double-parton interactions to the cross sections for $d+A \rightarrow \pi^0\pi^0X$ are not negligible. This mechanism is illustrated in Figure 4.20. They find that such contributions become important at large forward rapidities, and especially in the case for *d+A* scattering. Whether or not this mechanism provides an alternative explanation of the suppression of the away-side peak in $\pi^0$-$\pi^0$ is not settled. However, this new insight provides a strong argument for performing the proposed correlation studies in *p+A*, and not in *d+A* collisions. The higher luminosity in the upcoming 2015 p+A run will also enable to study more luminosity hungry processes, i.e. direct photon, photon – jet, photon - hadron correlations.

### *The gluon parton distribution function in the nuclear medium:*

The main emphasis of the 2015 and later *p+A* runs is to determine the initial conditions of the heavy ion nucleus before collision. Figure 4.21 [69] illustrates that our current understanding of nuclear parton distribution functions (nPDFs) is still very limited. The need to improve our knowledge on nPDFs is manifested in the Performance Milestone of Nuclear Physics DM18 (2012) "Determine gluon densities at low x in cold nuclei via p+Au or d+Au collisions"

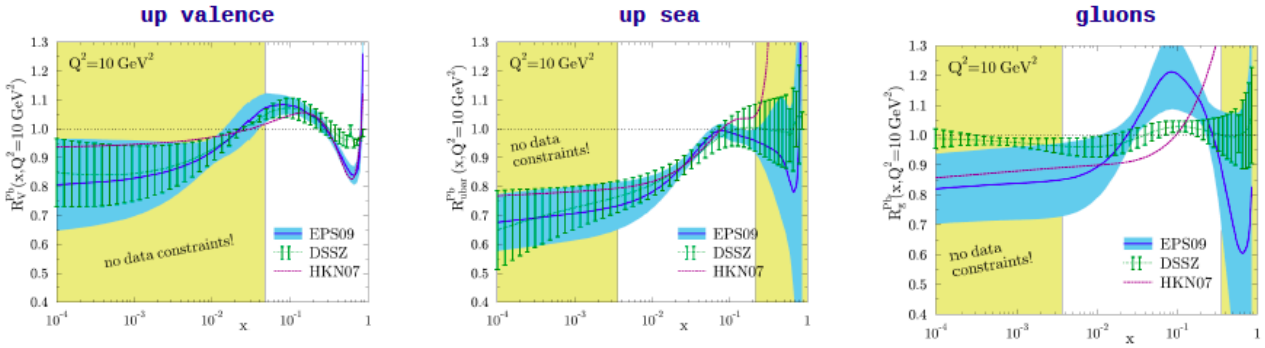


Figure 4.21: A summary of some of the most recent nPDFs. The central values and their uncertainties for up

valence, sea and gluons are shown. The yellow bands indicate regions in *x* where the fits are not constrained by data.

In measurements to date in d(p)+A collisions both the entrance and exit channels have components that interact strongly, leading to severe complications in the theoretical treatment. In d(p)+A collisions, these complications can be ameliorated by removing the strong interaction from the final state, using photons $W^{+/-}$, $Z^0$ and Drell-Yan electrons.
Direct photons are one of the key channels to separate strong interaction in the entrance and exit channels in d(p)+A collisions, because the have no strong interaction in the final state.
Figure 4.22 shows the $R_{pA}$ for direct photons in the rapidity range $3<\eta<4$ using the FMS and its pre-shower following an analysis as discussed in section 4.2.

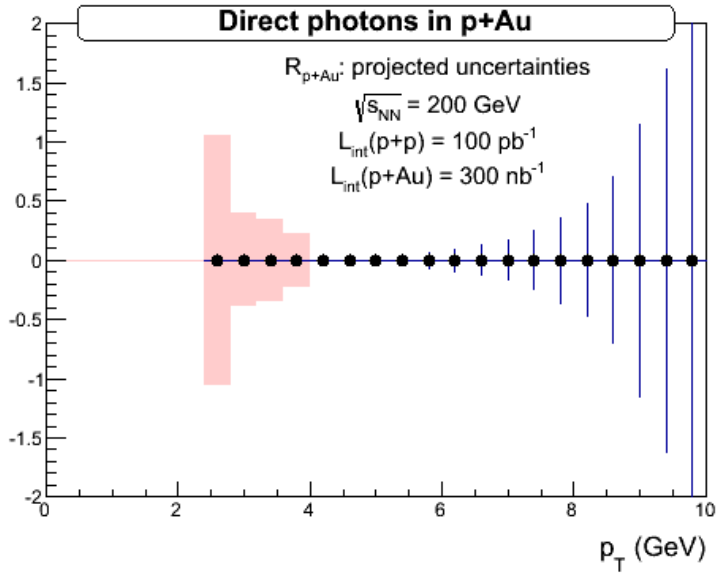


Figure 4.22: $R_{pA}$ for direct photons measured with the FMS and its preshower in the rapidity range $3<\eta<4$. The assumed detector performance and cuts applied are the same as for Figure . The statistical uncertainties are based on recorded luminosities of 100 $pb^{-1}$ for p+p and 300 $nb^{-1}$ for p+Au.
The systematic uncertainties are due to the remaining backgrounds (see Figure (left)).

*J/Ψ*-production in ultra-peripheral collisions (UPC) provides like direct photon measurements the unique opportunity if the J/Ψ is detected through its leptonic channel to study only the effects of strong interactions in the initial state. This measurement provides access to the spatial gluon distribution by measuring the distribution of dσ/dt. As follows from the optical analogy, the Fourier-transform of the square root of this distribution is the source distribution of the object probed. To study the gluon distribution in the gold nucleus, events need to be tagged were the photon is emitted from the proton. In UPC of heavy ions, the probability of an electromagnetic interaction is large with highly charged ions, but determining the momentum transfer from the grazing is experimentally not feasible due to extremely small scattering angles ($O(10^{-5})$ rad) at RHIC energies. Utilizing protons as a source for photons in p+A UPC will have an advantage since the kinematics of photons can be experimentally determined by reconstructing the scattered protons. To study STARs capabilities for such a measurement events were generated with the Sartre event generator [70,71], an p+A (e+A) event generator specialized for diffractive exclusive vector meson production based on the bSat dipole model [72] and its linearization, the bNonSat model [73]. In Figure 4.23 (left) the rapidity distribution for the *J/Ψ*-meson is shown for events the "UPC-photon" is emitted by the proton-beam, p-shine, and for events the photon is emitted by the Au-beam, Au-shine. To enhance the p-shine case the following cuts are applied:

- no hit in the ZDC to veto the Au-breakup to ensure coherent scattering.
- detecting the scattered proton in the RP ($-0.016 > -t > -0.2$ $GeV^2$)
- both J/ψ decay leptons are in $-1 < \eta < 4$

- cut on the $pt^2$ of the scattered Au, calculated as the $pt^2$ of the vector sum of the proton measured in the RP and the J/ψ to be larger than 0.02 GeV$^2$ (see Figure 4.23 right).

Figure 4.23 (middle) shows the resulting rapidity distribution for the *J/Ψ*-meson. The background from the Au-shine case has been suppressed basically completely. Unfortunately with an integrated luminosity of 300 nb$^{-1}$ only 1000 *J/Ψ*-mesons survive the cuts in the p-shine case. This statistics will not allow measuring dσ/dt for coherently produced *J/Ψ*-mesons. This distribution can be further used to obtain information about the gluon distribution in impact parameter space through a Fourier transform [74]. A high luminosity p+A run as discussed for the end of the decade will allow to measure g(x,Q$^2$,b) as function of A. In the 2015 p+A run the *J/Ψ*-meson rapidity distribution for both p-shine and Au-shine events can be measured and compared to models.

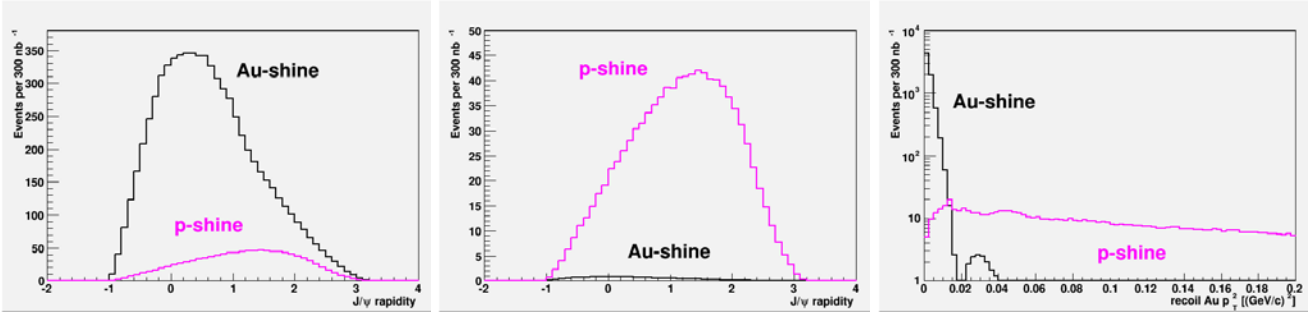


Figure 4-23: (left) Rapidity distribution for the *J/Ψ*-meson for p-shine and Au-shine events. (middle) Rapidity distribution for the *J/Ψ*-meson for p-shine and Au-shine events after applying all cuts listed. (right) $pt^2$ of the scattered Au, calculated as the $pt^2$ of the vector sum of the proton measured in the RP and the J/ψ.

### 4.5.2 Polarised observables

Single Transverse Spin Asymmetry in Polarized Proton-Nucleus Collisions: As a result of exciting recent theoretical developments, the scattering of a polarized proton on an unpolarized nuclear target appears to have the potential to extend and deepen our understanding of QCD. In the frame where the nucleus is relativistic, its wave function consists of densely packed quarks and gluons, which constantly split and merge with each other. At high enough energies the density of the gluons is so high that the saturation regime is reached, characterized by strong gluon fields and scattering cross sections close to the unitarity bound. The saturated wave function is often referred to as the Color Glass Condensate (CGC) and is reviewed in detail in [75].

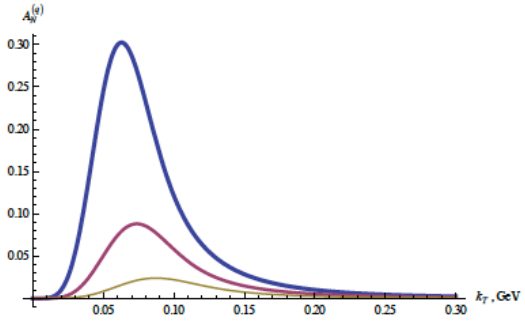


Figure 4-24: Quark SSA from Eq. (81) in [14] plotted as a function of $k_T$ for different values of the target radius: R = 1 fm (blue curve), R = 1.4 fm (red curve), and R = 2 fm (gold curve) for α = 0.7.

Scattering a polarized probe on this saturated nuclear wave function may provide a unique way of probing the gluon and quark transverse momentum distributions (TMDs). In particular, the single transverse spin asymmetry $A_N$ may provide access to the elusive nuclear Weizsaecker-Williams (WW) gluon distribution function [76], which is a solid prediction of the CGC formalism [77] but is

very difficult to measure experimentally. The nuclear effects on $A_N$ may shed important light on the strong interaction dynamics in nuclear collisions. While the theoretical approaches based on CGC physics predict that hadronic $A_N$ should decrease with increasing size of the nuclear target [78,79,80] (see Figure 4-24), some approaches based on perturbative QCD factorization predict that $A_N$ would stay approximately the same for all nuclear targets [81]. The asymmetry $A_N$ for prompt photons is also important to measure. The contribution to the photon $A_N$ from the Sivers effect [82] is expected to be non-zero, while the contributions of the Collins effect [83] and of the CGC-specific odderon-mediated contributions [84] to the photon $A_N$ are expected to be suppressed [79,85]. Clearly experimental data on polarized proton-nucleus collisions is desperately needed in order to distinguish different mechanisms for generating the single spin asymmetry $A_N$ in nuclear and hadronic collisions.

Figure 4-25 clearly shows that the requested statistics of 40 $pb^{-1}$ and 300 $nb^{-1}$ for p+p and p+Au, respectively, are sufficient to measure transverse spin observables in pA. The curves represent the theoretical prediction [79] for the suppression of SSA in the nuclear medium. This measurement will not only allow to get a handle on the saturation scale, but will also help to understand the underlying sub-process leading the big forward SSA in transverse polarized p+p. To distinguish further between the different theoretical models predicting a suppression of $A_N$ in p+A, it will be also essential to measure $A_N$ for direct photons. More details about the pre-shower in front of the FMS and its performance as well as the capabilities to measure $A_N$ for direct photons can be found in section 2.1.2.

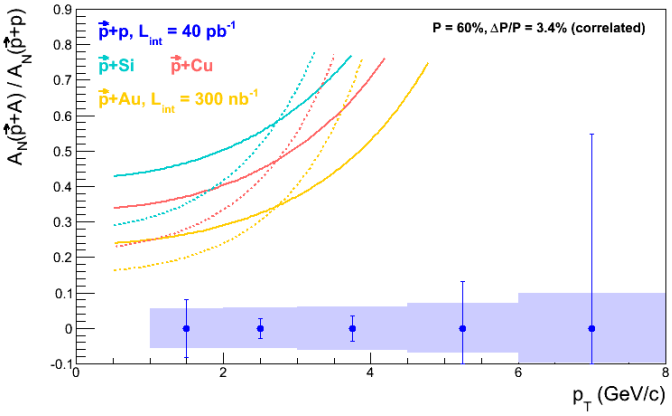


Figure4-25: The projected statistical and systematic uncertainties for the ratio of $A_N^{pA}/A_N^{pp}$ measured for $\pi^0$'s in the STAR FMS for the requested transverse p+p and p+A running. The colored curves follow Eq. 17 in Ref. [51] assuming $Q_s^p$ = 1 GeV (solid) and $Q_s^p$ = 0.5 GeV (dotted) with $Q_s^A = A^{1/3} Q_s^p$.

Access to the generalized parton distribution $E_g$: "How are the quarks and gluons, and their spins distributed in space and momentum inside the nucleon? What is the role of orbital motion of sea quarks and gluons in building the nucleon spin?" These are key questions, which need to be answered to understand overall nucleon properties like the spin structure of the proton. The formalism of generalized parton distributions (GPDs) provide till today the only theoretical framework, which allows some answers to the above questions [86]. The experimentally best way to constrain GPDs is through exclusive reactions in DIS, i.e., deeply virtual Compton scattering. RHIC with its possibility to collide transversely polarized protons with heavy nuclei has world-wide the unique opportunity to measure $A_N$ for exclusive J/ψ in ultra-peripheral $p^{\uparrow}$+Au collisions (UPC) [58,87]. A non-zero asymmetry would be the first signature of a non-zero GPD E for gluons, which is sensitive to spin-orbit correlations and is intimately connected with the orbital angular momentum carried by partons in the nucleon and thus with the proton spin puzzle. To measure $A_N$ for exclusive J/ψ in ultra-peripheral $p^{\uparrow}$+Au collisions provides an advantage in rate as the emission of the virtual photon from the gold nucleus is enhanced by $Z^2$ compared to ultra-peripheral $p^{\uparrow}$+p collisions. Detecting the scattered polarized proton in "Roman Pots" and vetoing the break-up of the

gold nucleus can ensure exclusivity of the process. The event generator SATRE [88], which also describes well the STAR results for $\rho^0$ results for UPC in Au+Au collisions, has been used to simulate exclusive J/ψ -production in $p^{\uparrow}$+Au UPC (see Figure 4-26 for the two contributing processes).

To select the J/ψ with the photon generated from the Au-beam cuts in the RP as installed for PHASE-II* need to be applied, at 200 GeV the RP PHASE-II* system has a *t*-acceptance from -0.016 GeV$^2$ to -0.2 GeV$^2$. Figure 4-26 shows the two processes generating a "UPC-photon" in pA. Figure 4-27 shows the probed $x$-$Q^2$ plane (left), if the photon is emitted by the gold beam and the *t*-spectra for the proton (right) for both processes generating the "UPC-photon". It can be seen that there is still some background coming from the case where the photon is emitted from the proton beam. The following cuts are applied:

- no hit in the RP phasing the Au-beam ($-t > -0.016$ GeV$^2$) or in the ZDC
- detecting the scattered proton in the RP ($-0.016 > -t > -0.2$ GeV$^2$)
- both J/ψ decay leptons are in $-1 < \eta < 4$
- cut on the $pt^2$ of the scattered Au, calculated as the $pt^2$ of the vector sum of the proton measured in the RP and the J/ψ to be less than 0.02 GeV$^2$

Figure 4-28 (left) shows the *t*-spectra for the proton and the rapidity distribution of the J/ψ -meson for both processes generating the "UPC-photon" after applying all the cuts. The background from the "proton-shine" events has been reduced significantly in the region of *t* accessible with the RPs. The final number of J/ψ's for a recorded luminosity of 300 nb$^{-1}$ is ~7k, which is enough to have a look to the $A_N$ as function of *t*. This measurement can be further improved with a high statistics p+A run in the later part of the decade and the high statistics p+p run in 2016.

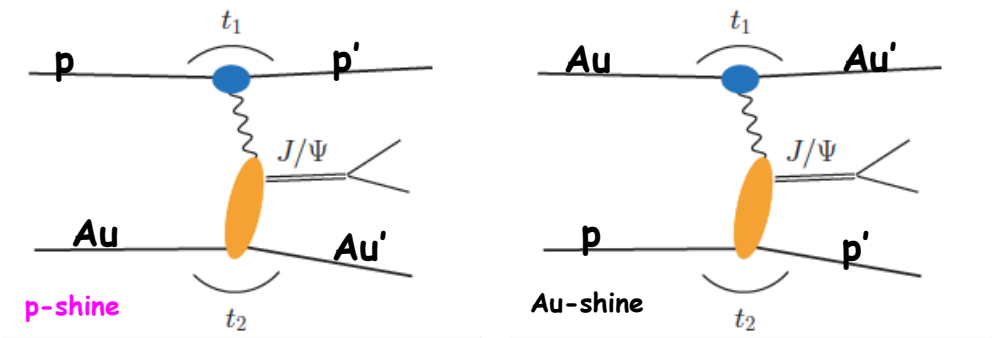


Figure 4-26: Possible processes to generate exclusive *J/ψ in* $p^{\uparrow}$+Au UPC in one case the photon is emitted by the proton beam, "p-shine" (left) in the other by the gold beam, "Au-shine" (right).

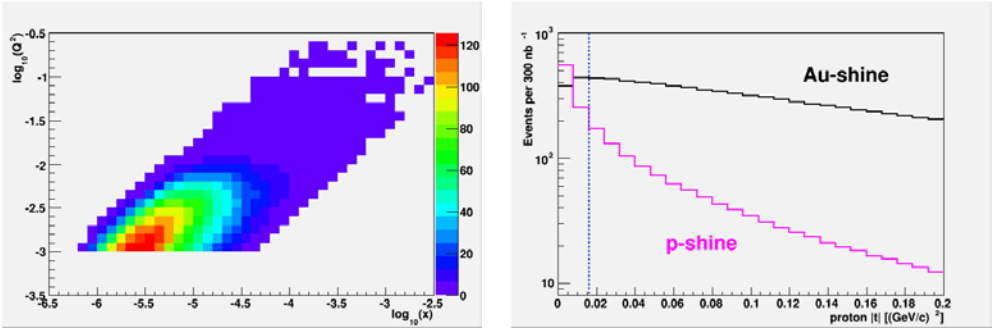


Figure 4-27: (left) The probed $x$-$Q^2$ distribution for Au-shine events. (right) The t-distribution for the proton for both event types. The vertical line indicates the start of the RP-acceptance.

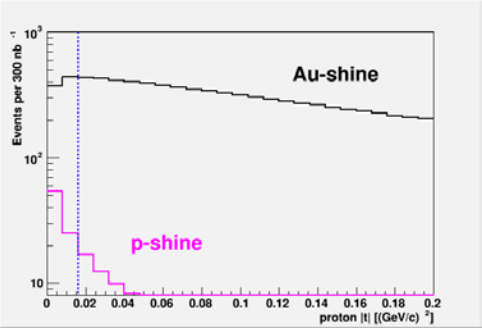


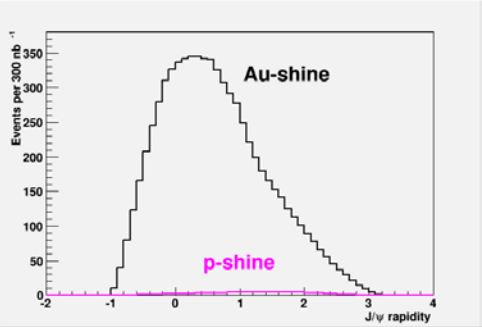


Figure 4-28: (left) The t-distribution for the proton for both event types after applying all cuts. The vertical line indicates the start of the RP-acceptance.
The J/ψ rapidity distribution for both events types after applying all cuts.

# 5. Run-16 Request

## 5.1 HFT Requests for Au+Au collisions in Run-16

In Run16, we are going to request a long Au+Au 200 GeV run to carry out the systematic measurements of heavy flavor hadrons with HFT and MTD. In particular, we are aiming for $\Lambda_c$ baryon and bottom hadrons through semi-leptonic channels as well as J/psi decays. We request a Au+Au 200 GeV run to collect 2B minimum bias good events with |Vz|<5cm and 1 $nb^{-1}$ sampled luminosity with EMC HT and dimuon triggers within |Vz|<5cm to perform these measurements.

The HFT-PXL detector planned for Run16 will be equipped with the Aluminum (Al) cable for inner ladders, while in the current Run14, most inner ladders are using Copper (Cu) cables. The material budget for an Al-cable ladder is reduced to about 0.37%X0 compared to 0.52%X0 for a Cu-cable ladder. This will significantly reduce the contribution from multiple columb scatterings to the pointing resolution, especially for low momentum particles, and thus improve the significance of reconstructed D0 mesons at low $p_T$. Figure 5.1 shows the significance ratio between the Al-cable and Cu-cable ladders for D0 mesons as a function of $p_T$. The improvement in the significant is about a factor of 1.6 for 1 GeV/c D0 mesons. In other words, the Figure-Of-Merit (FOM) statistics improvement with the same number of events in Run16 will be a factor of 2.5 for 1 GeV D0 mesons.

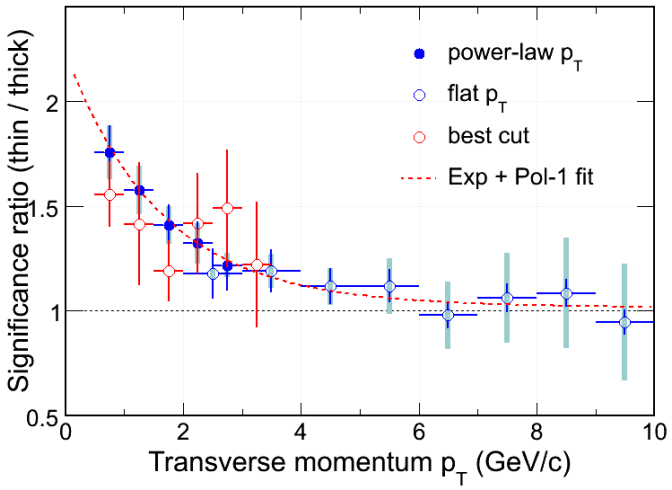


Figure 5.1 The ratio of $D^0$ meson significances between the Al-cable ladder (thin) and the Cu-cable ladder (thick) as a function of $D^0$ $p_T$ from simulation.

In addition, in Run16, we expect to have the SSD subsystem to participate the data taken in the full 200 GeV run period, while we don't have the SSD in the major HFT data collected in the current Run14. The SSD will improve the track matching and reduce the ghosting rate for the TPC tracks associating with the PXL hits. The improvement is about 10% for the single track efficiency with the additional SSD layer, thus effectively 20% in the D0-mesons reconstructed with two charged tracks.

We request to collect 2B minimum bias good events in Run16, compared to 1B goal in Run14. Therefore, the effective FOM increase considering the above detector configuration improvement is about a factor of 6 for low pT D0 when comparing Run16 with Run14. This is a significant improvement which will allow us to perform more differential studies on the charmed hadron

production including charm correlations. In the meantime, the improved statistics as well as the pointing resolution for low momentum tracks will make the $\Lambda_c$ measurement feasible ($c\tau$ of $\Lambda_c$ ~ 60 μm). Figure 5.2 shows the estimated statistical errors on the $\Lambda_c/D^0$ enhancement factor ($R_{cp}(\Lambda_c)/R_{cp}(D^0)$) for two scenarios: no enhancement and the same enhancement as Λ/Ks based on the 2B minimum bias data plus an additional 250M central triggered dataset. With these datasets, we will be able to distinguish these two scenarios with significance more than 3σ.

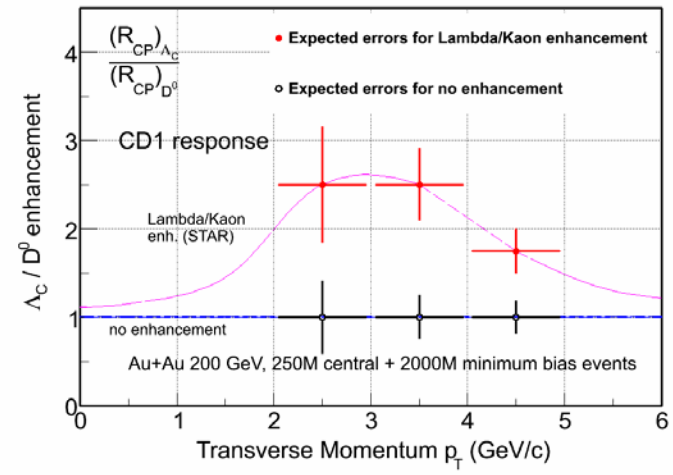


Figure 5.2 Statistical error estimation on the $\Lambda_c/D^0$ enhancement factor ($R_{cp}(\Lambda_c)/R_{cp}(D^0)$) measurement for two scenarios: no enhancement and the same enhancement as Λ/Ks with 2B minimum bias events and additional 250M central triggered events in Au+Au 200 GeV.

To collect 2B minimum bias data within 14 weeks requires a DAQ recording rate of 600 Hz for good minimum bias events and 70 HFT DAQ hours per week. To reach this DAQ rate, we would need the online VPD Vz resolution to be ~ 1cm or better. Compared to the 3.5 cm resolution in central collisions achieved in Run14, this improvement will increase the good event purity of the trigger events using the online Vz cut from 60% now in Run14 to more than 95% in Run16. A proposal to improve trigger electronics for this purpose has been approved by STAR Collaboration. The 600 Hz tape recording rate would require 800-900Hz L0 rate if we run the same protection configuration for the minbias trigger as Run14, which is achievable. The 70 DAQ hours with HFT per week would require the CAD to optimize the beam luminosity profile for STAR for the HFT running. If the analysis from run14 dataset shows effective construction without pile-up protection and the complete set of HFT can take data effectively through the whole fill, we may be able to reach our target goal of 2 billion events within a 10-week run.

Another important goal in Run16 is to sample sufficient luminosity ($1nb^{-1}$ within |Vz|<5cm) with the HFT for the measurements of bottom production. We expect the 56MHz RF will be fully commissioned in Run14 and become operational in Run16. This will improve the luminosity fraction within |Vz|<5cm from 8% so far in Run14 to about 15% in Run16. With the optimized beam luminosity profile, assuming 60% uptime for the STAR trigger and DAQ and the HFT can take 60% of the total available luminosity in the store, we should be able to reach the goal of $1nb^{-1}$ sampled luminosity within |Vz|<5cm within 14 weeks. The physics datasets will be collected through the dimuon trigger from the MTD to measure the displaced J/psi's from bottom decays and the single HT trigger from the EMC to measure the single electrons or dielectrons to form the displaced J/psi's.

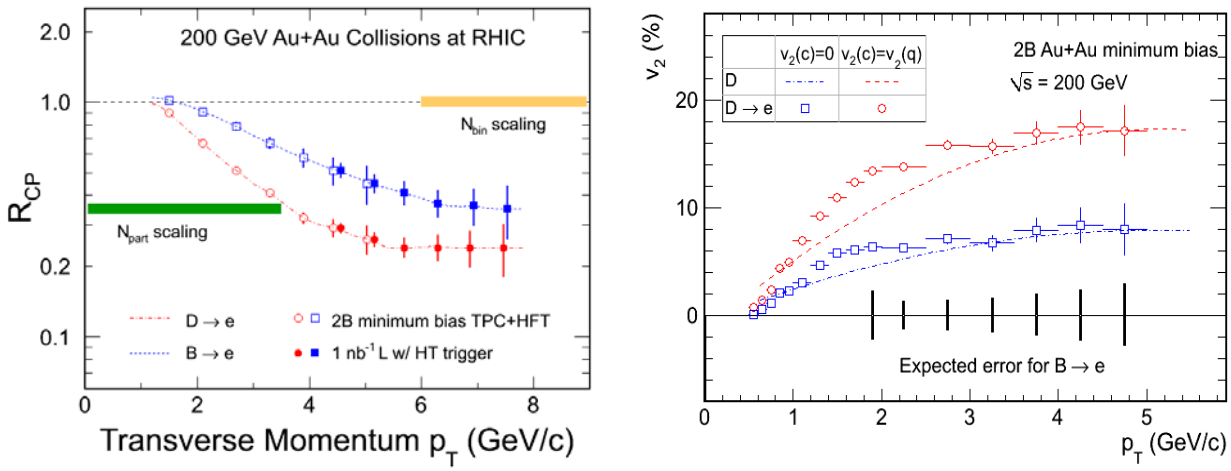


Figure 5.3 (Left) ) Projected statistical uncertainties for the $R_{CP}$ of electrons from charm and bottom decays separately with HFT. The estimate is based on 2B minimum bias event sample plus 1 nb$^{-1}$ sampled luminosity with HT triggers collected within $|V_z|<5$cm. (Right) Projected statistical uncertainties for charm and bottom decay electron $v_2$ with 2B minimum bias events.

### 5.2 High Luminosity Quarkonia program

A large-area and cost-effective Muon Telescope Detector (MTD) at mid-rapidity was fully installed at STAR for Run 14. The Time-of-Flight system it utilizes is based on multi-gap resistive plate chambers with precise timing and hit position. Among many exciting perspectives, we will be able to collect a large sample of *J/ψ* events for spectra and elliptic flow measurements (Figure 5.5left plot), to separate different Upsilon states (Figure 5.5 right plot) with a clear advantage over electron decay channels due to the reduced Bremsstrahlung radiation and Dalitz decay background, and to provide a unique measurement of $\mu-e$ correlations from heavy-flavor decays.

The open charm production rate is high enough at RHIC that the coalescence process becomes relevant for charmonium production. Knowledge of the total production cross-section for charm quarks is also essential as a baseline for J/ψ measurements. From a precise measurement of the spectra and the production ratios of charm hadron states, we will be able to extrapolate to the total yield for charm quark production. A unique advantage of STAR due to its full azimuthal coverage is the detailed studies of charm-charm correlations. The angular correlation will be modified in heavy ion collisions due to the interactions between the heavy quarks and the medium. Measurements of the direct D-Dbar and e-μ correlations are sensitive to the effect of 'partonic wind' on charm quark correlations in high-energy nuclear collisions and the thermalization in high-energy nuclear collisions. Meanwhile, the semi-leptonic decays of heavy-flavor pairs are important component of dilepton spectra. Only such correlation measurements can provide experimental tool to separate QGP thermal radiation from the heavy-flavor decays in the dilepton spectra.

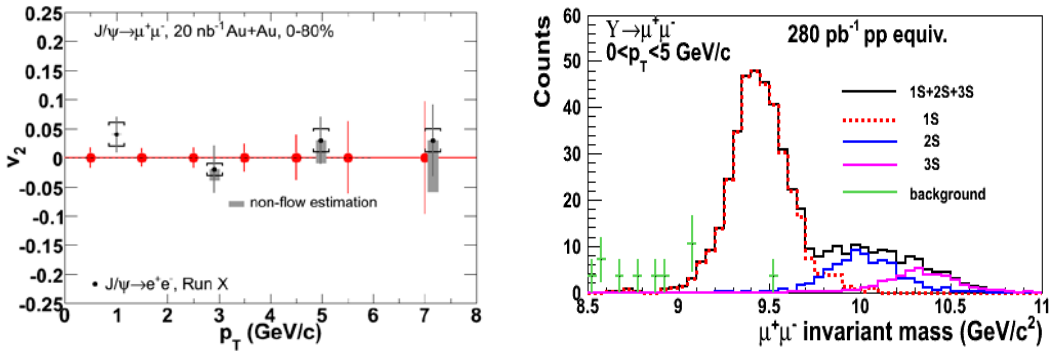


Figure 5.5: (Left) Projection of J/psi (from muon pairs) $v_2$ measurement from MTD. Data with error bars are from [13]. (Right) Projected Upsilon line-shapes of the 1S, 2S and 3S states and backgrounds measured in the MTD from 280 $pb^{-1}$ Au+Au collisions at RHIC.

Measurements of the in-medium dissociation probability of the different quarkonium states are expected to provide an estimate of the initial temperature of the system. Dissociation of quarkonium in a thermal QCD system would ultimately provide evidence of color screening and free quarks. The $J/\psi$(1S) is the lightest and most abundantly produced quarkonium state accessible in experiment. However, significant decay contributions from excited states and the final state production via coalescence complicate the situation. $\Upsilon$ (1S, 2S, 3S) states provide a natural thermometer since they are bottomia of three consecutive states. The ground state has a binding energy of 1.1 GeV and is way above the temperature reached at RHIC. However, the 2S and 3S states have binding energy at 0.54 and 0.2 GeV, respectively, and can be dissolved at RHIC. MTD provides the measurements allowing separate these three states at RHIC through the di-muon channel. The separation is made possible by MTD with reduced Bremsstrahlung radiation and enhanced trigger capability. Comparison of low-$p_T$ $J/\psi$ and $\Upsilon$ yields at RHIC and LHC and study of the $J/\psi$ azimuthal anisotropy could quantitatively further constrain the model interpretation. These requirements call for a comprehensive experimental quarkonium program at RHIC. The combined measurements by HFT and MTD from STAR offer a unique and comprehensive heavy flavor program to explore these exciting physics opportunities.

A transition to a different state is not only characterized by the increase of temperature, but also by the changes of degree of freedom and symmetries. The long-sought signature of such a transition is chiral symmetry restoration. The experimental procedure of detecting signature related to the restoration is to study the in-medium dilepton decay of vector mesons. The spectral function from the remnant hadronic structure should transit to a smooth spectrum of QGP thermal radiation with increasing temperature and density. Great progress has been made in the last decade at SPS and RHIC. It has been experimentally demonstrated that the hadronic spectral function has been greatly modified in the medium. However, a quantitative assessment of its temperature dependence is absent. This requires consistency between thermal radiation at high temperature (dominant at RHIC) and modified hadronic decay (dominant at SPS) close to the phase transition. At RHIC energies and above, such dilepton measurements are hindered by the dominant “irreducible” background from semileptonic decay of open heavy-flavor pairs. STAR has demonstrated its unique capability of di-electron measurement with the combination of large-coverage TPC, EMC and TOF. With HFT and MTD upgrades, contribution to the dilepton spectra from the open heavy-flavor pair correlation is measurable with D-Dbar and e-μ correlation measurements all at mid-rapidity.

**5.2.1 Run-16 requests:** Run 14 started the physics program with the full MTD. The primary focus of this MTD run is on Quarkonia at RHIC energies, using muons to remove the issue of Bremsstrahlung tails in their line-shapes. This is most important in the separation of the Upsilon 1S from the (2S, 3S) states, all three of which are expected to be suppressed differently in the QGP. We expect to sample 12 $nb^{-1}$ 200 GeV Au+Au luminosities in Run 14 for Upsilon measurements. We would like to request to sample at least 8 $nb^{-1}$ 200 GeV Au+Au luminosities in Run 2016 to complete the goal. Figure 5.6 shows a projected line-shape with the MTD, showing that the 1S can be clearly separated from the 2S+3S, while the 2S and 3S can be separated statistically assuming a large statistics sample and good control over the line-shape. Table 5.1 shows an estimate for the required luminosity for measurements of the 2S+3S and the 3S separately. A measurement at p+p collisions at 510 GeV will provide an important check on the systematics of the yield ratios extrapolated from other energies. Figure 5.6 shows the projected $R_{AA}$ for all the three separated states, taking into account the p+p reference from the average of the world data.

| **Collision system** | **Mini. lumi. for 10% uncertainty on ϒ(3S)** | **Mini. lumi. for 10% uncertainty on ϒ(2S+3S)** |
|---|---|---|
| p+p 510 GeV | 140 $pb^{-1}$ | 50 $pb^{-1}$ |
| Au+Au 200 GeV | 10 $nb^{-1}$ | 3.8 $nb^{-1}$ |

Table 5.1: Estimated luminosities for ϒ(2S, 3S) measurements.

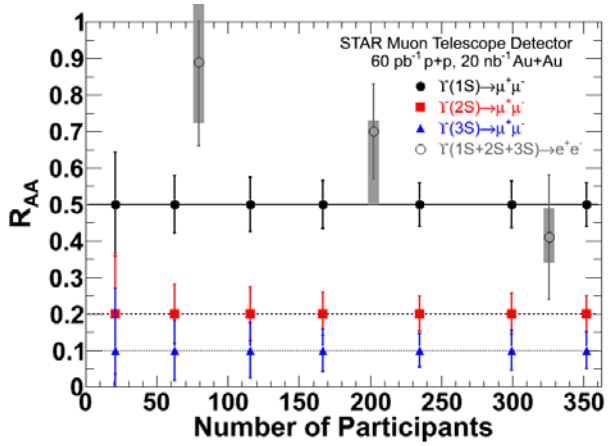


Figure 5.6 : Projected errors on $R_{AA}$ of Upsilon 1S+2S+3S measured by the STAR MTD from the 20 $nb^{-1}$ Au+Au and 60 $nb^{-1}$ p+p collisions (reference data).

The STAR MTD allows for the measurements of electron-muon correlations, where the electron and muon are both measured at mid-rapidity. The dominant source of these correlations at intermediate mass is from the decay of charm-anticharm pairs, since in thermal production of dilepton pairs electrons are paired with positrons, and muons with antimuons.

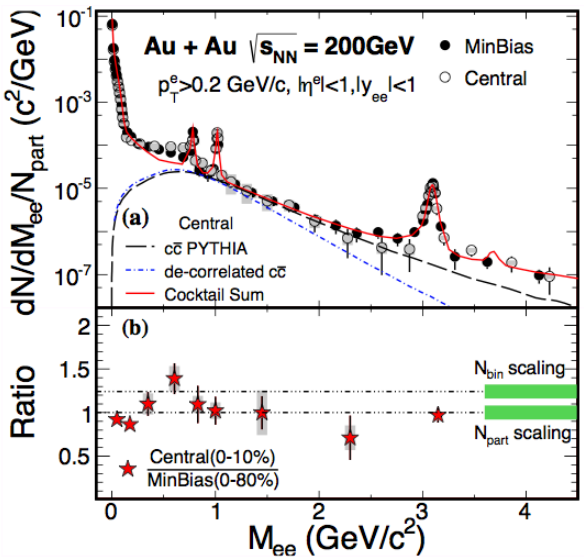


Figure 5.7: Central and minimum bias di-electron invariant mass distributions normalized by $N_{part}$, from Run 10 Au+Au collisions. Black line shows the cocktail contribution from fully correlated charm-anticharm pairs, assuming a cross section of 0.80 mb. Blue line shows the contribution if charm is angularly decorrelated and momentum distributions softened to match non-photonic electron $R_{AA}$.

Figure 5.7 shows the existing minimum bias and central di-electron pair invariant mass distributions normalized by $N_{part}$. According to the cocktail, the correlated charm contribution dominates the contribution in the intermediate mass range from 1 to 3 GeV/$c^2$. In this figure, the correlated charm contribution is from PYTHIA, assuming no decorrelation in medium and rescaled to match a charm cross section of 0.8mb. Both of these assumptions introduce a large uncertainty, due to the possibility of charm energy loss and decorrelation in the medium, both of which would decrease the contribution in this mass range. There are hints of suppression in central as compared to minimum-bias data. This uncertainty prevents the extraction of any signal from QGP radiation, which in the absence of decorrelation is approximately an order of magnitude below the charm contribution. The only way to make progress is to directly measure the correlated charm contribution in heavy ion collisions: electron-muon correlations provide one method to do so.

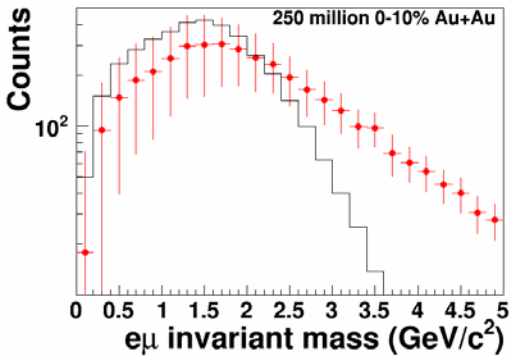


Figure 5.8: Projected electron-muon invariant mass distribution from 250M top 10% central Au+Au events with full MTD coverage. Red points assume full correlation and momentum distributions from PYTHIA while the black histogram assumes full decorrelation and softening of the charm momentum distribution to match non-photonic electron $R_{AA}$.

In Run 12 p+p collisions at $\sqrt{s}$ =200 GeV STAR established that we can trigger on electron-muon pairs with one leg in the MTD and the other leg in the Barrel Electromagnetic Calorimeter (BEMC) at a transverse energy threshold of 1.9 GeV. This was a very clean trigger, running at prescale 1

with a very low rate (~10's of Hz) in the p+p collisions. The total sampled luminosity in run 12 was 23 $pb^{-1}$. However, in Run 14 Au+Au collisions at $\sqrt{s}$ =200 GeV, the trigger on transverse energy threshold of 1.9 GeV was not effective. Instead, we triggered on electron-muon pairs with one leg in the MTD and the other leg in the BEMC at a transverse energy threshold of 3.0 GeV. We expect to sample 3 $nb^{-1}$ 200 GeV Au+Au luminosities in Run 14 for this trigger, which will enable us to do first electron-muon azimuthal correlation measurements in heavy ion collisions. In Run 2016, we can also sample a fraction of the delivered luminosity with a central trigger, which enables the kinematic cuts to be relaxed to allow for lower energy electrons, identified via the ToF and TPC dE/dx. Figure 5.8 shows the projected uncertainty in the electron-muon invariant mass distribution for 250 M central 0-10% Au+Au events, assuming the PYTHIA fully correlated charm contribution. For comparison, the black histogram shows the maximal reduction in the distribution, assuming full angular decorrelation and suppression of the charm singles distribution following measured non-photonic electron $R_{AA}$. The proposed measurement can clearly distinguish this extreme scenario from the fully correlated PYTHIA scenario. The downside of such triggered datasets is that they select specific regions of the invariant mass vs. $p_T$ plane, and so need detailed comparisons with unbiased data and simulations under energy loss scenarios to interpret correctly.

### 5.3 Long-range rapidity correlations and flow in Au+Au collisions with forward Calorimeter

While the STAR detector has excellent capabilities of detecting particles at midrapidity, an upgrade of hadronic calorimeters with azimuthal granularity in the forward rapidity region is highly valuable, and will significantly enhance STAR's competitiveness to other experiments at RHIC. This has been unambiguously demonstrated by recent results from the LHC experiments. As an example, the forward hadronic calorimeter (HF) at CMS is the only detector component used in all CMS heavy ion publications so far, which cover the pseudorapidity range 2.9 < |eta| < 5.2.The HFs at CMS have been playing a crucial role in several important areas of the heavy ion program: **Minimum bias trigger, event selection; Centrality determination and trigger; Event plane determination.** Installing forward hadronic calorimeters in STAR as early as in 2016 will significantly benefit STAR heavy flavor program in determining charm meson $v_2$ with minimum non-flow contamination. With a high luminosity AuAu run, azimuthal anisotropy $v_2$ of high $p_T$ jets or hadrons can also be determined more precisely using forward EP angle, which will provide much better constraints on path length dependence of jet quenching at RHIC.

The HCal will help maintain the ability of STAR to study long range azimuthal correlations in 200 GeV Au+Au collisions. The correlations that give rise to the ridge and to v3 in heavy ion collisions are thought to arise mostly from the geometry of the initial overlap region. The extent to which those initial state correlations are manifested in the final state as v2 or v3 can provide an estimate of the viscosity of the Quark GluonPlasma. v3 however is known to depend on the pseudo-rapidity interval over which it is measured[89]. The longitudinal width of v3 and the correlation function provides a clear indication of the period when the correlation was established with longer range correlations coming from early phases of the evolution. By measuring correlations over a wider pseudo-rapidity interval, we can disentangle correlations that arise from different phases of the systems evolution and make a more reliable estimate of the transport properties of the QGP like viscosity.

### 5.4 Transversely polarized p+p running at $\sqrt{s}$ = 510 GeV

#### 5.4.1 Mid-rapidity $A_N$ for W-boson production

In addition to the physics motivations already discussed in section 2.1.2 and 4.2 there are two very basic questions in transverse spin physics, for which finding answers will be of fundamental interest for QCD. One is the question about the evolution of transverse dependent parton distribution functions and fragmentation functions, which is different from the well-known evolution following DGLAP [90]. The other important aspect is the process dependence and the color gauge invariance of the Sivers function. In SIDIS, the quark Sivers function is manifested in association with a final state effect from the exchange of (any number of) gluons between the struck quark and the remnants of the target nucleon. On the other hand, for the virtual photon production in the Drell-Yan process, and the $W^{\pm}$, $Z^0$ Boson production, the Sivers asymmetry appears as an initial state interaction effect. As a consequence, the quark Sivers functions are of opposite sign in these two processes and this non-universality is a fundamental prediction from the gauge invariance of QCD. The experimental test of this sign change is one of the open questions in hadronic physics and will provide a direct verification of QCD factorization. The transverse single spin asymmetries for direct photon production provide also access to this sign change through the Twist-3 formalism. The importance of measuring this sign change is also reflected in the fact that it was made a HP performance measure, HP13 (2015). The COMPASS experiment at CERN is pursuing this sign change using a pion beam and new initiatives have been proposed e.g. at FNAL.
As already discussed in section 2.1.2 STAR was able in a pilot run with transverse polarized p+p collisions at $\sqrt{s}$=500 GeV to measure the transverse single spin asymmetries $A_N$ for fully reconstructed $W^{\pm}$, $Z^0$ Bosons based on a recorded integrated luminosity of 25 $pb^{-1}$. Figure 5.9 shows the most up-to-date theoretical predictions for the transverse single spin asymmetries for $W^{\pm}$, $Z^0$ Bosons from reference [44] including TMD-evolution.

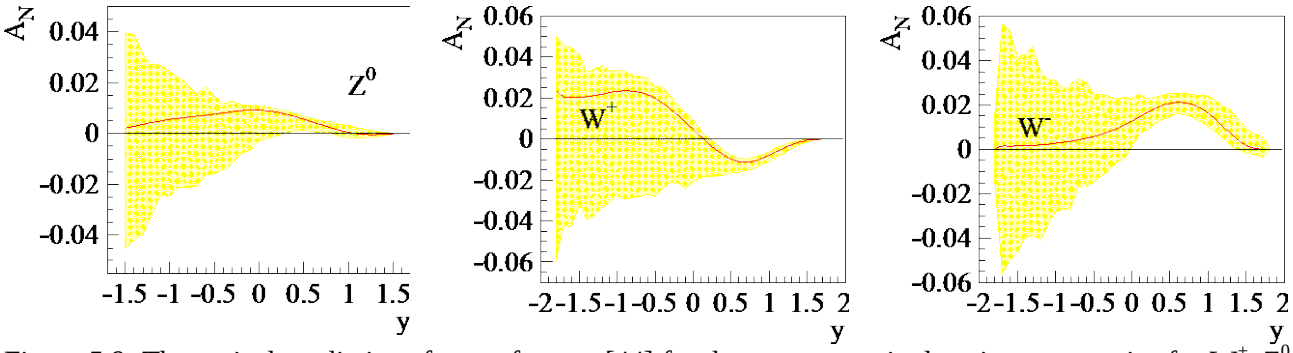


Figure 5.9: Theoretical predictions from reference [44] for the transverse single spin asymmetries for $W^{\pm}$, $Z^0$ Bosons for 0 GeV $< p_t <$ 3 GeV. The yellow bands represent the uncertainties for the asymmetry due to the unknown sea quark Sivers function.

The production of $W^{\pm}$ bosons at $\sqrt{s}$=500 GeV provides an ideal tool to study the spin-flavor structure of sea quarks inside the proton. The left-handed W boson only couples to (anti)quarks of a certain helicity, giving rise to large parity-violating single spin asymmetries in polarized p+p collisions at RHIC. In addition, the coupling of the W's to the weak charge correlates directly to quark flavor. Ignoring quark mixing, $W^{\pm}$ bosons are produced through $u+\bar{d}(d+\bar{u})$ interactions. A measurement of the transverse single spin asymmetry will provide the world wide first constraint on the sea quark Sivers function in a *x*-range, where the measured asymmetry in the $\bar{u}$ and $\bar{d}$ unpolarized sea quark distribution functions, as measured by E866 [91], can only be explained by strong non-pQCD contributions. Of course the same measurement is also able to access the sign change of the Sivers function. Figure 5.10 shows the projected uncertainties for transverse single spin asymmetries of $W^{\pm}$, $Z^0$ Bosons as function of rapidity and $p_T$ for a delivered integrated luminosity of 400 (900) $pb^{-1}$ and an average beam polarization of 55%. The 400 (900) $pb^{-1}$

correspond to 7 (14) weeks running and a dynamic β* squeeze through the fill. The dynamic β* squeeze provides a factor 2 increase of the luminosity in a fill as the luminosity profile through the fill is kept flat.

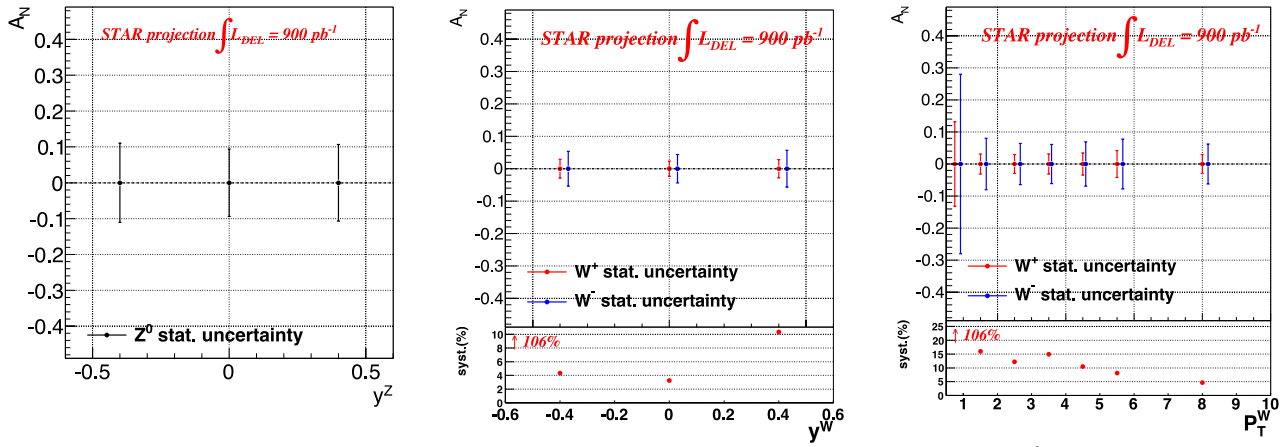


Figure 5.10: The projected uncertainties for transverse single spin asymmetries of $W^{\pm}$, $Z^0$ Bosons as function of rapidity and $p_T$ for a delivered integrated luminosity of 400 (900) $pb^{-1}$ and an average beam polarization of 55%.

A high statistics run at √s = 510 GeV in combination with the existing Run-12 data sample at √s = 200 GeV and the proposed √s = 200 GeV measurements in Run-15 gives the possibility to study the TMD evolution through the following processes:

- Interference fragmentation
- $A_N$ for direct photons
- $A_N$ for jet observables sensitive to the Sivers fct or transversity times Collins FF

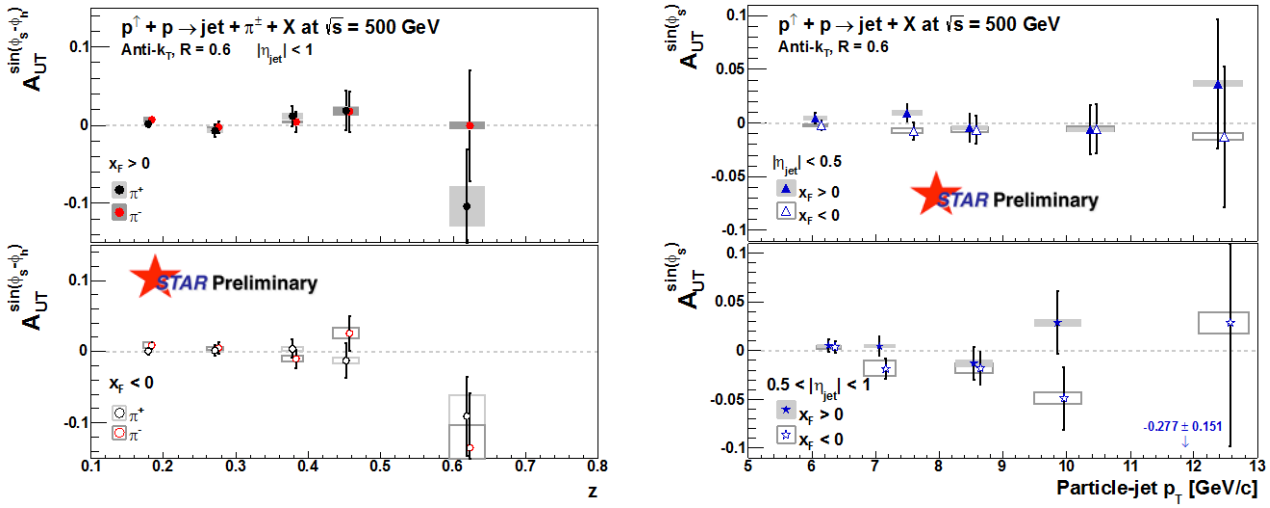


Figure 5.11: Transverse single spin asymmetries for hadron–jets (left) sensitive to the Collins mechanism and inclusive jets (right) sensitive to the sivers mechanism at √s=500 GeV from Run-11 (25 pb-1).

Figure 5.11 shows the transverse single spin asymmetries for hadron–jets (left) sensitive to the Collins mechanism and inclusive jets (right) sensitive to the Sivers mechanism for gluons at √s=500 GeV from Run-11 (25 $pb^{-1}$). A high luminosity run will provide the possibility to have enough statistics to test if the trends seen in the Collins-like jets at high *z* persist with higher luminosity as well as to make a high precision measurement of the gluon Sivers function in the Twist-3 formalism

through $A_N$ for inclusive jets. The uncertainties shown in Figure 5 will shrink by a factor 4 with the proposed Run-16. This measurement will be completely complementary to the results by the $A_N$DY collaboration done at $\sqrt{s}$=500 GeV for $\eta$>3 [92].

Transverse single spin asymmetries in direct photon production provide a different path access to this sign change through the Twist-3 formalism. Figure 5.12 right shows the statistical and systematic uncertainties for the direct photon $A_N$. The asymmetry can be measured up to $x_F \sim 0.7$ where the $\pi^0$ asymmetries are largest. Figure 5 left shows the level of achieved background suppression for charged particles as well as photons from decays, i.e. $\pi^0$, using the forward meson spectrometer (FMS) and its preshower following the analysis technique described in section 4.2.

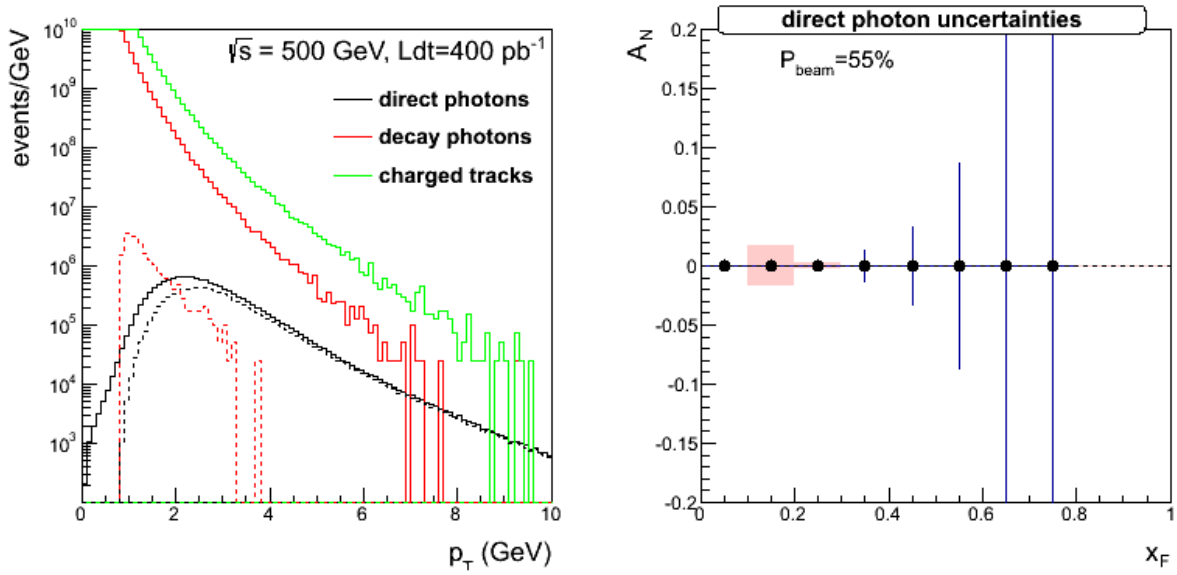


Figure 5.12: (left) The number of events at $\sqrt{s}$=500 GeV for a delivered luminosity of 400 pb$^{-1}$ for direct photons, charged hadrons and photons from decays, i.e. $\pi^0$ before (solid) and after (dashed) detector responses have been applied. (right) Statistical and systematic uncertainties for the direct photon $A_N$ after background subtraction.

STAR's capability to measure $A_N$ for direct photons, for $W^{\pm}$ and $Z^0$ bosons, and possibly for DY will provide the world-wide unique opportunity to simultaneously test TMD evolution, access the Sivers function for sea quarks, and test the predicted sign-change for the Sivers function with three different processes for two different theoretical approaches. It offers a viable path to address performance measure HP13 at RHIC.

# 6. Detector and Upgrades relevant to BUR

## 6.1 The Phase-II* Upgrade of the Roman Pots around STAR

In their 2011 report the PAC recommended that a solution is found to run the physics program with tagged forward protons under normal conditions or concurrently with the rest of the RHIC program. Thus to enable measurements like diffraction in p+p and p+A, the Roman Pots are required to be relocated to the DX-D0 region. To stage the cost of the full implementation of this upgrade an intermediate phase-II* in Run 15-16 will be realized as described below:
Roman Pot in STAR Phase-I, Phase-II* and Phase-II:

- Current configuration (Phase-I): two horizontal (at 55.5m) and two vertical (at 58.5m) Roman Pots (RPs) each in outgoing Yellow and Blue beam (Detector: 75x45mm$^2$) [data taking in Run-9]
- **Phase-II*:** reconfiguration of Phase-I detectors. Two vertical RP each at ~15.8 m and at ~17.6 m (Detector: Phase-I detector) [installation in 2014, data taking ready for Run-15]
- Phase-II: two vertical + one horizontal and two vertical and one horizontal RPs each (new Si-Detector: 100x70mm$^2$)

A schematic layout of Phase-II* is shown in Figure and Figure.

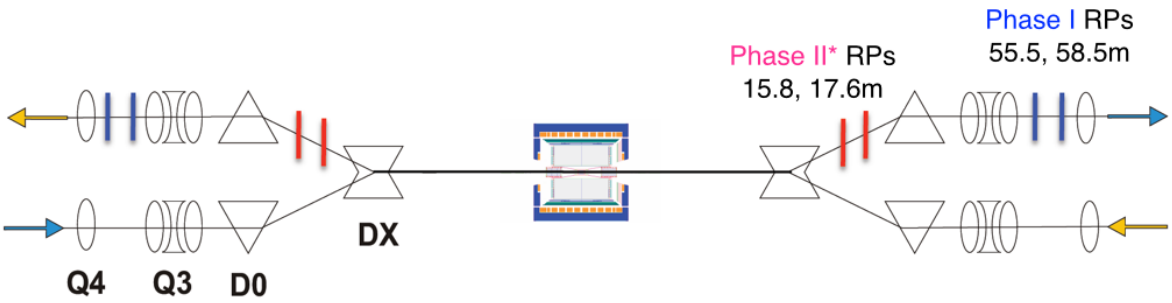


Figure 6.1: The layout of the RPs with the STAR detector (not to scale). The Phase-I RPs setup to detect scattered protons with low-*t* are located after two dipole magnets (DX, D0) and three quadruples at 55.5 m and 58.5 m from the interaction point (IP), respectively. For measuring protons with higher-*t* (Phase-II*), sets of RPs will be positioned between DX and D0 magnets, at 15.8 m and 17.6 m from IP.

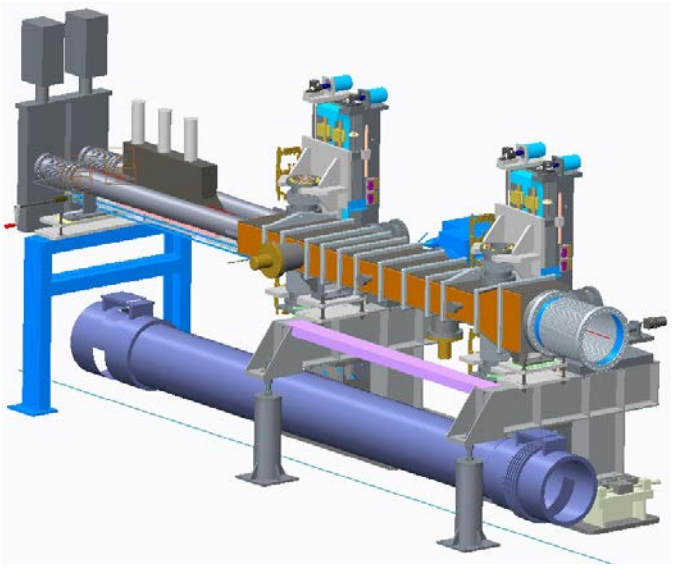

Figure 6.2: Layout of the design of the new DX-D0 chamber showing the Roman Pot stations. They will be installed in 2014.

Phase-II* has comparable *t* acceptance till 0.8 $GeV^2$ as Phase-II, for physics studies at high t the full Phase-II needs to be realized. The design and location of Phase-II* identified in collaboration with the CAD experts, allows the full implementation of Phase-II at a latter time. To have Phase-II* realized for Run-15 the design of the vacuum pipe needs to be finalized this summer, such that parts can be order and fabricated in time that the installation of the new vacuum chamber and the Roman Pots can be realized in the shutdown summer 2014.
The Roman Pot detectors used for the pp2pp experiment [93] and STAR Run-9 [94] installed in the location of Phase-II*, will be used to tag very forward protons, thus selecting processes, in which the proton stays intact.

## 6.2 A Preshower for the FMS

STAR is building a preshower detector in front of the FMS, which will help distinguish photons, electrons/positrons and charged hadrons. This detector will be comprised of two layers of perpendicularly arranged scintillator slats (PS1 and PS2), followed by a lead converter and a subsequent third layer of scintillator slats (PS3). PS1 and PS2 will be used to identify neutral particles (photons) from charged particles (hadrons and electrons), while PS3 after the converter will help separating electromagnetic showers (photons and electrons) from charged hadrons.
The preshower detector will be located in front of the FMS at a little less than 7 m downstream of the nominal interaction point in STAR and will cover a transverse area of about 2x2 $m^2$ with a 40x40 $cm^2$ cutout in the center for the beam pipe. The preshower layers will be divided into quadrants. The detector will be segmented to ~80 scintillator slats per layer, and the granularity of the array is going to match that of the FMS loosely as indicated in Figure .

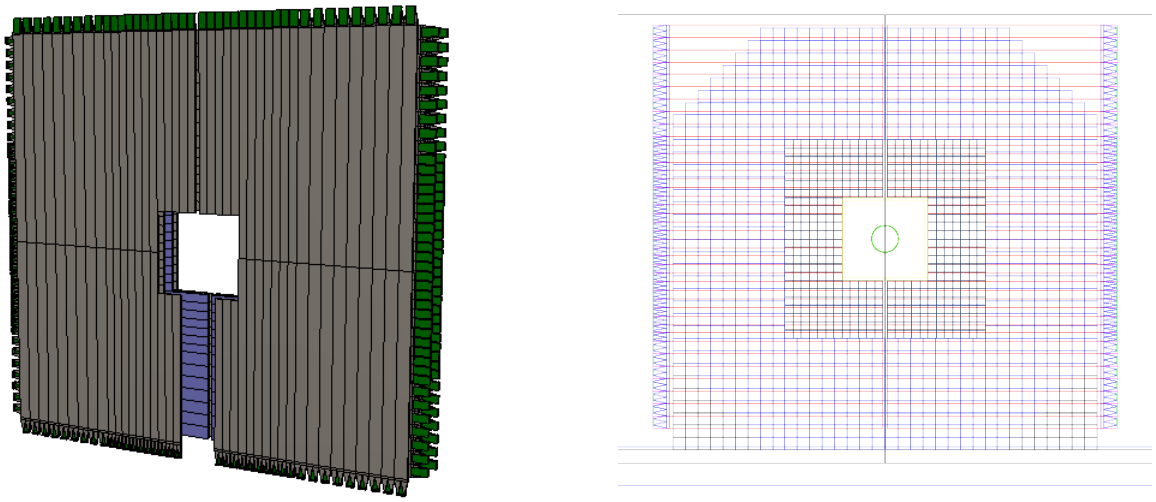

Figure 6.3: Geometry of the layers of a preshower detector in front of the FMS electromagnetic calorimeter in STAR. Left: Layered setup of scintillators (grey) with a Pb converter (blue) and SiPM and FEE board (green). Right: Matching of granularity of preshower (layer 3, red) with the tower size of the FMS (black and blue).

Due to up to 400 gauss of magnetic field from the STAR solenoid magnet, SiPMs (MPPC) were chosen for the readout instead of conventional PMT. The scintillation light from a scintillator slat will be read out by two 3x3mm Hamamatsu S12572-050P (PS1 & PS2) and S12572-025P (PS3) MPPC (SiPM), which will be mounted on a FEE board and attached to light guides at the end of the scintillator slat as shown in Figure . The initial tests of the SiPM and scintillator slats have been finished. The construction of the detector will take place summer 2014, followed by testing and installation to STAR before the 2015 RHIC run.

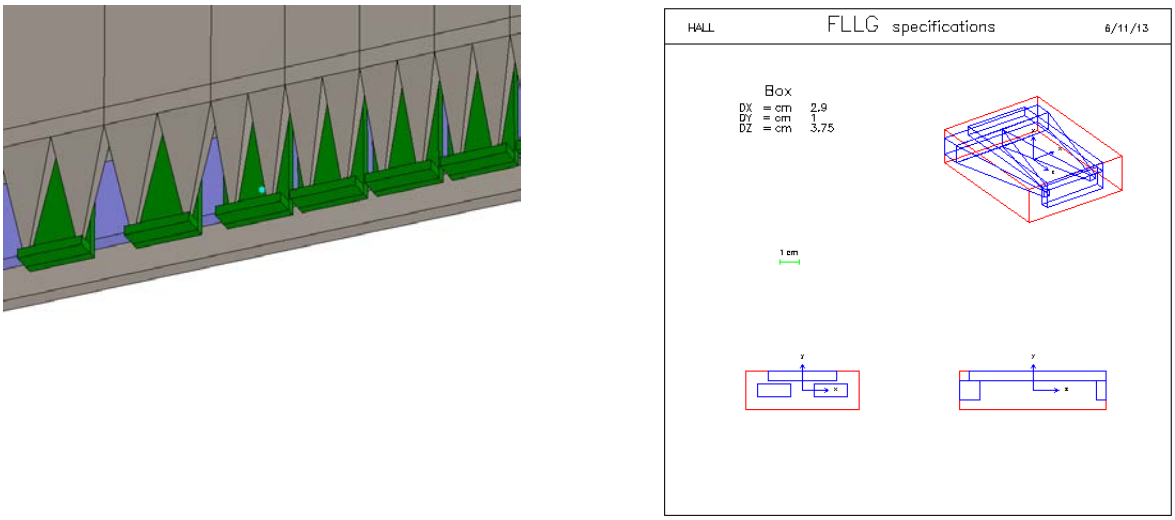


Figure 6.4: To keep the taper angle small while making it compact, there will be one light guide with a “two mountain structure” glued at each end of a scintillator slat. A small board with two SiPM will be attached to the end of the light guides. The FEE board will be mounted along the light guide for compactness as well as to give mechanical stability.

## 6.3 Run16 Forward Electromagnetic and Hadronic Calorimeter Options

The ultimate test for the TMD evolution would be to measure $A_N$ for $W^{\pm}$, $Z^0$ Boson and DY production. To obtain a significant measurement of $A_N$ for DY production, the DY leptons need to

be detected at rapidities 2 to 4 for a lepton pair mass of 4 $GeV^2$ and bigger. This is a highly non-trivial measurement, as backgrounds mainly due to QCD2→2 processes need to be suppressed by a factor ~$10^6$.

### 6.3.1 FMS with preshower and post-shower for Drell-Yan

Current preliminary studies indicate that the needed background suppression factor for an initial measurement for $A_N$ DY could be achieved by adding a new postshower behind the existing FMS and its preshower for Run-16. The design of such a postshower could be copied right from the FMS preshower (see section 6.2), but dropping the 3rd layer. More detailed simulations on the achievable signal to background level as well the statistical precision for the asymmetry measurement are still continuing over the next months.

### 6.3.2 Pixelization of E864 HCAL and re-configuring FGT

For a polarized DY experiment on a time scale competitive to other world efforts, one of the best solutions is to deploy the E864 calorimeter[95], with suitable modifications to emphasize its electromagnetic response. Pixelization of the E864 calorimeter into cells of transverse size comparable to the Moliere radius of electromagnetic showers, is an essential modification to the calorimeter for its use in detecting virtual photons decaying to $e^+e^-$ pairs. Conceptual proposal[96] with existing detector construction and on-going R&D efforts:

- a pixelized E864 calorimeter is deployed as a forward calorimeter;
- a preshower detector presently under construction performs robustly; and
- existing gas electron multiplier detectors work to provide forward tracking with good efficiency at high rate;

---


[1] *Beam-Energy Dependence of Directed Flow of Protons, Antiprotons and Pions in Au+Au Collisions* by Phys. Rev. Lett. arXiv:1401.3043

[2] *Observation of an energy-dependent difference in elliptic flow between particles and antiparticles in relativistic heavy ion collisions* Phys. Rev. Lett. 110 (2013) 142301

[3] *Energy dependence of moments of net-proton multiplicity distributions at RHIC* Phys. Rev. Lett. 112 (2014) 32302

[4] *Measurement of J/psi Azimuthal Anisotropy in Au+Au Collisions at $\sqrt{s_{NN}}$ = 200 GeV* Phys. Rev. Lett. 111 (2013) 52301

[5] *Jet-Hadron Correlations in $\sqrt{s_{NN}}$ = 200 GeV Au+Au and p+p Collisions* Accepted by Phys. Rev. Lett. arXiv:1302.6184

[6] *Experimental studies of di-jets in Au+Au collisions using angular correlations with respect to back-to-back leading hadrons* Phys.Rev. C87 (2013) 4, 044903

[7] *Event-plane dependent dihadron correlations with harmonic vn subtraction in Au+Au Collisions at $\sqrt{s_{NN}}$ =200 GeV* Accepted Phys.Rev. C (Rapid comm) *arXiv:1404.1070v1*

[8] B. Abelev et al. [STAR Collaboration], Studying Parton Energy Loss in Heavy-Ion Collisions via Direct-Photon and Charged-Particle Azimuthal Correlations, Phys. Rev. C 82 (2010) 34909

[9] *Freeze-out Dynamics via Charged Kaon Femtoscopy in $\sqrt{s_{NN}}$ =200 GeV Central Au+Au Collisions* Phys. Rev. C 88 (2013) 34906

[10] *Third Harmonic Flow of Charged Particles in Au+Au Collisions at $\sqrt{s_{NN}}$ = 200 GeV* Phys. Rev. C 88 (2013) 14904

[11] *System Size Dependence of Transverse Momentum Correlations at RHIC* Phys. Rev. C 87 (2013) 64902

[12] *Elliptic flow of identified hadrons in Au+Au collisions at $\sqrt{s_{NN}}$ =$ 7.7--62.4 GeV* Phys. Rev. C 88 (2013) 14902

[13] *Beam energy dependence of moments of the net-charge multiplicity distributions in Au+Au collisions at RHIC* Submitted Feb. 7, 2014 to Phys. Rev. Lett arXiv:1402.1558

[14] *Fluctuations of charge separation perpendicular to the event plane and local parity violation in $\sqrt{s_{NN}}$ =200 GeV Au+Au collisions at RHIC* Phys. Rev. C 88 (2013) 64911

*[15] Measurement of Charge Multiplicity Asymmetry Correlations in High Energy Nucleus-Nucleus Collisions at 200 GeV Submitted Mar. 4, 2013 to Phys. Rev C. arXiv:1303.0901*
*[16] Beam-energy dependence of charge separation along the magnetic field in Au+Au collisions at RHIC – Submitted Apr.7 2014 to Phys. Rev. Lett. arXiv:1404.1433*
[17] Y. Burnier, D. E. Kharzeev, J. Liao, and H.-U. Yee, Chiral Magnetic Wave at Finite Baryon Density and the Electric Quadrupole Moment of the Quark-Gluon Plasma, Phys. Rev. Lett. 107, 052303
[18] A. Bzdak, P. Bozek, Contributions to the event-by-event charge asymmetry dependence for the elliptic flow of π+π+ and π−π− in heavy-ion collisions, Physics Letters B 726 (2013) 239-243
[19] D. Kharzeev and M. Nardi, Phys.Lett.B **507**, 121 (2001); M.L. Miller, K. Reygers, S. J. Sanders and P. Steinberg, Ann.Rev. Nucl.Part.Sci. **57**, 205 (2007).
[20] B. Schenke, P. Tribedy and R. Venugopalan,Phys.Rev. C **86**, 034908 (2012);
B. Schenke, P. Tribedy and R. Venugopalan,
``Initial state geometry and fluctuations in Au+Au, Cu+Au and U+U collisions at RHIC,"
arXiv:1403.2232 [nucl-th].
*[21] Observation of D0 meson nuclear modifications in Au+Au collisions at $\sqrt{s_{NN}}$ = 200 GeV, arXiv:1404.6185, submitted to PRL*
[22] NPE v2 in Au+Au 39, 62 and 200 GeV, should be submitted to PLB before QM2014
[23] Elliptic flow of non-photonic electrons in Au+Au collisions at $\sqrt{s_{NN}}$ = 200, 62.4 and 39 GeV, *arXiv:1405.6348 submitted to PLB.*
*[24] J/Ψ production at high transverse momenta in p+p and Au+Au collisions at $\sqrt{s_{NN}}$ = 200 GeV Phys. Lett. B 722 (2013) 55*
*[25] Suppression of Y Production in d+Au and Au+Au Collisions at $\sqrt{s_{NN}}$ = 200 GeV*
*Submitted Dec. 16, 2013 to PLB, arXiv:1312.3675*
*[26] J/Ψ production at low $p_T$ in Au+Au and Cu+Cu collisions at $\sqrt{s_{NN}}$ = 200 GeV at STAR Submitted Oct. 14, 2013 to Phys. Rev.C arXiv:1310.3563*
*[27] J/Ψ polarization in p+p collisions at $\sqrt{s_{NN}}$ = 200 GeV in STAR Submitted Nov. 7, 2013 to Phys. Lett.B, arXiv: 1311.1621*
*[28] Dielectron Mass Spectra from Au+Au Collisions at $\sqrt{s_{NN}}$ = 200 GeV Submitted Dec. 30, 2013 to Phys. Rev. Lett. arXiv:1312.7397*
[29] Dilepton Production in Heavy-Ion Collisions, R. Rapp, PoS CPOD2013, 008 (2013) (todo: check if ref. is correct)
*[30] Di-electron elliptic flow at mid-rapidity in Au+Au collisions at 200 GeV Submitted to Phys. Rev. C arXiv:124-2.1791*
[31] Long-range angular correlations on the near and away side in p-Pb collisions at sNN=5.02 TeV - ALICE Collaboration (Abelev, Betty et al.) Phys.Lett. B719 (2013)
[32] Observation of Associated Near-Side and Away-Side Long-Range Correlations in sNN=5.02 TeV Proton-Lead Collisions with the ATLAS Detector , G. Aad, et al., Phys.Rev.Lett. 110 (2013) 182302.
[33] Quadrupole Anisotropy in Dihadron Azimuthal Correlations in Central d+Au Collisions at sNN=200 GeV, A. Adare, et al., (PHENIX Collab) Phys.Rev.Lett. 111 (2013) 212301
[34] L. Adamczyk et al., Neutral pion cross section and spin asymmetries at intermediate pseudorapidity in polarized proton collisions at √s = 200 GeV, Phys. Rev. D **89** (2014) 012001; arXiv:1309.1800
[35] L. Adamczyk et al., Measurement of longitudinal spin asymmetries for weak boson production in polarized proton-proton collisions at RHIC, submitted to PRL; arXiv:1404.6880
[36] L. Adamczyk et al., Precision Measurement of the Longitudinal Double-spin Asymmetry for Inclusive Jet Production in Polarized Proton Collisions at √s = 200 GeV, submitted to PRL; arXiv:14
[37] M. Aggarwal *et al.*, Phys. Rev. Lett. **106**, 062002 (2011), arXiv: 1009.0326
[38] E.C. Aschenauer et al., The RHIC Spin Program: Achievements and Future Opportunities, arXiv:1304.0079
[39] R. D. Ball et al., Nucl. Phys. B 849, 112 (2011) [Errata: ibid 854, 926 (2012) and 855, 927 (2012)];
R. D. Ball et al., Nucl. Phys. B 855, 608 (2012).
[40] D. de Florian, R. Sassot, M. Stratmann, and W. Vogelsang, arXiv:1404.4293
[41] B. I. Abelev *et al.*, Phys. Rev. Lett. **101**, 222001 (2008), arXiv: 0801.2990
[42] L. Adamczyk et al.,Transverse Single-Spin Asymmetry and Cross-Section for $\pi^0$ and η Mesons at Large Feynman-x in Polarized p+p Collisions at √s=200 GeV, Phys. Rev. D **86** (2012) 051101; arXiv:1205.6826
[43] HERMES Collaboration, Phys. Rev. Lett. **94** (2005) 012002;
COMPASS Collaboration, Phys. Lett. **B673** (2009) 127;
The Jefferson Lab Hall A Collaboration, Phys. Rev. Lett. **107** (2011) 072003.
[44] Z.-B. Kang and J.-W. Qiu, Testing the Time-Reversal Modified Universality of the Sivers Function, Phys. Rev. Lett. **103** (2009) 172001, arXiv:0903.3629
[45] A.Metz and J. Zhou, Transverse spin asymmetries for W-production in proton-proton collisions, Phys. Lett. B **700**

(2011) 11, arXiv:1006.3097
M.G. Echevarria, A. Idilbi, Z.-B. Kang and I. Vitev, QCD Evolution of the Sivers Asymmetry, Phys. Rev. D **89** (2014) 074013, arXiv:1401.5078
[46] S. Fazio, talk at DIS-2014, http://indico.cern.ch/event/258017/session/11/contribution/219/material/slides/0.pptx
[47] A. Adare et al. (PHENIX Collaboration) Phys. Rev. Lett. 107, 142301 (2011); B. Trzeciak for STAR Collaboration, QM 2012 proceedings; M. Wysocki for PHENIX Collaboration, QM 2012 proceedings.
[48] Brian Page, Indiana University Cyclotron Facility, Di-jet Cross Section and Double Spin Assymmetry at Mid-Rapidity from Polarized p=P Collisions at √s=200 GeV at RHIC, https://drupal.star.bnl.gov/STAR/files/thesis_Page.pdf
[49] L. Gamberg and Z.-B. Kang, Phys.Lett. B718 (2012) 181-188
[50] W. Ochs, J. Phys. **G40** (2013) 043001.
[51] E. Gregory et al., JHEP10 (2012) 170.
[52] HERMES Collaboration, A. Airapetian et al., Phys. Lett., B577:37–46, 2003. arXiv:hep-ex/0307023
HERMES Collaboration, A. Airapetian et al., Phys. Lett. B684:114–118, 2010. arXiv:0906.2478
[53] W. Brooks and H. Hakobyan, Nucl. Phys, A830:361c–368c, 2009. arXiv:0907.4606
[54] W. Brooks, Physics with nuclei at an Electron Ion Collider. 2010. arXiv:1008.0131.
[55] E866 Collaboration, M. Vasilev et al., Phys. Rev. Lett., 83:2304–2307, 1999. arXiv:hep-ex/9906010
[56] BRAHMS Collaboration, I. Arsene et al., Phys.Rev.Lett. 93, 242303 (2004), nucl-ex/0403005.
[57] STAR Collaboration, J. Adams et al., Phys.Rev.Lett. 97, 152302 (2006), nucl-ex/0602011.
[58] PHENIX Collaboration, A. Adare et al., Phys.Rev.Lett. 107, 172301 (2011), 1105.5112.
[59] J. L. Albacete and C. Marquet, Phys.Rev.Lett. 105, 162301 (2010), 1005.4065.
[60] ALICE Collaboration, B. Abelev et al., (2012), 1210.4520.
[61] P. Tribedy and R. Venugopalan, Phys.Lett. B710, 125 (2012), 1112.2445.
[62] J. L. Albacete, A. Dumitru, H. Fujii, and Y. Nara, (2012), 1209.2001.
[63] I. Helenius, K. J. Eskola, H. Honkanen, and C. A. Salgado, (2012), 1207.6869.
[64] Z.-B. Kang and F. Yuan, Phys.Rev. D84, 034019 (2011), 1106.1375.
[65] E. Braidot for the STAR Collaboration, arXiv:1008.3989 [nucl-ex].
[66] C. Marquet, Nucl. Phys. **A 796**, 41 (2007) [arXiv:0708.0231 [hep-ph]].
[67] J. L. Albacete and C. Marquet, arXiv:1005.4065 [hep-ph].
[68] M. Strikman and W. Vogelsang, arXiv:1009.6123 [hep-ph].
[69] H. Paukkunen, DIS-2014, http://indico.cern.ch/event/258017/session/1/contribution/222/material/slides/0.pdf
[70] T. Toll and T. Ullrich, arXiv:1307.8059 [hep-ph] (2013).
[71] T. Toll and T. Ullrich, Phys. Rev. **C 87**, 024913 (2013).
[72] H. Kowalski, L. Motyka, G. Watt, Phys. Rev. **D 74**, 074016 (2006).
[73] H. Kowalski and D. Teaney, Phys. Rev. **D 68**, 114005 (2003).
[74] S. Munier, A. M. Stasto and A. H. Mueller, Nucl. Phys. **B603**, 427 (2001).
[75] H. Weigert, Prog. Part. Nucl. Phys. **55** (2005) 461.
E. Iancu and R. Venugopalan, hep-ph/0303204.
F. Gelis, E. Iancu, J. Jalilian-Marian, and R. Venugopalan, Ann. Rev. Nucl. Part. Sci. 60 (2010) 463.
Y. V. Kovchegov and E. Levin, Quantum Chromodynamics at High Energy. Cambridge University Press, 2012.
J. Jalilian-Marian and Y. V. Kovchegov, Prog. Part. Nucl. Phys. 56 (2006) 104.
[76] A. Metz and J. Zhou, Phys. Rev. D **84** (2011) 051503.
F. Dominguez, J.-W. Qiu, B.-W. Xiao, and F. Yuan, Phys.Rev. D **85** (2012) 045003; J. Jalilian-Marian, A. Kovner, L. D. McLerran, and H. Weigert, Phys. Rev. D **55** (1997) 5414.
[77] Y. V. Kovchegov and A. H. Mueller, Nucl. Phys. **B529** (1998) 451.
F. Dominguez, C. Marquet, B.-W. Xiao, and F. Yuan, Phys. Rev. D **83** (2011) 105005.
[78] D. Boer, A. Dumitru, and A. Hayashigaki, Phys. Rev. D **74** (2006) 074018.
D. Boer and A. Dumitru, Phys. Lett. **B556** (2003) 33.
D. Boer, A. Utermann, and E. Wessels, Phys. Lett. **B671** (2009) 91.
[79] Z.-B. Kang and F. Yuan, Phys. Rev. D **84** (2011) 034019.
[80] Y. V. Kovchegov and M. D. Sievert, Phys. Rev. D **86** (2012) 034028.
[81] J.-W. Qiu, talk at the workshop on "Forward Physics at RHIC", RIKEN BNL Research Center, BNL, 2012.
[82] D. W. Sivers, Phys. Rev. D **41** (1990) 83.
[83] J. C. Collins, Phys. Lett. **B536** (2002) 43.
[84] M. Walker *et al*., arXiv:1107.0917.
[85] L. Gamberg and Z.-B. Kang, arXiv:1208.1962.
[86] D. Mueller, Fortschr. Phys. **42** (1994) 171; X.-D. Ji, Phys. Rev. Lett. **78**, 610 (1997); J. Phys. **G24** (1998) 1181; K. Kumericki, D. Mueller, and K. Passek-Kumericki, Nucl. Phys. **B794** (2008) 244; K. Kumericki and D. Mueller,

arXiv:1205.6967.
[87] S. Klein and J. Nystrand, hep-ph/0310223.
[88] T. Toll and T. Ullrich, Phys.Rev. **C 87** (2013) 024913
[89] STAR Collaboration, arXiv:1301.2187
[90] J. Collins, arXiv:1212.5974
[91] E.A. Hawker et al., "Measurement of the Light Antiquark Flavor Asymmetry in the Nucleon Sea", Phys. Rev. Lett. 80, 3715 (1998)
[92] L.C. Bland et al. [AnDY Collaboration], arXiv:1304.1454
[93] S. Bültmann et al., Phys. Lett. **B579** (2004) 245.
S. Bültmann et al., Nucl. Instr. Meth. **A535** (2004) 415.
S. Bültmann et al., Phys. Lett. **B632** (2006) 167.
S. Bültmann et al., Phys. Lett. **B647** (2007) 98.
[94] L. Adamczyk et al., Phys. Lett. **B719** (2013) 62.
[95] Armstrong et al, NIM A 406, 227, 1998
[96] https://drupal.star.bnl.gov/STAR/system/files/HCAL_proposal_140510.pdf
http://www.bnl.gov/npp/docs/pac0611/DY_pro_110516_final.2.pdf